TECHNISCHE UNIVERSITÄT WIEN
Vienna University of Technology

Master thesis

NK-92 metabolism and comparison of time-resolved cytotoxicity measurement methods

carried out for the purpose of obtaining the degree of Dipl.-Ing.

submitted at TU Wien

Faculty of Technical Chemistry

by

Karim Selmi, BSc

Mat.No.: 01427306

under the supervision of:

Univ.Prof. Dipl.-Ing. Dr.nat.techn. Oliver Spadiut

Bence Kozma, PhD

Valentin von Werz, MSc

Institute of Chemical, Environmental and Bioscience Engineering E166

Eidesstattliche Erklärung

Ich erkläre an Eides statt, dass ich die vorliegende Arbeit selbstständig und ohne fremde Hilfe verfasst, andere als die angegebenen Quellen und Hilfsmittel nicht benutzt bzw. die wörtlich oder sinngemäß entnommenen Stellen als solche kenntlich gemacht habe. Zudem bestätige ich, dass keine künstliche Intelligenz (KI) für die Verfassung der Arbeit bzw. für Teile der Arbeit zum Einsatz gekommen ist.

Wien, am 12.03.2024

Karim Selmi

Einverständniserklärung zur Plagiatsprüfung

Ich nehme zur Kenntnis, dass die vorgelegte Arbeit mit geeigneten und dem derzeitigen Stand der Technik entsprechenden Mitteln (Plagiat-Erkennungssoftware) elektronisch-technisch überprüft wird. Dies stellt einerseits sicher, dass bei der Erstellung der vorgelegten Arbeit die hohen Qualitätsvorgaben im Rahmen der ausgegebenen der an der TU Wien geltenden Regeln zur Sicherung guter wissenschaftlicher Praxis - „Code of Conduct“ (Mitteilungsblatt 2007, 26. Stück, Nr. 257 idgF.) an der TU Wien eingehalten wurden. Zum anderen werden durch einen Abgleich mit anderen studentischen Abschlussarbeiten Verletzungen meines persönlichen Urheberrechts vermieden.

Wien, am 12.03.2024

Karim Selmi

Acknowledgements

I would like to express my appreciation to Univ. Prof. Oliver Spadiut for taking over the supervision of this thesis and for welcoming me in his research group.

Further I thank Bence for his constructive ideas and support in coordination of the work. I would also like to express my gratitude to Valentin for creating an enjoyable and appreciative working atmosphere and for all the scientific input and support in the laboratory. A big thank you to Philipp, who not only supported me through our close collaboration but also kept me motivated with his cheerfulness and moral support.

I am also grateful to my parents and my siblings for being always there for me.

Lastly, I want to thank my life companion Sophie for her never-ending encouragement and emotional support, which were invaluable throughout my academic journey.

Table of content

Abstract

NK-92 is a highly cytotoxic natural killer cell line, with favourable properties for application in adoptive cell therapy. Relations between NK-92 metabolism and cytotoxic function are yet to be elucidated and the use of different cytotoxicity assays prevents comparison between experiments. Here NK-92 metabolism-cytotoxicity relationships were investigated, and three commonly used cytotoxicity methods were compared.

NK-92 cells were cultured for 21 days in a pseudo-static setup with a daily sampling procedure. Cell clustering was analysed via brightfield microscopy and metabolite concentrations were measured in the culture via amino acid HPLC and enzymatic assays. Cytotoxicity measurement at effector to target ratios (E:T) of 1:1 and 5:1, after 4 h of co-culture with K-562 via LDH release assay, calcein release assay and a flow cytometry-based method were performed and compared.

Correlations were found between metabolite concentrations, metabolite rates, aggregate formation, and cell count. Results of the three cytotoxicity methods showed no significant difference at 5:1 E:T. The results of the calcein release assay were significantly higher than those of the other two methods at 1:1 E:T. A correlation between spontaneous LDH release from NK-92 cells and the ratio of necrotic and apoptotic target cells was identified, indicating a potential role of spontaneous LDH release as soft sensor for the mode of killing of NK-92.

Kurzfassung

NK-92 ist eine stark zytotoxische Zelllinie der natürlichen Killerzellen, die vorteilhafte Eigenschaften für die Anwendung in der adoptiven Zelltherapie aufweist. Zu den Zusammenhängen zwischen Metabolismus und zytotoxischer Funktionalität von NK-92 ist noch wenig bekannt, während für die Zytotoxizitätsbestimmung verschiedene Messmethoden herangezogen werden, was einen Vergleich zwischen verschiedenen Experimenten erschwert. In dieser Arbeit wurden Metabolismus-Zytotoxizitätszusammenhänge untersucht und drei verschiedene Methoden zur Zytotoxizitätsmessung anhand von NK-92 verglichen.

NK-92 Zellen wurden über 21 Tage hinweg auf pseudostatische Weise, unter täglicher Probenahme expandiert. Die Bildung von Zellaggregaten wurde mittels Breitfeldmikroskopie analysiert und die Konzentration zahlreicher Metabolite wurde mittels einer Aminosäure HPLC Methode und enzymatischer Tests bestimmt. Zytotoxizitätsmessungen bei einem Verhältnis von Effektorzellen zu Zielzellen (E:T) von 5:1 und 1:1 und einer co-Inkubationsdauer von 4 h mit K-562 Zellen mittels Laktatdehydrogenase-Freisetzung, Calceinfreisetzung und einer Durchflusszytometrie basierten Methode wurden durchgeführt und miteinander verglichen.

Korrelationen zwischen Metabolitkonzentrationen und- Aufnahme/Produktionsraten, Aggregatbildung und Zellzahlen konnten festgestellt werden. Die Ergebnisse der Zytotoxizitätsmessung wiesen bei E:T=5:1 keine signifikanten Unterschiede auf, während die Zytotoxizitätswerte bei E:T=1:1 für die Calceinfreisetzung signifikant höher als jene der beiden anderen Methoden waren. Zusätzlich wurde ein Zusammenhang zwischen der spontanen LDH-Freisetzung der NK-92 Zellen und dem Verhältnis zwischen nekrotischen und apoptotischen Zielzellen nach der co-Inkubation gefunden.

1 Introduction

1.1 NK cell characteristics

Natural killer (NK) cells are lymphocytes of the innate immune system and serve as an important first line of defence against tumours and several pathogens, due to their ability to directly lyse target cells and secrete cytokines and chemokines, initiating further immune responses[1]. NK cells are generally identified by the absence of CD3 and the T cell receptor and the simultaneous presence of CD56 on their cell surface[2]. These cells, which make up 5-20% of circulating lymphocytes in humans, develop in the bone marrow and in secondary lymphoid tissues (SLTs) including tonsils, spleen and lymph nodes[3]. NK cell development (see Figure 1) starts from hematopoietic stem cells, which differentiate into $CD45RA^{+}$ lymphoid-primed multipotential progenitors, which further transition into common lymphoid progenitors (CLPs) with the ability to make lineage commitments into Pro-B, Pre-T, NK progenitors (NKPs) or other innate lymphoid cells[3]. The irreversible transition of CLPs into NKPs is marked by the expression of CD122, while the appearance of abundant CD56 marks the transition of immature NK cells into mature NK cells[3]. Most of the $CD56^{bright}$ population converts into a major $CD56^{dim}/CD16^{-}$ -and a minor $CD56^{dim}/CD16^{+}$ subpopulation[3]. Based on the expression of CD56, mature NK cells can be classified into a $CD56^{bright}$ population which resides primarily in the SLTs and is a potent producer of inflammatory cytokines and a $CD56^{dim}$ subset exhibiting more pronounced cytolytic functions, representing the majority of circulating NK cells in humans[3]. NK cell biology is strongly influenced by cytokines, as signalling through the common gamma chain, which serves as signalling subunit for interleukin-2 (IL-2), IL-4, IL-7, IL-9, IL-15 and IL-21 is required for development, homeostasis and function of NK cells[3].

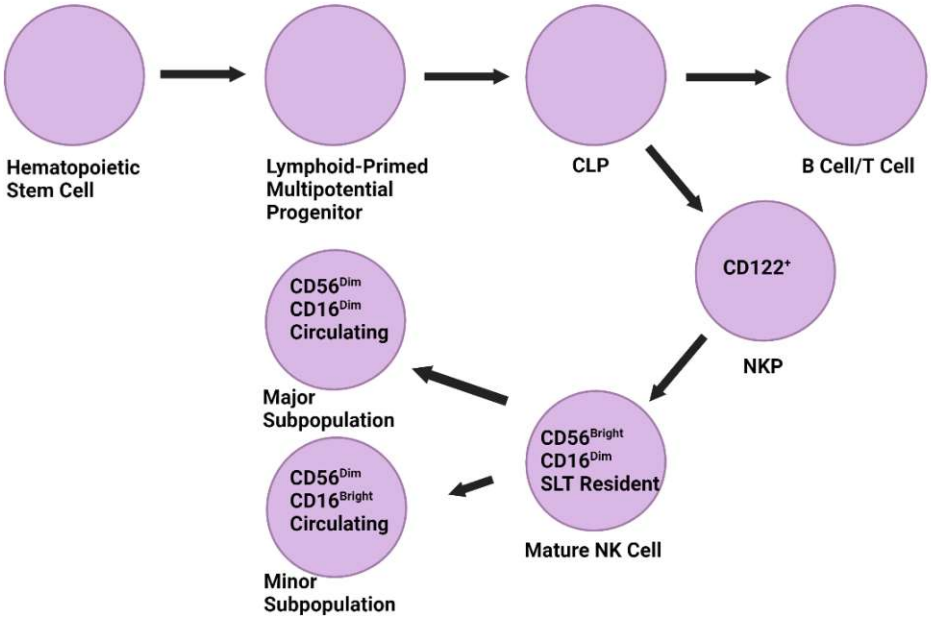

Figure 1: Overview of NK cell development Depicted is a scheme of the development of NK cells starting from hematopoietic stem cells. The commitment to NK cell development is marked with the transition from common lymphoid progenitors (CLP) to NK progenitors. NK cell development results in two circulating subpopulations with low CD56 expression and a secondary lymphoid tissues (SLT)-residing population with higher CD56 expression. This image was created with Biorender.com, adapted from reference[3].

While NK cells kill target cells via similar cytotoxic mechanisms as $CD8^+$ T cells, they have the ability to do so without prior sensitisation as their activation is not dependent on T cell receptors[3, 4]. NK cell activation is controlled by an equilibrium of activating and inhibitory signals, originating from activating and- inhibitory receptors on the NK-cell surface (see Figure 2)[5]. Healthy cells continuously express molecules, such as the major histocompatibility complex class I (MHC I), representing a major source of inhibitory signals[5]. Virus-infected and tumour cells often lack MHC I leading to lower inhibitory signalling[5]. Additionally, cellular stress associated with viral infections and tumorigenesis leads to an upregulation of ligands for activating receptors[5]. Another activating signal can be target cell-bound antibodies which are recognised by the activating receptors CD16a and CD32c[6]. Thus, the involvement of CD16a and CD32c in activation is referred to as antibody dependent cellular cytotoxicity (ADCC) [6]. NK cell activating receptors (NKRs) do not contain signalling domains in their cytoplasmatic tails, but associate with receptor-associated adaptor molecules, to enable signal transduction[3]. These adaptor molecules, including FcεRIγ, CD3ζ, and DAP12, are transmembrane-anchored proteins containing immunoreceptor tyrosine-based activation motifs (ITAMs)[7]. Upon engagement of a NKR with a ligand, ITAMs are phosphorylated, inducing a downstream signalling pathway that leads to the release of calcium from the endoplasmic reticulum, leading to target cell killing and cytokine production[5]. Inhibitory receptors, which contain immunoreceptor tyrosine-based inhibitory motifs (ITIMs) in their cytoplasmatic domain, counteract the activating signalling. This inhibition takes place as phosphatases are recruited by ITIMs upon ligand engagement with inhibitory receptors, which in turn deactivate proteins involved in ITAM signalling[5].

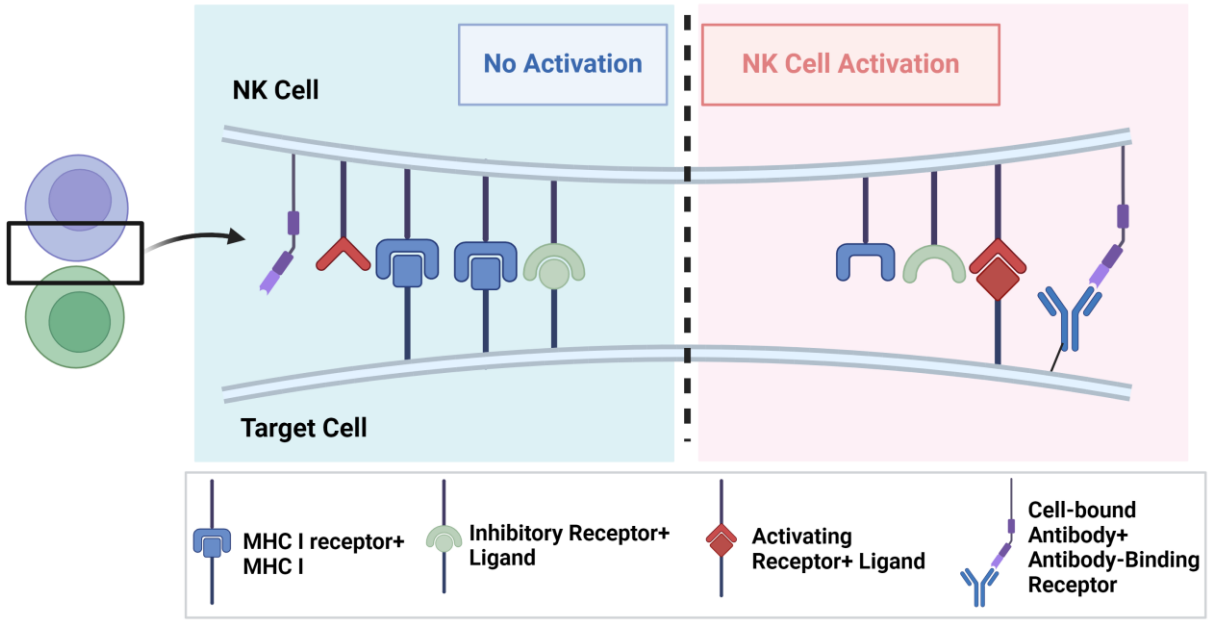

Figure 2: Scheme of NK cell activation Malignant- and virally infected cells express ligands of NK cell activating receptors. Upon binding of activating receptors to their ligands NK cell activating signals are transmitted. Target cell-bound antibodies are also ligands of activating receptors and their involvement in NK cell activation is referred to as antibody dependent cellular cytotoxicity (ADCC). Major histocompatibility complex I (MHC I) and other ligands, which are continuously expressed by healthy cells are bound by inhibitory receptors leading to signals that counteract activating signalling. The balance between the cumulated activating and inhibitory signalling is decisive for NK cell activation. The image was created with BioRender.com and reference[3].

Once this interplay between activating and inhibitory signalling results in NK cell activation, NK cells secrete a wide variety of pro-inflammatory cytokines, such as interferon-γ, tumour necrosis factor-α, IL-5, IL-10 and IL13 and exert cytolytic functions, also referred to as cytotoxic activity, which can take place via two distinct killing pathways[5].

One cytotoxic pathway involves the secretion of lytic molecules, predominantly perforin various granzymes, eventually leading to target cell death[8]. Perforin is a protein, that forms pores in the plasma membrane of the target cell, while granzymes are serine proteases, which are capable of induction of apoptosis[9]. These lytic molecules are stored within specialised secretory organelles, known as lytic granules inside the effector cell[10, 11]. When a target cell is identified, intensive contact between the effector and target cell is established via the formation of an immunological synapse[12]. Subsequently the lytic granules are polarized towards the immunological synapse[12]. Here perforin and granzymes are released into the synaptic cleft, via fusion of lytic granules with the plasma membrane[12]. The synaptic cleft is the interface between effector and target cell, formed by the immunological synapse[12]. It is not fully elucidated whether the pores formed by perforin directly allow granzymes to enter into the target cell cytosol or if the pore formation triggers endocytosis transporting granzymes and perforin into the target cell[9]. If the local cell membrane damage caused by perforin cannot be restored the target cell undergoes necrosis[13]. If the target cell is able to restore the cell membrane the introduced granzymes lead to apoptosis[13]. This differentiation between necrotic and apoptotic cell death is based on cell morphology characteristics occurring during cell death[13]. Necrotic cell death is characterized by cell swelling and lysis, whereas apoptosis comprises cell shrinkage followed by plasma membrane blebbing and separation of cell fragments into

apoptotic bodies[14]. However, also mixed forms of these two categories of cell death occur in NK cell-induced cytotoxicity[13].

The other cytotoxic pathway is the death receptor-induced target cell apoptosis[8]. Here, death receptors, on the target cell are engaged by binding of ligands expressed on NK cells, which induces apoptosis of the target cell[8]. The three different ligands, capable of apoptosis induction are TNF, Fas ligand (FasL) and TNF-related apoptosis-inducing ligand (TRAIL). TNF is a secreted cytokine, while the latter two are expressed on the NK cell surface[8].

1.2 NK cells for cancer treatment

Adoptive cell therapies (ACT) have emerged in recent decades as promising approaches to make use of the endogenous cytotoxic activity of immune cells in cancer treatment[15]. In contrast to conventional cancer treatments, such as surgery, chemotherapy and radiotherapy, ACT has the advantage of exhibiting more permanent anti-tumour directed effects[16]. In ACT immune cells from autologous or allogeneic sources are expanded and transformed *ex vivo* and (re)introduced into the patient[17, 18]. While the term autologous describes the use of the patient's own cells, allogeneic sources can be donors or cell lines[19]. Besides the application of T cells, NK cells have drawn attention as platform for ACT, due to the essential role of NK cells in tumour-immunosurveillance, which was highlighted by the association of increased cancer susceptibility and metastasis with diminished NK cell activity in clinical studies[20, 21]. However, autologous NK cell therapy has shown limited results in ACT, so that the focus of research shifted towards allogeneic NK cell therapy[22, 23]

Beyond the use of native immune cells, strategies to improve their specificity and activity against cancerous cells via genetic engineering have been introduced[24]. These strategies include modifications for the expression of antigen-specific T-cell receptors and chimeric antigen receptors (CAR)[25]. In particular, the use of CAR-T cells has been successful with eight CAR-T cell therapies, being approved for therapy[16]. However, CAR-T cell immunotherapy still has some challenges which have yet to be overcome, such as the occurrence of cytokine release syndrome (CRS) and neurotoxicity[16]. Another drawback of CAR-T cell therapy is the limitation of its allogeneic application due to the risk of graft versus host disease (GvHD) and host versus graft rejection (HvGR)[16]. In contrast, NK cells exhibit lower GvHD, HvGR, CRS and neurotoxicity risks[2]. An additional advantage of CAR-NK cells is the availability of CAR-independent pathways for anti-tumour activity[2]. Thus, research in the field of CAR-NK cell immunotherapy has gained significant interest, with 39 ongoing clinical trials and 35 preclinical trials as of October 2022[26]. Notably, out of the 35 preclinical trials, 26 use NK-92 cells as a source while 7 of the studies use primary NK cells (peripheral blood, cord blood and induced pluripotent stem cells)[26]. The remaining preclinical trials use other NK cell lines, such as KHYG and YTS as sources[26].

The high proportion of preclinical trials using NK-cell lines as source is reflected in the advantages of utilizing NK cell lines for CAR-NK immunotherapy over primary NK cell sources. For the use of blood derived NK cells for allogeneic NK cell immunotherapy, an additional purification step removing T-lymphocytes is necessary, as these cells are also enriched in the leukapheresis collection to obtain NK cells[19]. This additional purification step is time-consuming and expensive, and results in a loss of NK cells[19]. However, NK cell lines are continuously growing at high growth rates *in vitro* and do not show source-depending variabilities, making them suitable as "off-the-shelf" products for ACT[19]. Apart from that it is

more difficult to genetically engineer primary NK cells for CAR expression compared to NK cell lines[19].

1.3 Cytotoxicity measurement

An important part of ACT is to characterise the cells before injection into the patient, which includes the determination of NK cell function[27]. NK cell function involves the release of cytokines as well as cytolytic activity.[28] So the evaluation of NK cell function can be focused on either of these two[28]. Cytokine release can for instancebe measured by flow cytometry after an intracellular staining procedure or by quantification of released cytokines via enzyme-linked immunosorbent assay[29]. A prerequisite to determine cytokine release is prior stimulation, either via chemicals or through co-culture with target cells[30]. The cytolytic activity, or cytotoxicity, on the other hand can be measured via indirect and direct measurement methods[29]. An example for an indirect method is the CD107a assay, which measures the amount of secreted lytic granules[29]. Direct cytotoxicity measurement methods allow the quantification of either lysed or necrotic and apoptotic target cells after co-culturing of effector and target cells[29]. For a long time, the standard method for direct cytotoxicity determination was the chromium release assay, which involves radioactive labelling of the target cells with ^{51}Cr, followed by co-incubation with effector cells[30]. The release of ^{51}Cr from dead cells into the supernatant can be measured via gamma counting and is used to determine the cytotoxicity[31]. However, the chromium release assay comes with several disadvantages, including high material costs and radiation safety training and licensing[31, 32]. For this reason, several alternative cytotoxicity assays have been introduced, including the measurement of enzymes released from dead target cells and the measurement of fluorochromes released from prelabelled targets[33-35]. The use of flow cytometry-based methods provides several advantages, such as the facilitation to assess the E:T ratio as well as the effector cell viability at the end of the assay[36]. Additionally, these methods allow for further characterisation of the effector cell phenotype and enable discrimination between apoptotic and necrotic cells among the target cells without the use of image-based methods[37, 38]. However, some of these new methods have yet to be compared to each other. Accordingly, it is not possible to compare the outcome of experiments, which use different cytotoxicity determination methods to each other. This would require further understanding of differences between methods or the establishment of a new standard method. Furthermore, the outcome of a cytotoxicity assay is influenced by numerous parameters, such as the incubation time and effector to target ratio of the co-culture, target cell types, as well as cell densities of both effector- and target cell cultures just to name a few. This even makes a comparison between experiments applying the same methods difficult.

1.4 NK cell expansion

To perform clinical trials on NK cell ACT large numbers of NK cells are needed for infusion, ranging from $5x10^6$ to $1x10^8$ $CD3^-$ $CD56^+$ NK cells per kilogram bodyweight[39]. This points out the importance of the efficient *ex vivo* expansion of NK cells, to reach large cell numbers with high purity and potency, which has been a major hurdle in NK cell clinical trials[40]. The efficiency and product quality of NK cell expansion processes can be influenced by various factors, such as the choice of culture vessels, medium composition, the addition of ILs, the choice between feeder cell-based and feeder cell-free systems and the NK cell source[39]. To provide an overview, each of these factors will be elucidated in this section.

Regarding the culture vessel type, lymphocytes are usually expanded under static conditions in well-plates, T-flasks, and bags, which includes the periodical division and refilling of the

culture[23]. While it is convenient to work under static culture conditions, due to easy handling and scalability, low shear stress during culture and low vessel costs, static culturing methods still have disadvantages compared to dynamic cultures[41]. These are on the one hand a lack of homogeneity of nutrient availability in the culture and on the other hand the lack of the possibility of online process analytics[42]. Furthermore, static cultures are often performed in batch format, leading to time-dependent changes in nutrient concentrations, being an additional source of potential change of phenotype compositions[43]. The expansion of NK cells in more elaborated dynamic systems has already been reported[41]. The use of stirred bioreactors for example was reported to lead to a 7-fold increase in total NK cell production, compared to static cultures after 33 days of cultivation[41]. Also the expansion of NK cells in perfusion reactors was reported and was claimed to result in a highly pure NK cell product[43].

Another important point is the addition of cytokines and feeder cells to the culture[39]. Feeder cells are cells or cell lines which are used to further stimulate NK cell proliferation by adding them during the expansion process, with the most frequently used example being K562 cells[39]. Usually cytokines, such as IL-2, Il-15, IL-12, IL-18 and IL-21 are added to the culture to reach increased proliferation and improved cytotoxic function[39]. Additionally, in the case of primary NK cells, feeder cell-based systems are needed to ensure sufficiently high proliferation[39].

As the products of these expansion processes are determined for the use in ACT, product safety is an important aspect regarding NK cell production[27]. For this reason, $CD3^+$ T cells and $CD19^+$ B cells, which are contained in peripheral blood need to be removed before the expansion process as these cells cause graft versus host disease and passenger lymphocyte syndrome in patients[20]. This purification can either be performed via CD3/CD19 depletion or via CD3 depletion followed by CD56 enrichment, via antibody coated magnetic beads[39]. If a feeder cell-based system is used for expansion, the feeder cells must be stringently qualified by viral- and mycoplasma testing and their removal from the product after the expansion process is necessary[39].

The necessity for the above-mentioned purification steps is in general dependent on the NK cell source selection[39]. To acquire NK cells for ACT various sources are available, including peripheral blood mononuclear cells (PBMCs), umbilical cord blood (UCB) and NK cell lines[39]. PBMCs and UCB for example contain CD3 expressing T cells, which need to be removed[39, 44]. Furthermore, the ratio of NK cells derived from leukapheresis of PBMCs is generally low and highly variable and regarding UCB the low volume per unit should be considered[39, 45]. An alternative to primary NK cell sources is NK cell lines, whereas NK-92 is the only NK cell line approved by the FDA for clinical use[26]. Advantages of using NK-92 are that no removal of other cell populations is necessary and its ability of unlimited proliferation, which makes it a rapidly available, abundant and cost efficient source for ACT[26]. A drawback of NK cell lines is that irradiation of the cells is necessary prior to infusion, due to their tumorigenicity[27]. Good manufacturing practice compliant protocols for the expansion of NK-92 cells have already been introduced[46-48]. The reported methods are carried out in culture bags in X-Vivo 10 serum-free medium supplemented with 2.5% human serum and 500 U/ml IL2, with one protocol yielding in a 218-250 fold expansion over 15-17 days[47].

Another important factor, which has an influence on the efficiency of NK cell expansion is the media composition[41]. Examples are reported influences of amino acid levels on T cell proliferation and of fatty acid levels on NK-92 cell proliferation[49, 50]. Since NK cell metabolism was reported to have an influence on anti-tumour directed NK cell function, the media

composition can be expected to additionally have an influence on the effector function of the produced NK cells[41]. Hence, a deeper understanding of the relations between NK cell metabolism and effector functions could help to define critical process parameters and therefore could drive the optimisation of expansion processes, regarding process stability, product yields and product quality.

1.5 NK-92 cell line

NK-92 is a cell line derived from the mononuclear blood cells of a patient diagnosed with an aggressive NK cell lymphoma[19]. NK-92 cells are grown in suspension, forming cell aggregates with individual cells being 10-12 µm in diameter[19]. The cells are dependent on the presence of IL-2 in the culture medium for continuous growth[19]. In comparison to enriched and activated, blood derived NK cells, NK-92 shows a consistently high cytotoxic activity against malignant cells, which is due to multiple reasons[19]. Firstly NK-92 cells contain larger amounts of granzymes than blood-derived NK cells[19]. Other reasons include that NK-92 cells express various activating receptors, while only expressing one inhibitory receptor of the KIR family and their ability to perform serial killing to a greater extent than blood-derived NK cells[19]. However, NK-92 cells do not express CD16 and thus cannot perform ADCC[51]. Their consistently high cytotoxic activity makes NK-92 a suitable model organism for research on target cell recognition and killing mechanisms of NK cells[52].

While NK-92 has been studied intensively, only little is known about relationships between process parameters (PPs) applied in NK-92 expansion and quality attributes (QAs) such as cell growth and cytotoxicity[19]. Deeper understanding of these relationships would allow optimization of NK-92 production processes, especially since relations between metabolism and cytotoxic activity of NK cells have already been reported[41].

1.6 Goals

For an efficient optimisation of the yield and product quality of NK-92 expansion processes in compliance with the concept of quality by design, a fundamental understanding of PP-QA relations is essential. However, these relations are poorly understood for NK-92 processes. Moreover, multiple different methods are currently used for the assessment of cytotoxicity, being an important QA. Thus, a direct comparison of these methods would reveal potential limits of the comparability of results derived from different cytotoxicity assays.

Therefore, this thesis aimed to investigate the relationship between different PPs of a static NK-92 culture over a period of 21 days and to simultaneously compare three different, commonly used approaches of measuring the cytotoxicity under time resolved conditions.

Within this scope NK-92 cells were expanded in a pre-established setup, that allowed daily sampling of the culture[53]. Multiple metabolites and amino acids were tracked throughout the process. Additionally, aggregate formation in the culture was monitored via brightfield microscopy. Employment of image analysis software allowed the acquisition of aggregate morphology data. The cytotoxicity against K-562 cells was determined from daily samples via three different cytotoxicity assays. Correlation analysis was performed on all acquired data and the results were interpreted.

The laboratory work for this thesis was performed in collaboration with Philipp Brunmayr, MSc to obtain a shared database. However, the data evaluation was performed independently.

2 Materials and Methods

2.1 Cell Maintenance

NK-92 cells, purchased from the American Type Culture Collection (ATCC) were maintained in Stem Cell Growth Medium (SCGM) (CellGenix) supplemented with 5% fetal bovine serum (FBS) (ATCC) and 2 mM GlutaMAX (Thermo Fisher Scientific Inc.). K-562 cells (ATCC) were maintained in Iscove's Modified Dubelcco's Medium (IMDM) (gibco) supplemented with 10% FBS. All cells were cultured at 37°C and 5% CO_2 in a humidified atmosphere. The viable cell concentration was kept between $0.7x10^6$ and $1.0x10^6$ viable cells/ml with media renewal in 48 h intervals.

2.2 NK-92 expansion and daily sampling process

For the observation of cell-related parameters of the NK-92 cells throughout a process duration of 21 days, NK-92 cells were cultivated according to a preestablished protocol, including the daily removal of a representative sample of the culture. K-562 cells, which were required for determination of the cytotoxicity of the sampled NK-92 cells, were cultured in parallel.

NK-92 cultures were initiated at $1x10^5$ cells/ml in triplicates in T175 flasks with 50 ml NK-92 medium. The cultures were refreshed by daily exchange of 20% of the culture volume with fresh medium and supplemented with 500 IU/ml human interleukin-2 (IL-2) IS Premium grade (Milteny Biotec) every 48 h.

To perform daily cytotoxicity assessment and quantitative metabolite determination of the NK-92 cultures, samples of NK-92 and K-562 cultures were collected, and cell count, and viability were determined daily over a process duration of 21 process days. For cell count and viability determination a 20 µl aliquot of cell suspension was mixed with 20 µl of trypan blue solution (0.4%) (gibco). 10 µl of the mixture were pipetted onto a cell counting chamber slide. Cell count and viability were then determined in triplicates via a bright field image-based automated cell counter device (Countess II) (Thermo Fisher Scientific). The automated cell counter additionally measures the average cell size of the sample.

An overview of the sampling process is given in figure 3. To quantify possible medium evaporation during the process, all flasks were weighed before and after each sampling and refilling step. For refilling of the sampled culture volume T175 flasks containing 50 ml of fresh NK-92 medium were kept at 37°C and 5% CO_2, which are later referred to as stability flasks. A 10 ml sample of the culture was taken and transferred into a 15 ml tube (later referred to as culture sample). Subsequently the culture was refilled with 10 ml of preconditioned NK-92 medium from the stability flask. A 10 ml sample was additionally transferred from the stability flask into a 15 ml tube (later referred to as stability sample) and the stability flask was then refilled with 10 ml of fresh NK-92 medium. The culture sample was centrifuged (5 min, 300 g). A fraction of 500 µl of the culture supernatant and of the stability sample was used respectively to determine the pH via a pH-meter. Another fraction of 800 µl of the culture supernatant and the stability sample was used respectively to quantify metabolites via enzyme-based assays and amino acids via a preestablished high performance liquid chromatography (HPLC) method (see sections 2.3 and 2.4). Following the viability assessment via trypan blue exclusion and cell count determination, the cells were employed for subsequent cytotoxicity determination.

The K-562 culture was resuspended by pipetting and a 5 ml sample was transferred into a 15 ml tube. The culture was refilled with 5 ml of fresh K-562 medium. The sample was centrifuged for 5 min at 300 g and the supernatant was discarded. The sampled K-562 cells were resuspended in serum-free IMDM. An aliquot of 20 µl of the cell suspension was used for cell count and viability determination. The remaining cell suspension was split into two fractions and further used for subsequent cytotoxicity assays.

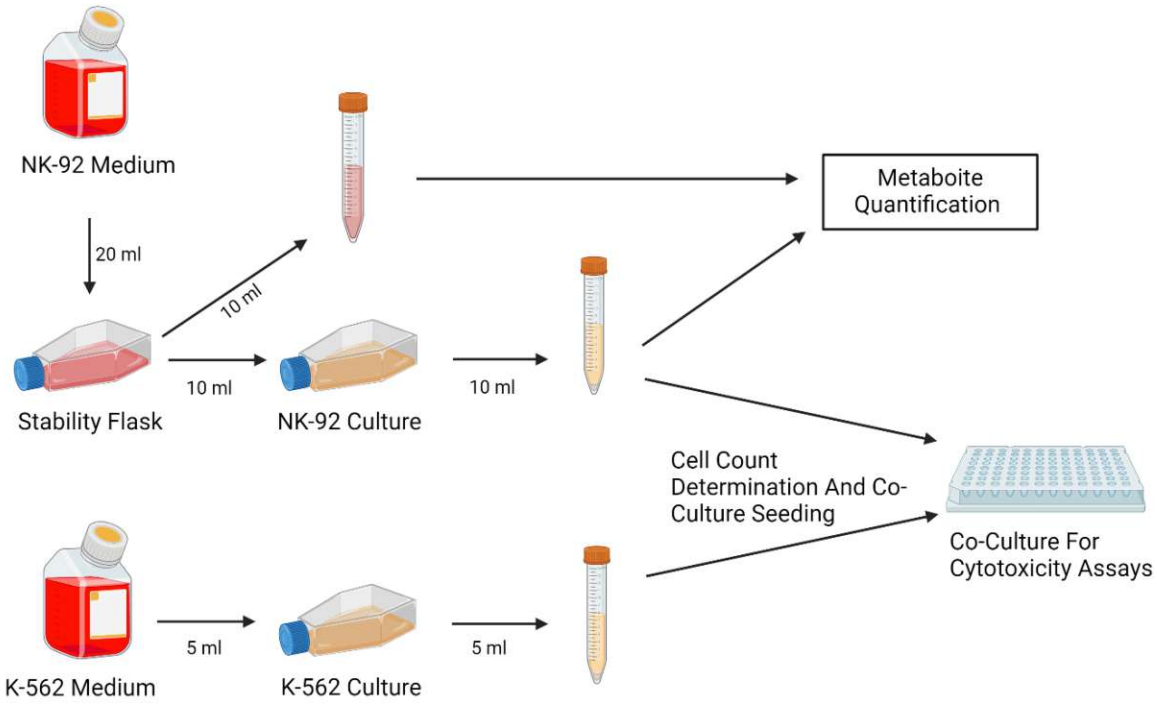

Figure 3: Scheme of NK-92 and K-562 culture sampling process and subsequent use of supernatants and cells
A 10 ml sample of the NK-92 culture was taken, after resuspension of the culture via pipetting, and transferred into a 15 ml tube. The NK-92 culture was then replenished with 10 ml of pre-conditioned NK-92 medium from the stability flask. A sample of 10 ml deriving from the stability flask was transferred into another 15 ml tube and the stability flask was replenished with fresh NK-92 medium. A 5 ml sample of the K-562 culture was transferred into another 15 ml tube and the culture was replenished with fresh K-562 medium. Cells in the culture samples were separated via centrifugation (300 g, 5 min). The NK-92 culture supernatant and the stability flask sample were used for metabolite quantification, and the cells were used for co-culture seeding. This image was created with BioRender.com

2.2.1 Calculation of the specific growth rate of the NK-92 cultures

To gain a better overview of the growth behaviour, the specific growth rate (µ) was calculated from the measured NK-92 cell counts, which considers the dilution of the culture during the sampling process as well as the number of cells removed from the culture. µ was calculated according to equation 2, which is obtained from equation 1 by separation of variables and subsequent integration under the assumption of a constant growth rate. However, it is pointed out that µ is only constant during maximal growth, which cannot be assumed throughout the whole NK-92 culture process, as a lag-phase is expected at the start of the process and limitations or inhibitions can occur in the process.

$$\frac{dc_x}{dt} = \mu * c_x$$

Equation 1

μ…	*growth rate (h^{-1})*
c_x…	*cell concentration (cells/ml)*

$$\mu\ (h^{-1}) = ln(\frac{c_x(t_{0+24})}{c_x(t_0)}) : 24\ h$$

Equation 2

μ…	*growth rate (h^{-1})*
$c_x(t_0)$…	*viable cell concentration at timepoint t_0 (cells/ml)*
$c_x(t_{0+24})$…	*viable cell concentration 24 h after timepoint t_0 (cells/ml)*

2.3 Microscopy images of standard culture

NK-92 cells form cell aggregates, also referred to as clusters, when grown in static suspension cultures[19]. To examine the morphology and number of cell aggregates in the NK-92 cultures, microscopy images of the culture were taken at 4X magnification with a bright field microscope equipped with a camera (Axiocam 208 color) (ZEISS) on every process day, followed by an image analysis using the open-source software ilastik (1.4.0) (https://www.ilastik.org/) and CellProfiler (4.2.4) (https://cellprofiler.org/), to obtain the average aggregate count and average aggregate diameter. As sampling of the culture is accompanied by disruption of cell aggregates, the microscopy images were taken prior to the sampling process. The area of the T175 culture flasks was divided into 16 equally sized squares. The culture was photographed once in each of the segments, to achieve representativeness of the culture images.

Due to debris formation in NK-92 cultures the use of the software CellProfiler, resulted in errors in the identification of clusters in previous test runs. Therefore, the software ilastik was additionally used to avoid these errors. The workflow used to identify cell aggregates consisted of a pixel classification step via ilastik, training the program to differentiate between pixels belonging to cells or to the background by manual assignment. The trained program created probability maps from the culture images, which enhanced the following cluster identification via cell profiler, due to favourable contrasts of the probability maps compared to the original culture images. The result of the cluster identification via cell profiler was data including cluster sizes and cluster counts. The workflow of the image analysis is summarised in table 1.

Table 1: Workflow for aggregate morphology data acquisition from microscopy images In a first step inhomogeneous illumination of the microscopy images was removed and sharper borders were created around cells and cell aggregates. Cell aggregates were then identified and aggregate morphology data acquired by employing an adjusted pipeline in the image analysis software CellProfiler.

ilastik (input=original microscopy image; output=probability map)	
Module	**Description of function**
Pixel identification	Creates a probability map in which a pixel is shown in colour if the probability that it is part of a cell and not the background is over a certain threshold. Results in sharper borders around objects and removal of inhomogeneous illumination.
CellProfiler (input=probability map; output=image with outlined clusters and cluster morphology data)	
Module	**Description of function**
ColorToGrey + CorrectIlluminationCalculate	Converts the input image into a grayscale image
IdentifyPrimaryObjects	Creates outlines around clusters within a predefined size range
MeasureObjectSizeShape	Outputs the area, eccentricity and form factor of the outlined clusters
OverlayOutlines	Creates an overlay of the produced outlines on the original image

To enhance the identification of cell aggregates via cell profiler, the pixel classification function of the open-source software ilastik was used. To train the Random Forest classifier, the background and cells were annotated manually in multiple culture images. The trained classifier was then applied to all culture images, resulting in probability maps of each image. In the probability map a pixel is coloured if the probability that it belongs to a predefined class is over a certain threshold. Thus, the probability map exhibits sharper borders around cells and no uneven illumination in contrast to the original microscopy images. The probability maps were exported in .tiff format. An example of an input culture image and the corresponding probability map is depicted in figure 4. The resulting probability maps were then used as input for the identification of cell aggregates via cell profiler.

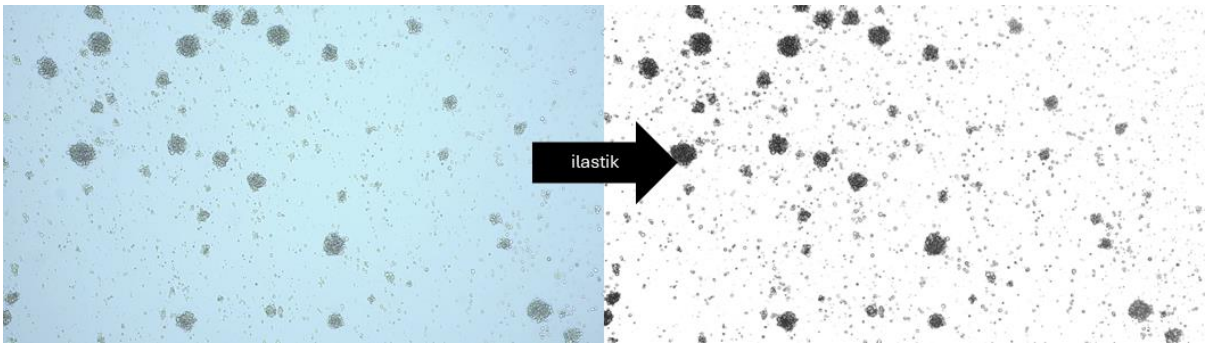

Figure 4: Example of input- and output images of pixel identification via ilastik On the left the input image for pixel identification via ilastik is depicted and the output image on the right. A trained random forest classifier assigns each pixel to the two classes background and aggregates. The output image is a probability map, where a pixel is shown coloured when the probability that it belongs to the aggregate class is over a certain threshold. Advantages of the output image over the original image are sharper borders around cells/aggregates and the removal of inhomogeneous illumination.

A pipeline consisting of multiple modules was assembled in the open-source software CellProfiler with the goal of creating outlines around cell aggregates and acquiring morphology data for each aggregate. To convert the output images from ilastik into grayscale images the ColorToGray and CorrectIlluminationCalculate functions were used. The IdentifyPrimaryObjects function was used to create outlines around aggregates within a predefined size range. Aggregates and cells that are outside the predefined size range are not outlined. Here, the triple length of the average cell diameter was chosen as lower limit of the size range. The lower limit could not be decreased, as this created outlines around accumulations of cell debris particles in previous test runs. The upper limit was set higher than the diameter of the largest aggregates among the sample images. The MeasureObjectSizeShape function measures several area and shape features of the outlined primary objects. With the OverlayOutlines function an overlay of the outlines over the original images was created, to enable a visual validation of the object identification (figure 5). The output data consisted of the area (pixel), eccentricity and form factor of each of the identified primary objects.

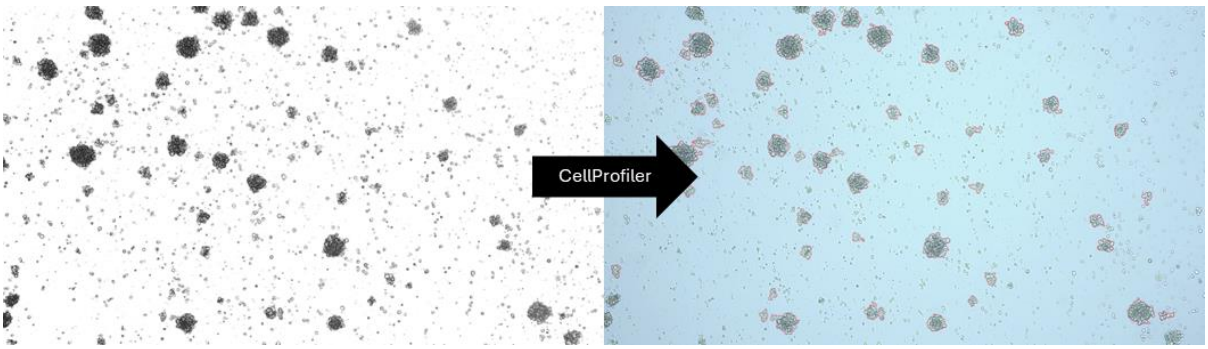

Figure 5: Example of input and output images of object identification via CellProfiler On the left the output image of the pixel classification via ilastik is depicted and the output image of the aggregate identification on the right. After transformation of the input image into grayscale, outlines were created around cell aggregates within a predefined size range using the IdentifyPrimaryObjects module. The limit of the size range was triple the

diameter of an average NK-92 cell, as lower values have resulted in outlines around debris accumulations. Aggregate morphology data, including the area, of outlined aggregates were acquired and analysed.

As the single cell size exhibited a variation over the process time, it was necessary to consider both the size of aggregates, and the number of cells contained per aggregate for data analysis. The number of cells per aggregate was calculated according to equation 3, where the mean single cell area of the respective process day was used. On the Axiocam 208 color, 1 pixel is equivalent to 1.85 µm. With the consideration of the augmentation factor of 4 and the crop factor of 0.5 the length of a pixel results in 0.925 µm and the area of a pixel is accordingly 0.86 μm^2 (equation 4). The calculated number of cells per aggregate does not represent an approximation of the actual number of cells per aggregate, as only the cross-sectional area of each aggregate but not its volume is considered in equation 3. However, this method still allows an interpretation of time dependent changes in the calculated number of cells per aggregate.

$$number\ of\ cells\ per\ aggregate = \frac{aggregate\ area\ (pixel) * pixel\ area\ (\frac{\mu m^2}{pixel})}{mean\ single\ cell\ area\ (\mu m^2)}$$

Equation 3

$$pixel\ area\ \left(\frac{\mu m^2}{pixel}\right) = \left(1.85\ (\mu m) * \frac{2}{4}\right)^2$$

Equation 4

2.4 Metabolite and amino acid measurement via enzyme-based assays

A fraction of 200 µl of the NK-92 culture supernatant was transferred into a 1.5 ml tube and directly used for the quantification of various metabolites and the amino acids glutamate and glutamine via a Cedex Bio HT instrument (Roche). This device measures metabolite concentrations via enzymatic assays resulting in colour changes, that are detected photometrically. The enzymatic assays are performed fully automated by the device. The measurement principle of each of the measured metabolites is described below.

- Lactate dehydrogenase (LDH) activity: Lactate and oxidised nicotinamide adenine dinucleotide (NAD^+) are converted into pyruvate and reduced nicotinamide adenine dinucleotide (NADH) in the presence of LDH. The initial rate of NADH formation is measured photometrically.
- Lactate concentration: L-lactate is oxidised via lactate oxidase, yielding pyruvate and H_2O_2. The conversion of H_2O_2 via peroxidase a chromogen. The absorption of the chromogen is directly proportional to the concentration of L-lactate in the sample.
- Glucose concentration: Glucose is converted to glucose-6-phosphate (G6P) via hexokinase. G6P is oxidised by oxidised nicotinamide adenine dinucleotide phosphate $NADP^+$ in the presence of glucose-6-phosphate dehydrogenase. The rate of reduced nicotinamide adenine dinucleotide phosphate (NADPH) formation is measured photometrically and is directly proportional to the glucose concentration in the sample.
- Ammonia concentration: NH_4^+ is converted together with 2-oxoglutarate and NADPH in the presence of glutamate dehydrogenase into l-glutamate and $NADP^+$. The decrease

of NADPH is directly proportional to the concentration of NH_4^+ in the sample and is determined photometrically.

- Glutamine concentration: L-glutamine is converted to L-glutamate by glutaminase. L-glutamate is further oxidised by L-glutamate oxidase to α-ketoglutarate, ammonia and hydrogen peroxide. Hydrogen peroxide forms a chromogen in the presence of peroxidase. The formation of the chromogen is directly proportional to the glutamine concentration in the sample and is measured photometrically. To avoid any influence of already present glutamate in the sample, glutamate oxidase and catalase are added in a prior step.
- Glutamate concentration: L-glutamate is converted into α-ketoglutarate, ammonia and H_2O_2 via L-glutamate oxidase. H_2O_2 forms a chromogen in the presence of peroxidase. The chromogen formation is directly proportional to the concentration of L-glutamate in the sample and is determined photometrically.
- GlutaMAX + glutamine concentration: GlutaMAX, which is a dipeptide of alanine and glutamine, is hydrolysed via amino acid arylamidase to glutamine and alanine. The following steps are the same as for the measurement of glutamine. As a result, this assay measures the sum of GlutaMAX and free glutamine.
- Pyruvate concentration: Pyruvate is converted to L-lactate by NADH in the presence of LDH. The NADH decrease is measured photometrically.

2.5 Quantitative amino acid determination via HPLC

19 different amino acids were quantified via a pre-established HPLC method, which is based on a protocol by Agilent Technologies Ltd[54]. The method involves the separation of amino acids in the sample via reversed phase HPLC, followed by detection via a fluorescence detector operating at an excitation wavelength of 340 nm and an emission wavelength of 450 nm. For amino acid detection via fluorescence measurement, a derivatisation step with ortho-phthaldialdehyde (OPA) is required prior to the separation[55]. During the derivatisation amino acids react with OPA and 3-mercaptopropionic acid (3-MPA) under formation of fluorescent isoindoles[55]. For absolute quantification of amino acid concentrations from the obtained chromatograms a standard series was prepared and measured. Each standard and sample were supplemented with a defined amount of norvaline, serving as internal standard to account for differences between individual measurements.

2.5.1 Preparation of reagents, elution buffers and standards

Elution buffers were prepared as follow: A solution of 10 mM NaH_2PO_4 and 10 mM $Na_2B_4O_7$ in ultrapure water, adjusted to a pH of 8.2 with concentrated HCl (Buffer A) and a mixture of 45% v/v acetonitrile, 45% v/v. methanol and 10% v/v. ultrapure water (Buffer B) were prepared. A 400 mM aqueous solution of H_3BO_3 adjusted to a pH of 10.2 with 10 M NaOH was prepared (Borate buffer). For the derivatisation of amino acids, OPA was added to a final concentration of 372 mM to Borate buffer, followed by the addition of 3-MPA to a final concentration of 1% v/v shortly before the HPLC measurement (OPA final reagent). A 2.5 mM solution of asparagine, glutamine, and tryptophane in 0.1 M HCl was prepared and mixed in a 1:1 ratio with amino acid standard 18 AAS (Sigma-Aldrich). The final mixture is later referred to as all AA standard. The all AA standard was diluted with Buffer A to 10 different concentrations ranging from 0.01 mM to 0.63 mM (standard series). As internal standard a solution of 25 mM norvaline in 0.1 M HCl was prepared.

2.5.2 Measurement procedure

A fraction of 300 µl of the NK-92 culture supernatant and the stability sample were used respectively for the quantification of 19 amino acids via HPLC. Firstly, the samples were deproteinised by addition of perchloric acid (70%) (Carl Roth) to a final concentration of 0.25 mM and removing the formed precipitate by filtering the suspension through a 0.2 µm cellulose filter. This step was followed by the addition of the internal standard to final concentration of 1.25 mM norvaline to each sample and the standard series. Subsequently all samples, the standard series and the required reagents and solutions were loaded into the HPLC autosampler and the HPLC method was started. The method consisted of an automated derivatisation step, carried out by the robotic autosampler as described in table 2 followed by injection onto the separation column (Agilent AdvanceBio AAA LC column) at 40 °C and elution with a mobile phase gradient, described in table 3 at a flow rate of 1.2 ml/min.

Table 2: Auto sampler instructions for amino acid derivatisation Summarised are the steps carried out by the auto sampler for the derivatisation of amino acids, for detection via a fluorescence detector.

Draw 5 µl borate buffer
Draw 1 µl sample
Mix 6 µl in air 3X
Wait 15 s
Draw 1 µl OPA final reagent
Mix 7 µl in air 6X
Wait 60 s
Draw 1 µl Buffer A
Mix 8 µl in air 6X
Wait 60 s
Draw 3 µl 1 M acetic acid
Mix 11 µl in air 4X
Inject

Table 3: Summary of the HPLC gradient profile After equilibration of the separation column in the first step, samples are eluted with a linear gradient, followed by complete elution of residuals from the separation column at 100% buffer B.

Time (min)	% Buffer A	% Buffer B
0 (Injection time point)	98	2
0.2	98	2
6.8	43	57
7	0	100

2.5.3 Quantification of amino acid concentrations

With the measurement of the dilution series of the all AA standard a linear regression of the peak area to the amino acid concentration was calculated. Differences between individual measurements were considered by dividing the peak area of interest by the peak area of norvaline in the same sample. With the slope and intercept of the linear regression between peak area and concentration the corresponding concentration for each peak area was calculated.

2.6 Rate calculations

From the measured concentrations, the volumetric production rate for each metabolite and amino acid was calculated according to equation 6, based on the general mass balance described in equation 5, which was derived from reference[56]. To differentiate between the amount of glutamine and alanine deriving from the hydrolysation of GlutaMAX and the amount derived from the cells, the amount of GlutaMAX hydrolysed after addition to the culture was added to $n_{i,refill}$ for the calculation of the volumetric production rate of glutamine and alanine.

$$V_{in}c_{i,in} - V_{out}c_{i,out} + V_R r_i = V_R \frac{\partial c_i}{\partial t} + c_i \frac{(\partial V_R)}{\partial t}$$

Equation 5

V_{in}/V_{out}...	*volumetric flowrate into/out of the reactor (l/h)*
c_i...	*concentration of component I (mol/l)*
V_R...	*reactor volume (l)*
r_i...	*production rate of component I (mol/(l*h))*

$$r_i = \frac{n_i(t_{0+48}) - \left(n_i(t_0) + n_{i,refill}(t_0) + n_{i,refill}(t_{0+24}) - n_{i,sample}(t_0) - n_{i,sample}(t_{0+24})\right)}{V_{average} * 48\ h}$$

Equation 6

r_i...	*production rate of component I (mol/(l*h))*
$n_i(t_{0+48})$...	*amount of substance I in culture 48 h after timepoint t_0 (mol)*
$n_i(t_0)$...	*amount of substance I in culture at timepoint t_0 (mol)*
$n_{i,refill}(t_0)$...	*amount of substance I refilled to culture at timepoint t_0 (mol)*
$n_{i,refill}(t_{0+24})$...	*amount of substance I refilled to culture 24 h after timepoint t_0 (mol)*
$n_{i,sample}(t_0)$...	*amount of substance I removed from culture as sample after timepoint t_0 (mol)*
$n_{i,sample}(t_{0+24})$...	*amount of substance I removed from culture as sample 24 h after timepoint t_0(mol)*
$V_{average}$...	*average culture volume between timepoint t_0 and 48 h after t_0 (l)*

The specific production rates were calculated from the volumetric production rates according to equation 7.

$$q_i = r_i / VCC_{average}$$

Equation 7

q_i...	*specific production rate of substance I (mol/(10^6 cells*h))*
$VCC_{average}$...	*average viable cell concentration between timepoint t_0 and 48 h after t_0 (10^6 cells/l)*

2.7 NK-92 cytotoxicity determination

The cytotoxicity of NK-92 cells (effector cells) exerted against K-562 cells (target cells) was assessed via three different methods. All three methods involved a co-culture of effector- and target cells. The first two of these methods are based on the release of an endogenous enzyme or a fluorophore which was introduced in a prior labelling step into the target cells. Upon target cell lysis by effector cells, these substances are released into the supernatant and can then be quantified. The third method is a flow cytometry-based method, which requires staining of cells for markers associated with cell death and apoptosis after the co-culture.

Co-cultures were conducted in 96 well conical (V) bottom plates at an E:T ratio of 1:1 and 5:1, in a 1+1 mixture of NK-92 medium and K-562 medium at a total volume of 230 µl per well and an incubation time of 4 h at 37°C and 5% CO_2 in a humidified atmosphere. Wells containing either only effector (NK control wells) or only target cells (K-562 control wells) were additionally seeded as negative controls. Positive control wells contained only target cells, which were lysed by adding 2% v/v. Triton X-100 after 3.25 h of incubation time (Triton lysed wells). An additional well containing 10 times more K-562 cells than the K-562 control wells was seeded. (10x K-562 well). The plate layout is depicted in Figure 6 and the numbers of cells used are summarised in Table 4.

The co-cultures were performed in two different plates, whereas the only difference is that fluorescent- labelled target cells were used for plate 1 and unlabelled target cells were used for plate 2.

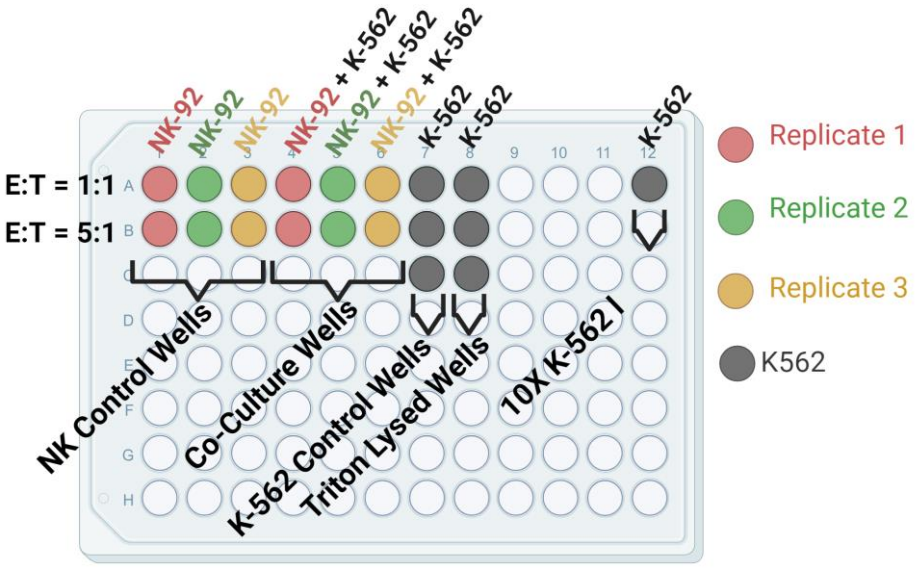

Figure 6: Schematic overview of co-culture plate layout. Two plates with identical layouts were seeded on each process day. One plate with calcein-labelled cells and the other plate with unlabelled K-562 cells. The plate was incubated at 37°C and 5% CO_2 for 4 h. Triton X-100 (2% v/v) was added to the wells marked as Triton lysed wells 45 min before the incubation time was over. The image was created with BioRender.com.

Table 4: Summary of cell numbers seeded in each well

	Co-culture wells		NK control wells	K-562 control wells	Triton lysed wells
E:T ratio	Number of viable NK cells per well	Number of viable K-562 cells per well	Number of viable NK-92 cells per well	Number of viable K-562 cells per well	Number of viable K-562 cells per well
1:1	$6{,}6x10^4$	$6{,}6x10^4$	$6{,}6x10^4$	$6{,}6x10^4$	$6{,}6x10^4$
5:1	$3{,}3x10^5$	$6{,}6x10^4$	$3{,}3x10^5$		

2.7.1 Cytotoxicity determination via calcein release

In this assay the release of the fluorophore calcein (emission maximum=449 nm) is used as an indicator for target cell lysis[33]. Target cells are labelled with calcein acetoxymethyl (AM), which permeates the cell membrane and is cleaved by intracellular esterases, yielding impermeable calcein[33]. After co-culture of effector and target cells the release of calcein is quantified in the co-culture supernatant fluorometrically. The percentage of lysed target cells is obtained by assigning 0% target cell lysis to the K-562 control well and 100% target cell lysis to the Triton lysed well and linear interpolation between the two values. The result is corrected with the spontaneous release of calcein, for which the K-562 control well is used.

Calcein AM (Calcein AM-Green, Invitrogen) was added to a suspension of $1x10^6$ K-562 cells per ml in serum-free IMDM to a final concentration of 15 µM. After an incubation time of 30 min at 37°C and 5% CO_2, the labelled cells were spun down for 5 min at 300 g and the supernatant was discarded. The labelled cells were washed twice with PBS by resuspending in 1 ml of PBS, centrifuging for 5 min at 300 g and discarding the supernatant.

After the incubation time of 4 h, the co-culture plate, containing the calcein-labelled target cells was centrifuged at 300 g for 5 min and 200 µl of supernatant from each well was transferred into a non-transparent 96 well flat bottom plate for the fluorescence measurement on a plate reader instrument (Spark, TECAN). The fluorescence in each well was measured at an excitation/emission of (485/520 nm). The measurements were performed in the automated gain adjustment mode of the plate reader instrument, as variations in the fluorescence of the samples were expected over the course of the process. With automated gain adjustment the plate reader determines the gain based on the highest signal on the plate. The cytotoxicity was calculated according to equation 8.

$$Cytotoxicity_{Calcein}(\%) = \frac{fluor._{co\ culture} - fluor._{K-562\ control}}{fluor._{K-562\ Triton} - fluor._{K-562\ control}} * 100$$

Equation 8

$fluor._{co\text{-}culture}$...	*fluorescence intensity in co-culture well (RFU)*
$fluor._{K\text{-}562\ only}$...	*fluorescence intensity in K-562 control-well (RFU)*
$fluor._{Triton}$...	*fluorescence intensity in K-562 triton lysed well (RFU)*

2.7.2 Cytotoxicity determination via LDH release

In this assay, the release of cytosolic LDH from lysed target cells is used as an indicator for the target cell lysis. After co-culture of effector and target cells the released LDH can be measured in the co-culture supernatant via an enzymatic assay. The percentage of lysed target cells is obtained by assigning 0% target cell lysis to the K-562 negative control well and 100% target cell lysis to the Triton lysed well and linear interpolation between the two values. As LDH in the co-culture supernatant can also be originated from effector cells, it is necessary to correct the result with a negative control describing the spontaneous release of LDH from effector cells, for which the NK only wells were used.

After fluorescence measurement for the calcein release assay, 150 µl of the co-culture supernatant was transferred into 1.5 ml tubes for measurement of the enzymatic LDH activity via an enzymatic assay as described in section 2.3.

The cytotoxicity was calculated according to equation 9. If the LDH activity in the NK-92 only well supernatant was below the detection limit, the mean value over all available sampling timepoints was used for the calculation of the cytotoxicity value.

$$Cytotoxicity_{LDH}(\%) = \frac{LDH_{co\ culture} - LDH_{K-562\ control} - LDH_{NK-92\ control}}{LDH_{K-562\ Triton} - LDH_{K-562\ control}} * 100$$

Equation 9

$LDH_{co\text{-}culture}$...	*volumetric LDH activity in co-culture supernatant (U/l))*
$LDH_{K\text{-}562\ control}$...	*volumetric LDH activity in K-562 control-well supernatant (U/l)*
$LDH_{NK\text{-}92\ control}$...	*volumetric LDH activity in N-K92 control-well supernatant (U/l)*
$LDH_{K\text{-}562\ Triton}$...	*volumetric LDH activity in K-562 Triton lysed-well supernatant (U/l)*

2.7.3 Cytotoxicity determination via flow cytometry-based method (FCM)

In this assay the cells are stained with fluorescent labelled antibodies and selective dyes after co-culture and subsequently analysed with a flow cytometer. To distinguish between effector and target cells, the cells were stained with a fluorescent labelled CD56 antibody, since CD56 is expressed on NK 92 cells but not on K-562 cells. To further distinguish between living and dead cells, the cells were labelled with Live or Dead Fixable Dead Stain (LIVE/DEAD) (AAT Bioquest), which is an amine reactive dye. Amine reactive dyes can penetrate damaged cell membranes and bind to amino groups in the cytoplasm, yielding in a fluorescent staining[57]. For viable cells, the staining is restricted to cell surface amino groups, resulting in a less intense fluorescence[57]. To additionally identify apoptotic cells, the cells were labelled with a fluorescent-labelled antibody, with binding specificity for phosphatidylserine (PS). In apoptotic cells PS is translocated from the inner side of the cell membrane to the outer surface of the plasma membrane[58]. The results of the flow cytometry were analysed using the flow cytometry analysis software FlowJo (10.8.1) (BD Biosciences). The software allows to iteratively exclude data points of cells from the analysis by applying gating strategies to the data, which allows analysis of cell populations of interest.

After the 4 h incubation time, the co-culture plate containing unlabelled K-562 cells, was centrifuged for 5 min at 300 g and the supernatant was discarded. The cell pellets were washed twice with 150 µl of PBS. The cell pellets were resuspended in 25 µl of a LIVE/DEAD pre-dilution (7.2 µl LIVE/DEAD in 1792 µl PBS). The plate was incubated for 30 min at 37 °C and 5% CO_2. After the incubation, the cells were washed twice with PBS. The cell pellets were resuspended in 25 µl of freshly prepared antibody dilution and the plate was incubated on ice, in the dark for 30 min. The composition of the antibody dilution is summarised in table 5. After incubation the cells were washed twice with 150 µl PBS. The cell pellets were then resuspended in 100 µl Fix/Perm buffer and incubated for 20 min on ice in the dark. After the incubation the cells were washed twice with Perm/Wash buffer and twice with PBS. The cells were resuspended in PBS and analysed on a Cytek Aurora instrument with SpectroFlo software (3.0.3).

Table 5: Composition of antibody dilution

Specificity - Fluorophore	Added volume	Final concentration (% v/v)
Brilliant Stain Buffer	559 µl	92.7
CD11a - PerCP/Cyanine 5.5	3.53 µl	0.59
CD25 - APC/Fire 750	3.53 µl	0.59
CD49d - Super Bright 600	3.53 µl	0.59
CD56 - PE-cF594	1.27 µl	0.21
CD69 - BUV737	3.53 µl	0.59
CD107a - PE-Cyanine5	3.53 µl	0.59
CD244 - PE	1.43 µl	0.24
CD314 - BV785	3.53 µl	0.59
CD335 - BV711	3.53 µl	0.59
CD337 - BUV395	12.5 µl	2.07
Phosphatidylserine - AF-488	4.3 µl	0.71

For calculation of the cytotoxicity, the percentage of viable target cells was determined via a multi-step gating strategy. The gating strategy is summarised in Figure 7. In the first step of the gating strategy small particles are excluded from further analysis, based on their forward scatter signal. The next step is the exclusion of doublets, which is a term for cells that are coherent to each other and thus pass by the detector together. Doublet exclusion is done by plotting the forward scatter signal intensity (FSC-H) against the forward scatter signal area (FSC-A). As the FSC-A is directly proportional to the FSC-H for single cells, the single cells are aligned along the diagonal of this plot. Doublets, however, show a higher FSC-A at the FSC-H of the equivalent single cells. For exclusion of the effector cells the FSC-A was plotted against the signal of the fluorescence channel at the emission maximum of the fluorescent-labelled CD56 antibody, and the $CD56^+$ effector cells were excluded. The resulting target cell population was analysed by plotting the signal of the fluorescent-labelled PS antibody against that of LIVE/DEAD. By considering the presence/absence of LIVE/DEAD and PS percentages of viable (LD^-PS^-), early apoptotic (LD^-PS^+), late apoptotic (LD^+PS^+) and necrotic (LD^+PS^-) populations were obtained (viability gate). Biases in setting the viability gate were avoided by setting the gate for the K-562 control and subsequently transferring it to the co-culture.

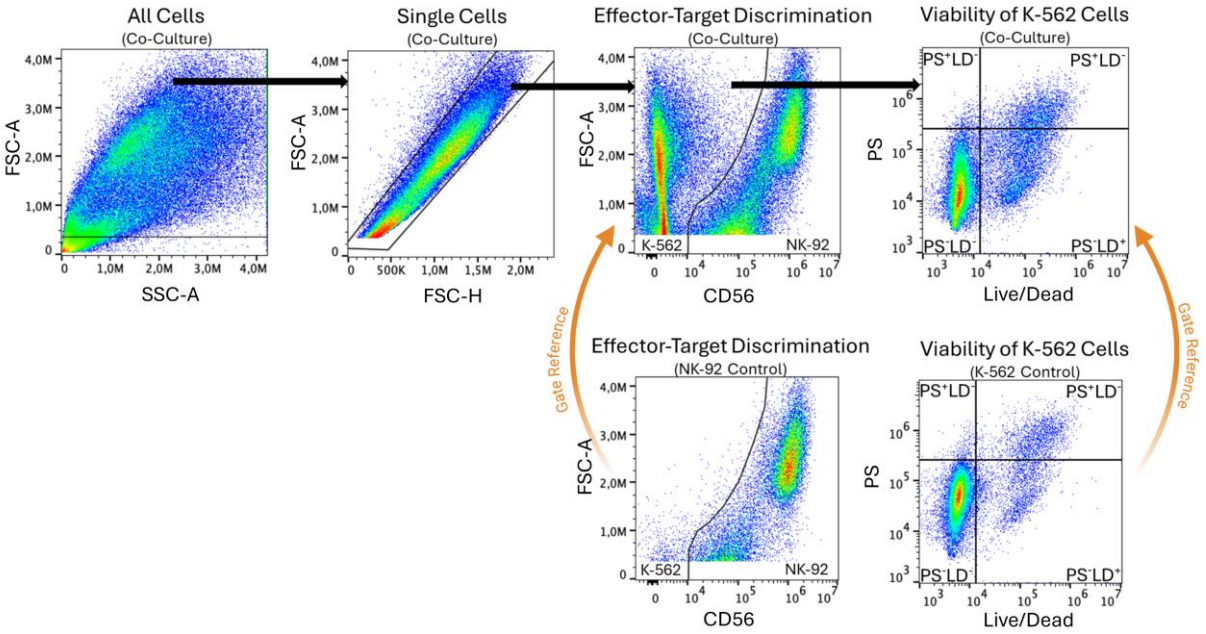

Figure 7: Gating strategy for identification of living, necrotic, early apoptotic and late apoptotic target cells The presence/absence of CD56 was used to distinguish the CD56 negative K-562 cells from the CD56 positive NK-92 cells. Based on the binding of the PS antibody and the presence of the amine reactive dye (Live/Dead) viable cells (PS^-LD^-) were distinguished from necrotic (PS^-LD^+), late apoptotic (PS^+LD^+), and early apoptotic (PS^+LD^-) cells.

For the calculation of the cytotoxicity, early apoptotic, late apoptotic, and necrotic cells were summarized as non-viable cells. With the proportion of events in the relevant gates the cytotoxicity was calculated according to equation 10.

$$cytotoxicity_{FCM}(\%) = \frac{prop.K-562\ viable_{K-562\ only} - prop.K-562\ viable_{co\ culture}}{prop.K-562\ viable_{K-562\ only}} * 100$$

Equation 10

prop. K-562 viable$_{K\text{-}562\ only}$…proportion of viable K-562 events to total K-562 events in K-562 only well
prop K-562 viable$_{co\text{-}culture}$…proportion of viable K-562 events to total K-562 events in co-culture well

2.8 Data pre-processing

As the acquired data were difficult to interpret, due to slow variations of the analysed process parameters over time, only every second data point is used for the time course plot of each process parameter and the cytotoxicity. Accordingly, only every second data point was used for the calculation of correlations.

To identify outliers among the metabolite concentration results of the biological triplicates, the difference of the concentration in one replicate to the mean of the concentration of the remaining two replicates was calculated for each metabolite concentration and each replicate. Consequently, outliers among these differences were identified via Grubbs' tests at α=0.05.

3 Results and discussion

3.1 Cell growth, cell size, viability and pH of the NK-92 culture (basic PPs)

Correlations among the basic PPs were calculated in form of Pearson correlation coefficients, considering the whole process duration as well as the two process phases individually. The correlations are summarized in form of matrices of the squared Pearson correlation coefficients (R^2 values) in figure 12. If the R^2 values are equal or higher 0.7 the correlation is considered as strong correlation.

Time course plots of the viable cell concentration (VCC) and viability of the NK-92 culture are depicted in Figure 8. During the first process days, an increase in the VCC can be observed until process day 8, followed by a plateau phase and another slight increase during the last days of the process for all three replicates. The viability of replicate B and C increases during the first process days, starting at around 82% on process day 0 and reaching a maximum of approximately 90% on day 2-4. After the maximum in viability is reached the viability drops back to 80%, followed by a slight recovery. The viability of replicate A does not vary as much as the other two replicates, but still shows a slight drop after process day 10. The VCC reached during the process is not limiting the growth, as NK-92 cells cultured at a VCC of $0.7x10^6$ and $1x10^6$ reached doubling times of 48 h in previous experiments. Thus, the cell concentration is not the reason for the decline in cell growth on process day 8.

As the three replicates show comparable patterns of the VCC over time, the mean of the three replicates is considered for all following process parameters.

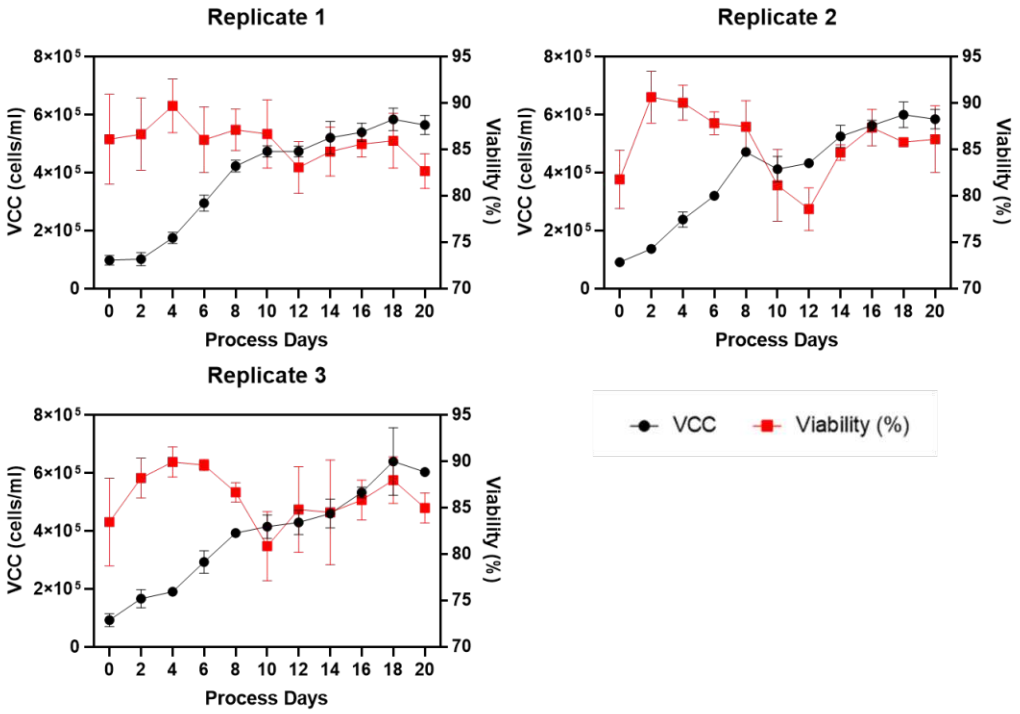

Figure 8: Time-course plots of VCC and viability of the NK-92 culture triplicates. The NK-92 culture sample was centrifuged and the cell pellet was resuspended in 1 ml serum-free SCGM. 20 µl of the cell suspension were used for cell count determination via trypan blue exclusion on a Countess II device in triplicates. Values represent the mean of triplicate measurements and error bars the standard deviation.

Time course plots of the growth rates are depicted in Figure 9. A large difference between the replicates can be observed at the beginning of the process, while the replicates start to match each other after process day 10. From process days 2-8 a higher growth rate can be observed, compared to the subsequent process days. Based on this difference in the growth rate, the process was divided into two process phases, as the different growth behaviour can be an indicator for changes in cell metabolism. To validate if the growth rates in the first and second process phase are significantly different from each other a two-tailed t-test was conducted, comparing all values of the first process phase to those of the second phase, at a significance level of α=0.05. A significant difference was confirmed with a p value of 0.0054.

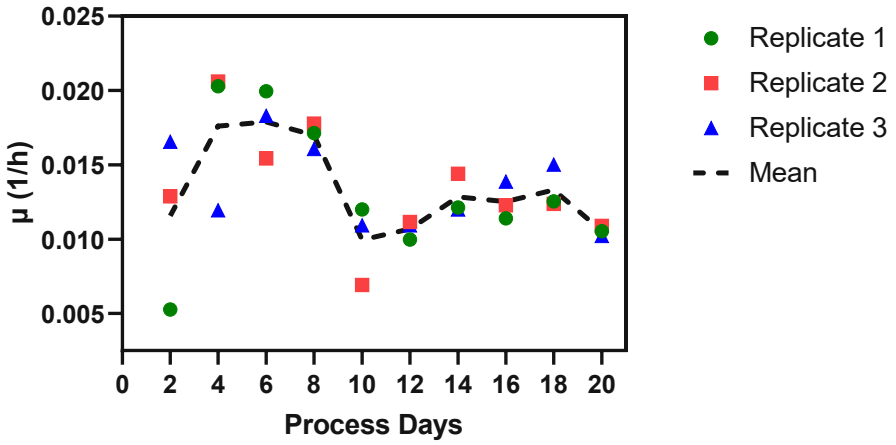

Figure 9: Time-course graph of the growth rate of the NK-92 cultures. The growth rates were calculated from the VCC of the NK-92 cultures using equation 2. Depicted are the mean values of two consecutive process days respectively.

The cell count determination additionally resulted in the acquisition of the average cell size in the measured samples. In Figure 10 it can be observed that the average cell size exhibits a strong increase from process day 0 to 2 from 17 µm to over 19 µm in diameter. From process day 2 to 8 a slight decrease in the average cell size can be observed, followed by a sharp decrease from process day 8 to 10, reaching the lowest values on process day 10 and 12. In the subsequent process days the average cell size rises back to a diameter of 18 µm followed by another drop at the end of the process. A possible reason for the variation of the average cell size is apoptotic volume decrease[59]. AVD could be resulting from osmotic stress, due to accumulation of metabolic byproducts[59]. Also, nutrient limitations or metabolite inhibitions can cause AVD[59]. If apoptotic volume decrease is the main reason for the average cell size variation, a correlation of the average cell size with the viability would be expected. A strong correlation between these two observables (R^2=0.73) was indeed observed over the whole process duration. Thus, the smaller average cell size at process day 0 seems to be a result of inhibitions or limitations, due to less frequent medium exchange and higher cell densities during the NK-92 preculture. The drop in the average cell size at the beginning of the second process phase could therefore also be a result of metabolite limitations or inhibitions. Also, the formation of large cell aggregates, which is favoured by higher cell concentrations, could lead to limited accessibility of nutrients, due to concentration gradients inside of aggregates[60].

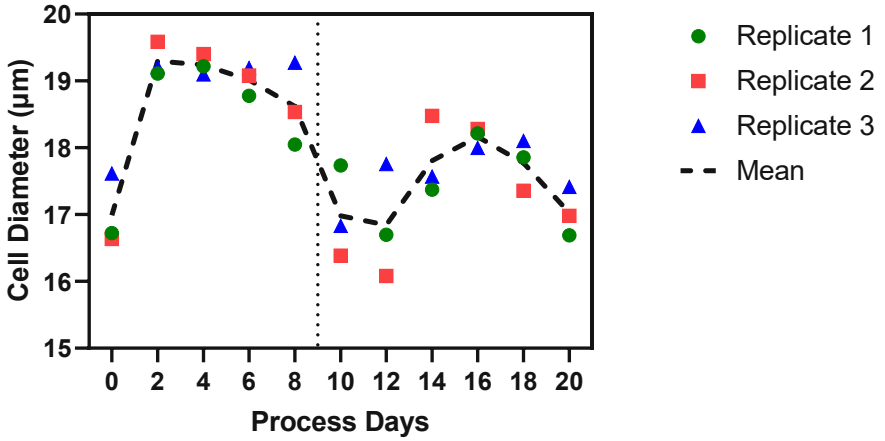

Figure 10: Time-course graph of cell diameter of the NK-92 cultures The average cell diameter is an additional result of the NK-92 cell count determination via the automated cell counting device. The dotted vertical line represents the separation between the two process phases.

3.1.1 pH in the culture supernatant

A time-course plot of the pH measured in the NK-92 culture supernatant is depicted in Figure 11. It can be observed that the pH of the culture continuously decreased from 7.7 to 7.2 over the first process phase, followed by a plateau between 7.3 and 7.4 in the second process phase.

It should be considered that the pH can affect the cell growth and viability of the culture[61] Consequences of too low pH values are endoplasmatic reticulum stress, unfolded protein response and apoptosis[62]. The physiological pH of human plasma is 7.4 and that of serum-free SCGM is 7.2 to 7.5 according to the manufacturer[62]. On the other hand, the pH of tumour microenvironments reaches values ranging from 5.5 to 7.0, which is largely linked to the extensive production of lactate by malignant cells[62]. Moreover, a study showed that the growth of T cells is even three times higher at a pH between 7.0 and 7.2 than at a pH of 7.4[63]. Thus, it can be assumed that the pH in the NK-92 culture did not reach levels, that negatively influenced the growth behaviour.

The main cause for the drop in the pH of cell cultures is the accumulation of acidic byproducts. In the case of malignant cell lines the most common of these byproducts are lactic acid, pyruvic acid, α-ketoglutarate, fumarate[64]. Also, the release of amino acids, such as glutamate and aspartate can contribute to the pH decrease[64]. The release of most of these metabolites was indeed observed, as described in the discussion of the metabolite production rates. The acidic byproduct production also results in the strong correlation between the VCC and pH in the culture (R^2=0.90), as increasing cell numbers lead to a higher release of byproducts. The slower decrease of the pH in the second process phase, indicates a decrease in the release of acidic byproducts. Thus, the metabolism either shifted in favour of aerobic pathways or the overall metabolic activity decelerated in the transition to the second process phase.

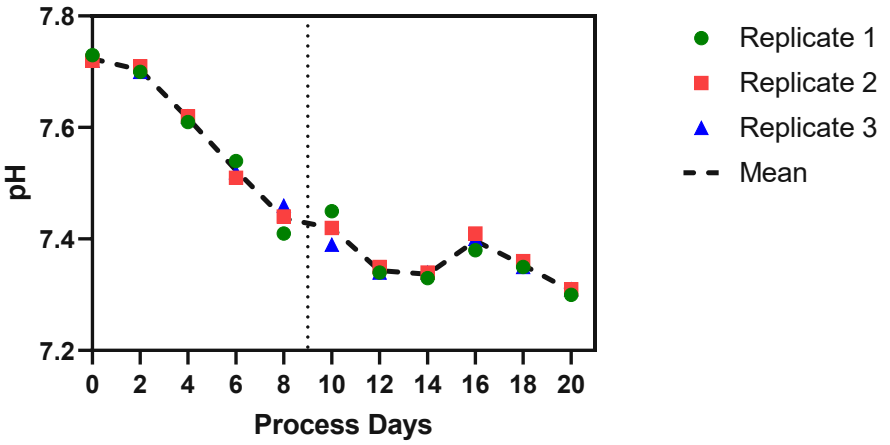

Figure 11: Time-course graph of measured pH in NK-92 culture supernatants The pH of the NK-92 cultures was measured via a pH probe directly from the supernatant of the centrifuged NK-92 culture samples. The dotted vertical line represents the separation between the two process phases.

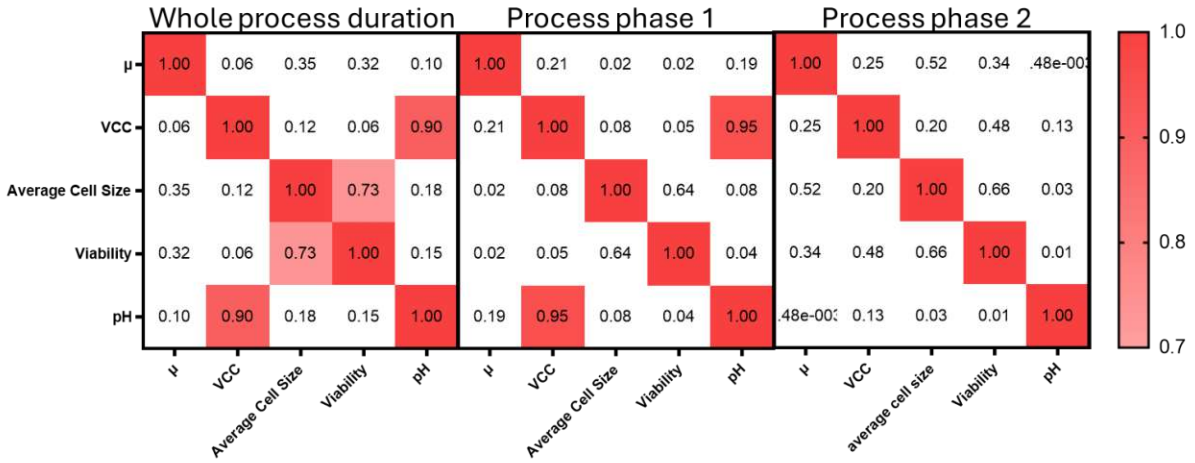

Figure 12: Matrices of R^2-values of the correlation between μ, VCC, average cell size, viability and pH of the NK-92 cultures Depicted are matrices of R^2 values of the correlation of NK-92 culture-related parameters derived from the cell count determination and the pH measurement in the culture supernatants.

3.2 Metabolite tracking of the NK-92 culture

Time course graphs of the concentrations of the amino acids and other metabolites, quantified in the NK-92 culture supernatant, are depicted in figure 13. From these plots it could be derived whether limiting or inhibiting concentrations of certain metabolites reached. Due to the pseudo-static cultivation method the metabolite concentration profiles cannot be directly interpreted, which is why the specific production rate of each metabolite was calculated. The specific production rates are plotted in Figure 14. For a more detailed interpretation of the data, correlations between metabolite concentrations and basic parameters, as well as between the specific production rates and basic parameters were calculated in form of Pearson correlation coefficients. The correlations are summarized in form of matrices of R^2 values in Figure 15 to Figure 20. If the R^2 values are equal or higher 0.7 the correlation is considered as strong correlation. In this section the most important metabolic pathways of the NK-92 cell line will be discussed, based on the process derived data. Subsequently the growth behaviour of the NK-

92 culture will be discussed for each of the two process phases respectively, including potential causes of the change in the growth.

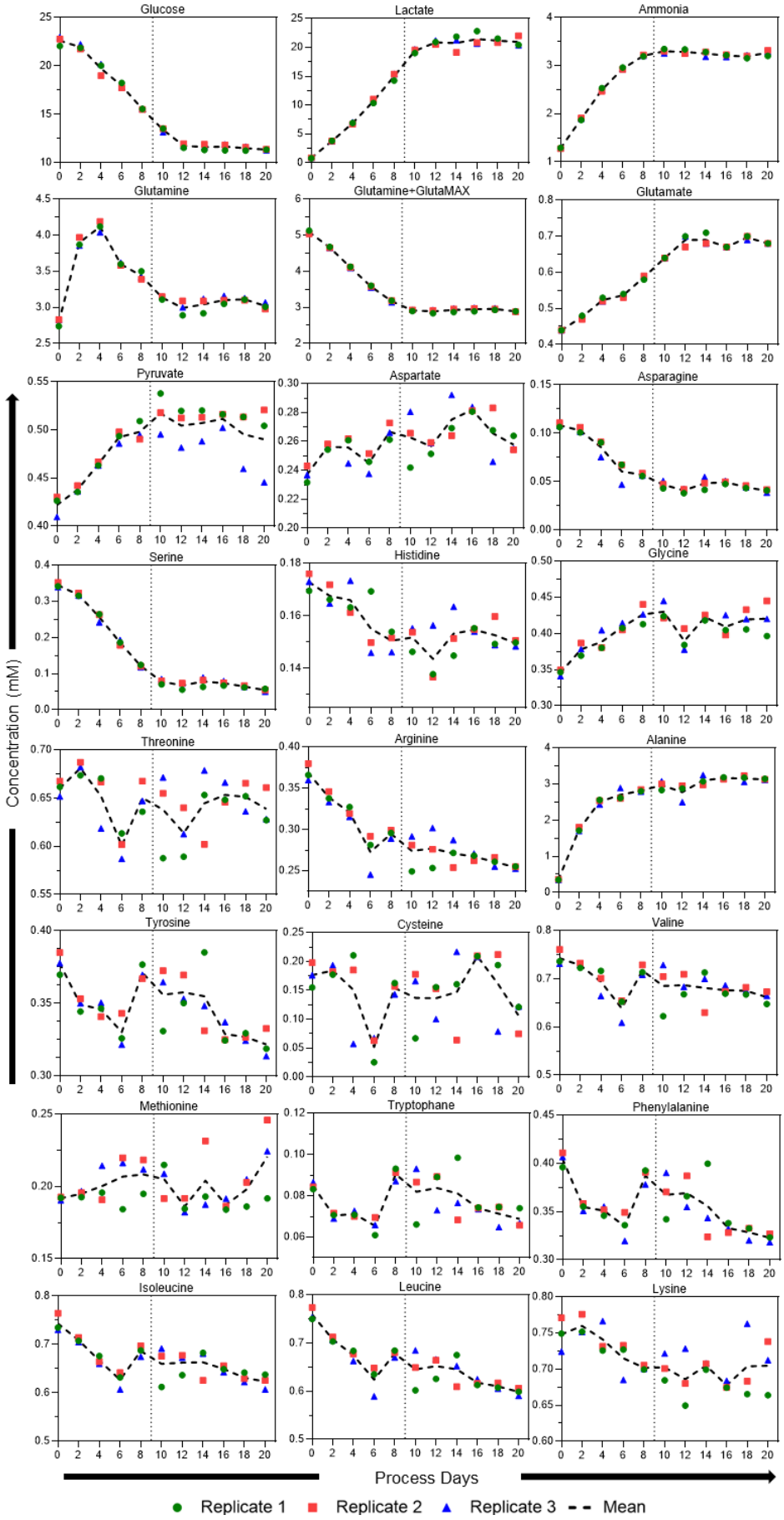

Figure 13: Time course graphs of metabolite concentrations in the NK-92 culture supernatant

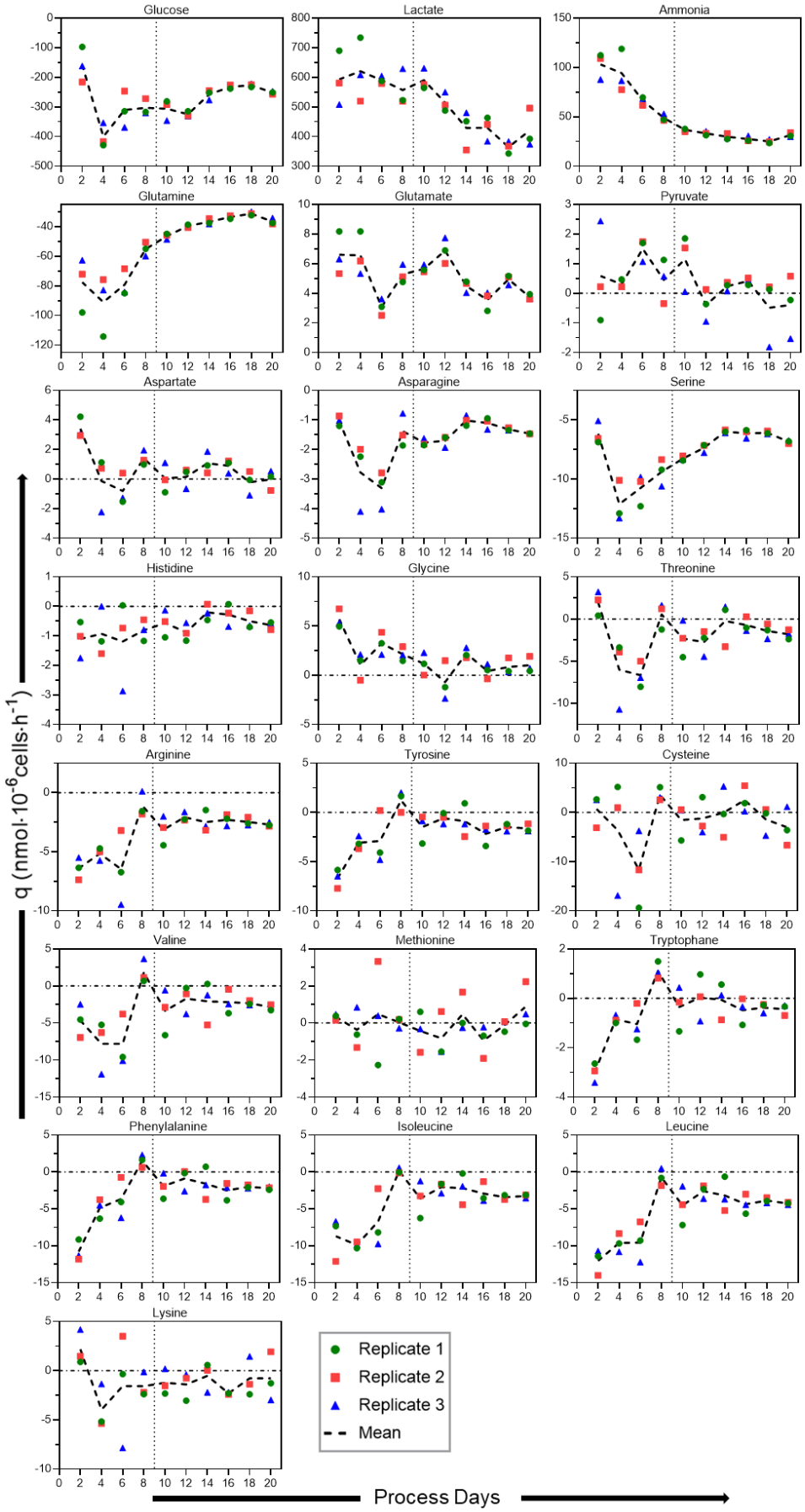

Figure 14: Time course graphs of specific production rates of metabolites in the NK-92 culture supernatant

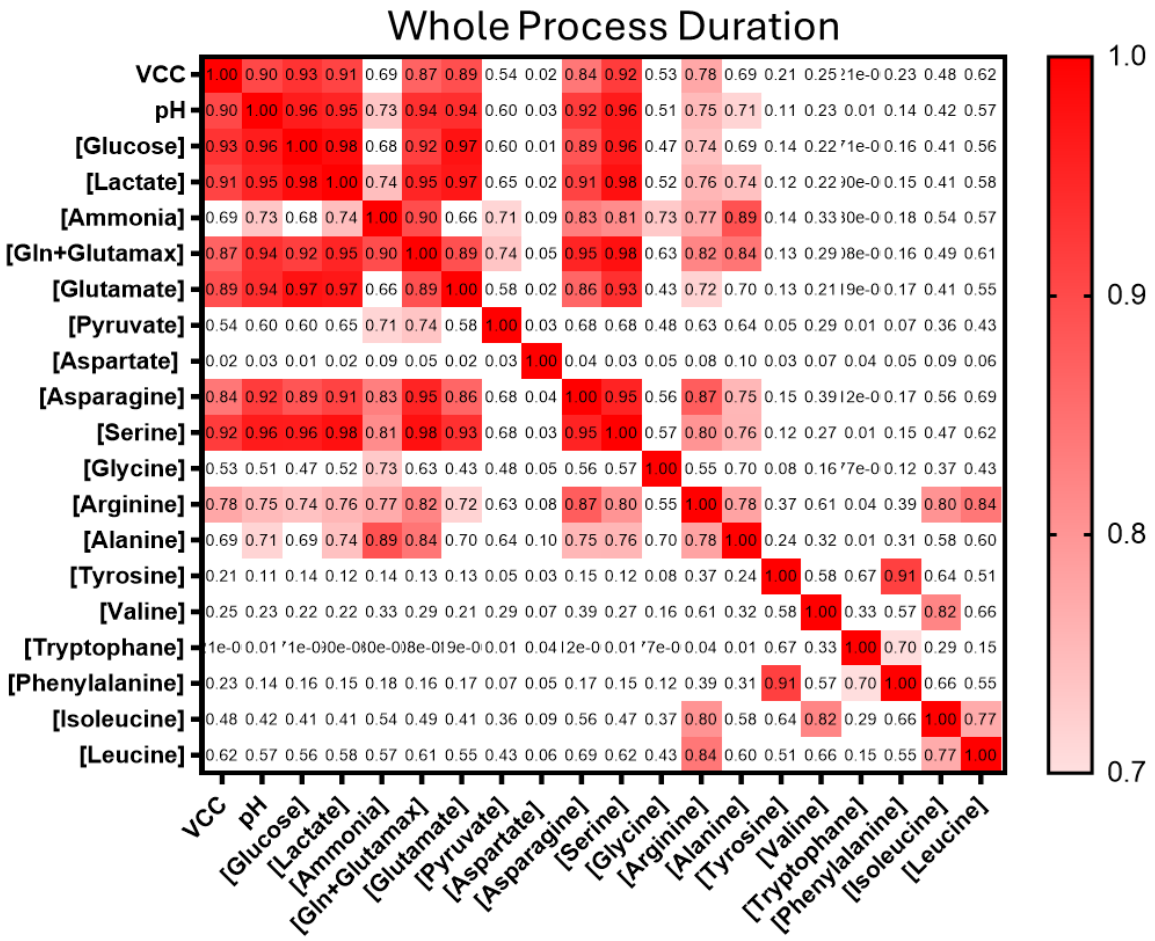

Figure 15: Matrix of R^2 values of the correlations between basic PPs and metabolite concentrations over the whole process duration Exclusively PPs exhibiting strong correlations with other PPs are depicted.

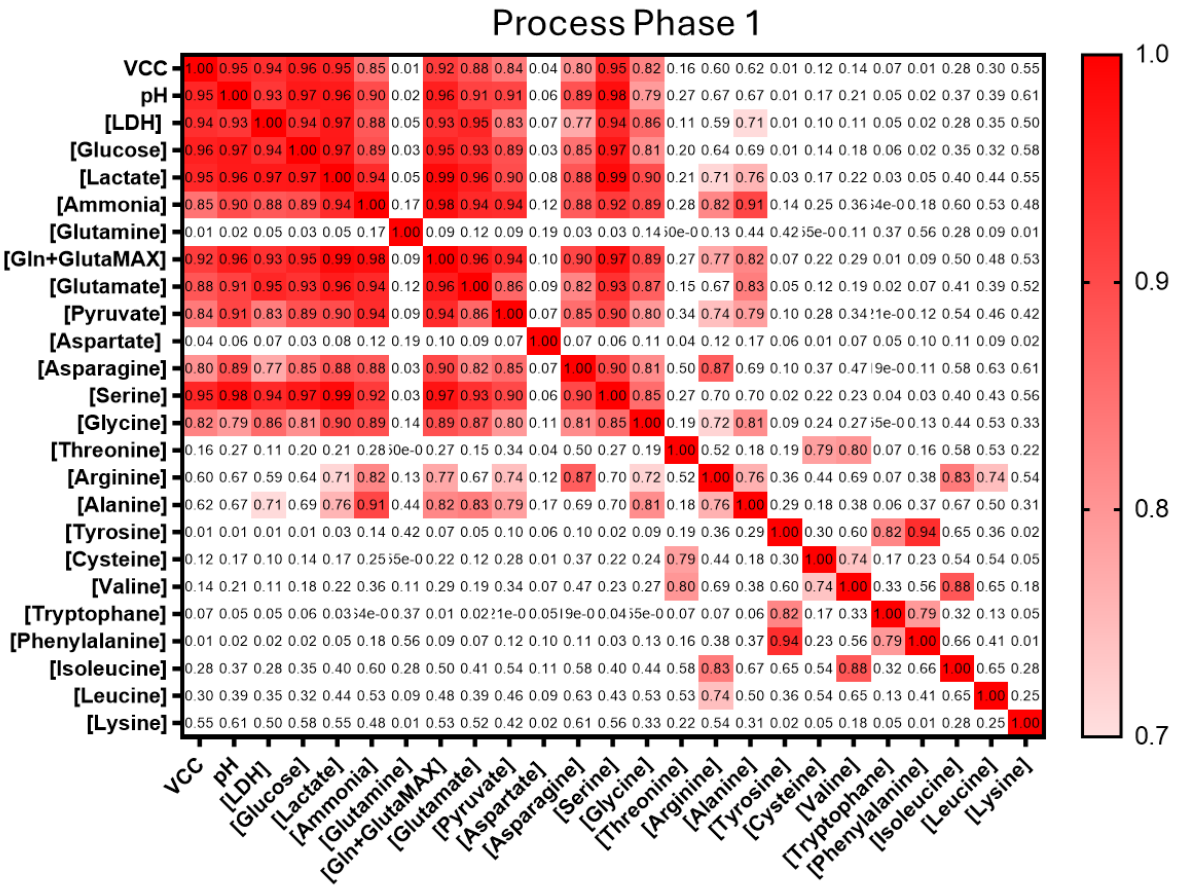

Figure 16: Matrix of R^2 values of the correlations between basic PPs and metabolite concentrations over process phase 1 Exclusively PPs exhibiting strong correlations with other PPs are depicted.

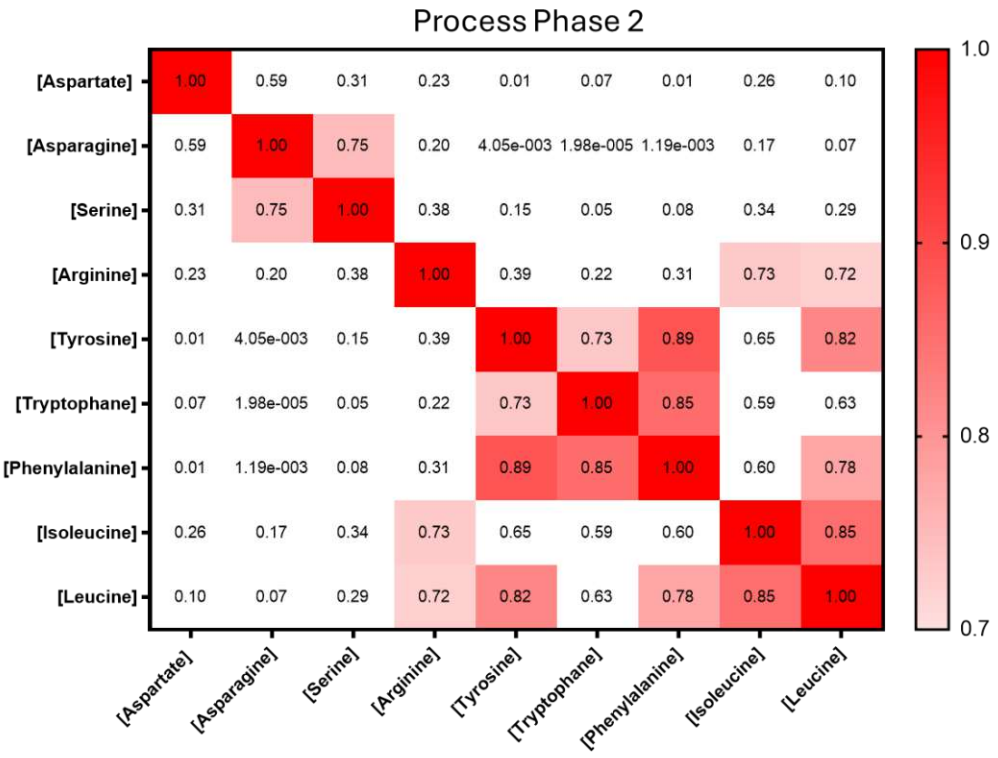

Figure 17: Matrix of R^2 values of the correlations between basic PPs and metabolite concentrations over process phase 2 Exclusively PPs exhibiting strong correlations with other PPs are depicted.

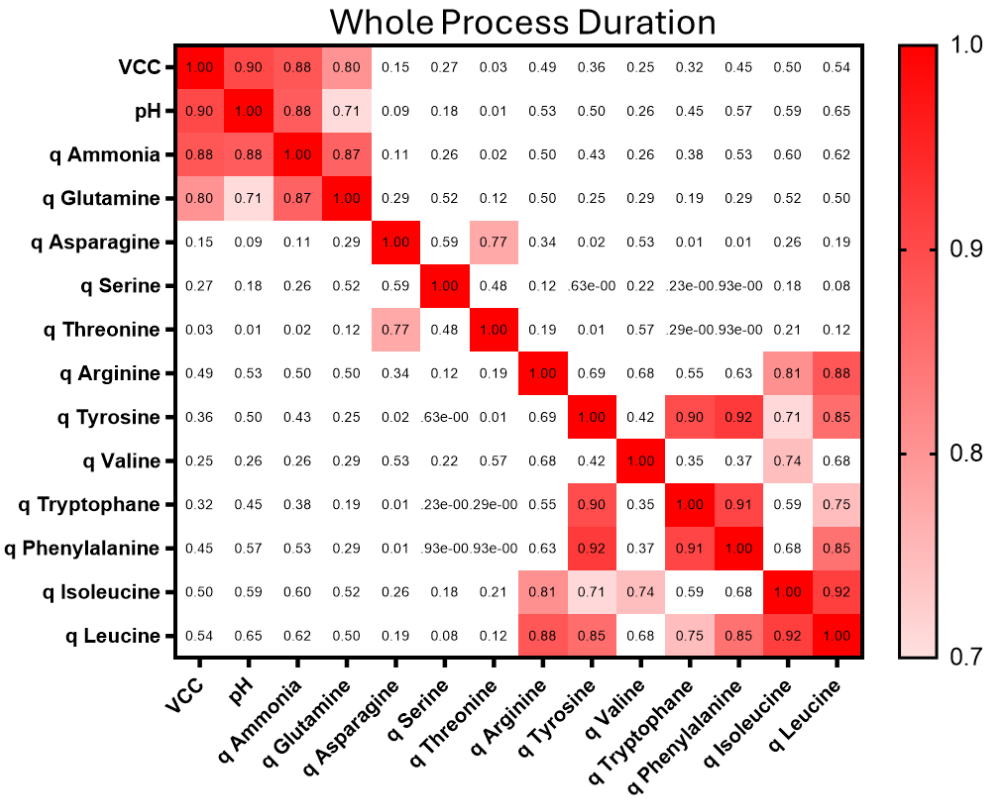

Figure 18: Matrix of R^2 values of the correlations between basic PPs and specific metabolite production rates over the whole process Exclusively PPs exhibiting strong correlations with other PPs are depicted.

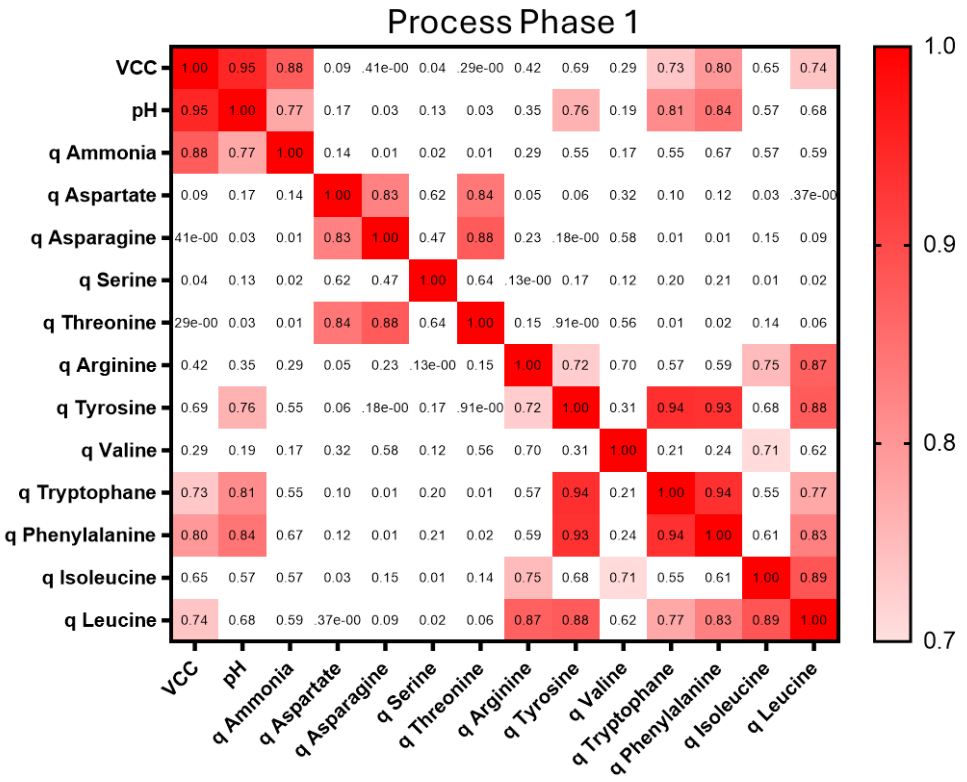

Figure 19: Matrix of R^2 values of the correlations between basic PPs and specific metabolite production rates over proess phase 1 Exclusively PPs exhibiting strong correlations with other PPs are depicted.

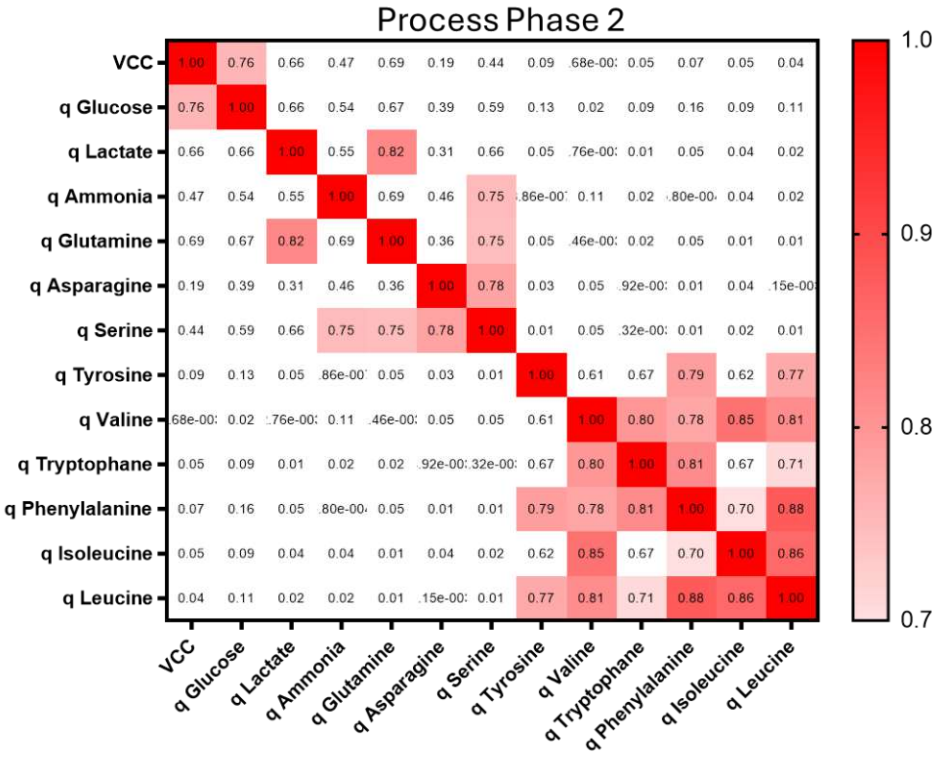

Figure 20: Matrix of R^2 values of the correlations between basic PPs and specific metabolite production rates over proess phase 2 Exclusively PPs exhibiting strong correlations with other PPs are depicted.

3.2.1 The Warburg effect

Since NK-92 is a malignant cell line, considering the Warburg effect (also known as aerobic glycolysis) is necessary. The Warburg effect is a hallmark of cancer, which is characterized by an increased glucose uptake and lactate production of cancer cells, even in the presence of sufficient oxygen[65]. Adenosyl triphosphate (ATP) production via oxidative phosphorylation (OXPHOS), however is not impaired[66]. Rather, the largely increased uptake of glucose enables the simultaneous production of lactate and maintenance of OXPHOS[66]. Thus, the Warburg effect fulfils the requirement of highly proliferative cells for elevated production of both ATP and glycolytic intermediates for biosynthetic pathways[65].

The main metabolic pathways of the Warburg effect are summarized in Figure 21. The produced lactate can be derived from both, glucose and glutamine. Glucose yields pyruvate via glycolysis, which is either transported into the mitochondria to fuel OXPHOS, or it is converted into lactate via LDH[67]. It has been reported that, in the case of primary NK cells, most of the produced pyruvate is converted into cytosolic citrate via the citrate-malate shuttle, fuelling OXPHOS[67, 68]. However, it can be expected that this metabolic pathway of pyruvate conversion into citrate is overshadowed by the high pyruvate production via the Warburg effect, resulting in pyruvate export and lactate production. Glutamine, which is the other major source of lactate, is converted into glutamate via glutaminase, besides its direct use for the synthesis of nucleotides and asparagine[69]. Glutamate is converted into α-ketoglutarate, which is further converted into malate in the TCA cycle[70]. Malate is then decarboxylated via the malate enzyme yielding pyruvate and NADPH[70]. The resulting pyruvate can again be converted into lactate via LDH.

Beyond the described role in lactate production, glutamate can also be converted into other amino acids, such as ornithine arginine and proline[70, 71].

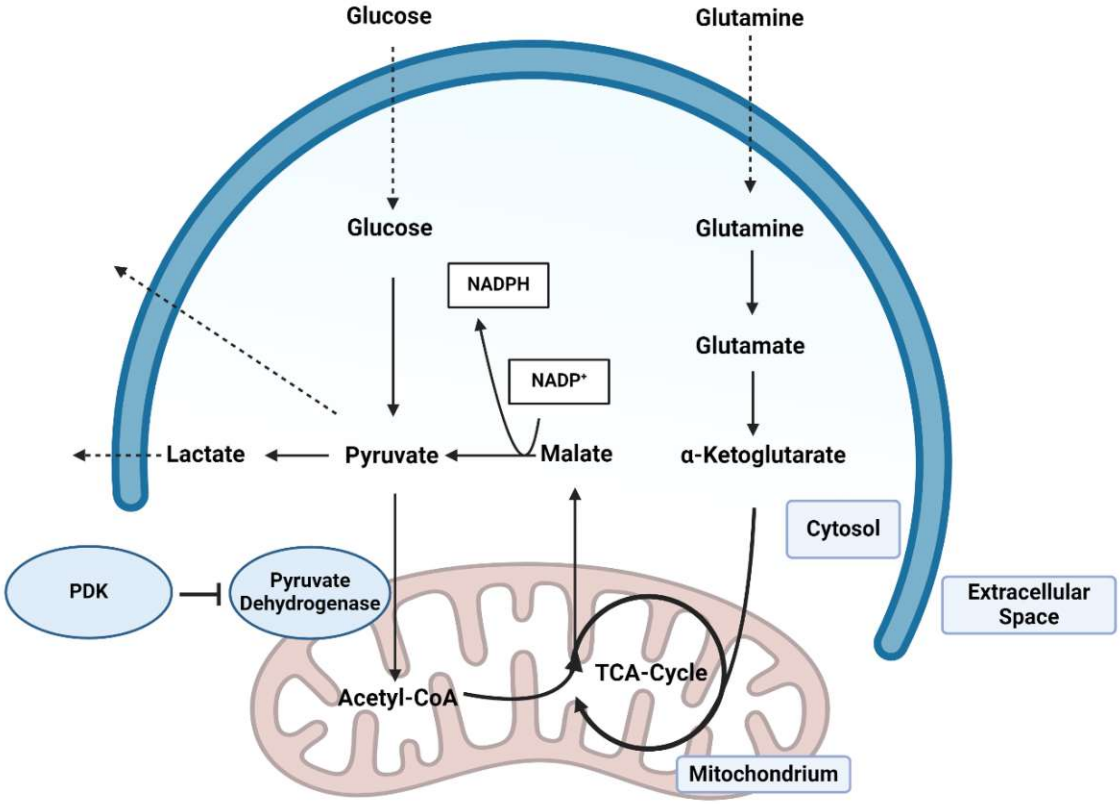

Figure 21: Main metabolic pathways of the Warburg effect The Warburg effect, which is an important feature of most malignant cells, is characterised by the production of lactate, despite the presence of adequate oxygen. Glucose, which is heavily consumed in the Warburg effect is primarily converted into lactate, while the entry of pyruvate into the mitochondria for oxidative phosphorylation (OXPHOS) is decreased by the inhibition of pyruvate dehydrogenase via pyruvate dehydrogenase kinase (PDK). Glutamine can fuel OXPHOS by the entry of α-ketoglutarate into the TCA cycle, and it produces NADPH for anabolic pathways via its conversion into pyruvate. This image was created with BioRender.com and references[65, 66, 69].

The production of lactate was indeed observed in the culture, with a high specific production in the first process phase, which started to decrease in the second process phase. The lactate production was concomitated by a high specific consumption of glucose and glutamine, which were also higher in the first phase of the process compared to the second phase. However, no strong correlation was observed between the specific production rate of lactate and glucose or lactate and glutamine. This was expected, as the catabolic pathways of glucose and glutamine do not exclusively result in lactate production as described above. Also, the production of pyruvate was observed from process days 0 to 10, followed by a low consumption of pyruvate at the end of the process. The release of pyruvate into the medium has already been described in previous studies and matches with the elevated consumption of glucose and glutamine in the

first process phase[72]. From these observations, it can be concluded that the Warburg effect indeed occurred in the metabolism of the NK-92 culture.

A decrease in glucose concentration can be observed during the first phase of the process from an initial concentration of 22.5 mM to 11 mM on process day 12. In the second process phase the concentration exhibits a plateau until the end of the process. As it was shown that NK-92 cells can be grown in media containing 5.5 mM glucose, it can be derived that the levels reached during the expansion process are not in a growth-limiting range[73].

Glucose is converted to pyruvate via glycolysis[67]. The resulting pyruvate can either be converted to lactate via LDH or it is transported into the mitochondria for OXPHOS[67]. However, it was reported that in the case of activated NK cells, most of the produced pyruvate is converted into cytosolic citrate via the citrate-malate shuttle, fuelling OXPHOS[67, 68]. This metabolic pathway of pyruvate conversion to citrate is overshadowed by the high pyruvate production via the Warburg effect, resulting in pyruvate export and lactate production.

3.2.2 Nucleotide synthesis and one-carbon metabolism

An important role of amino acids in strongly proliferating cells, is their use in nucleotide synthesis. Amino acids involved in nucleotide synthesis are glutamine, aspartate, serine, and glycine. Serine and glycine contribute to the nucleotide synthesis by their role in one-carbon metabolism. The one-carbon metabolism includes the tetrahydrofolate- (THF) and the methionine cycle[74]. THF serves as a one-carbon unit acceptor, resulting in formyl-THF, methyl-THF or methylene-THF, which can donate the one-carbon units for the biosynthesis of purine, thymidylate and for methionine recycling[74]. One-carbon metabolism is strongly upregulated in cancer cells, due to their increased on nucleotide synthesis[74, 75].

One of the possible pathways to provide one-carbon units to the THF cycle is the conversion of serine to glycine via serine hydroxymethyltransferase (SHMT)[74]. Low levels of serine in the culture medium have been reported to be accompanied by a decrease of intracellular serine levels and a decrease in cell proliferation for cancer cells.[76].

However, serine can also be newly synthesised from 3-phosphoglycerate (3PG), which is a glycolysis intermediate, and via the conversion of glycine into serine[76]. For serine *de novo* synthesis 3PG is first converted into 3-phosphohydroxypyruvate via phosphoglycerate dehydrogenase (PHGDH), which is further converted into serine in two consecutive steps, including glutamate consumption[76]. The *de novo* synthesis of serine from 3PG is regulated by the availability of serine itself[76]. Serine serves as an activator of the enzyme pyruvate kinase M2 (PKM2), which catalyses the conversion of phosphoenolpyruvate into pyruvate under ATP production[76]. Accordingly, serine deprivation yields in an accumulation of 3PG which favours the *de novo* synthesis of serine[76]. On the other hand, serine inhibits PHGDH activity which also leads to an acceleration in the serine synthesis pathway upon serine deprivation[76].

Serine showed the highest consumption over the whole process after glutamine, reaching a seventh of its' initial concentration. This indicates that the demand for serine exceeded the *de novo* synthesis capacity. A reason for the reliance on serine uptake can be the strong regulation of its' biosynthesis. This regulation might be necessary, as glutamate, which is required for serine synthesis, is also used for energy production via the Warburg effect. The high consumption of serine confirms the upregulation of one-carbon metabolism in the NK-92

process. Also, the strong correlation of the serine concentration with the VCC (R^2=0.92) confirms the important role of serine in nucleotide synthesis.

Glycine can be produced by the conversion of serine to glycine via the reversible SHMT pathway[77]. On the other hand, also glycine itself can contribute to the one-carbon metabolism via the glycine cleavage system, resulting in the conversion of glycine into ammonia and CO_2, while a one-carbon unit is donated to THF and NAD^+ is converted into NADH[77]. However, it has been shown that serine is used predominantly when both serine and glycine are available in the culture medium and that the addition of glycine to the culture medium does not rescue the proliferation, after deprivation of serine and glycine[74]. Too high intracellular glycine to serine concentrations lead to an inhibition of cell proliferation due to the conversion of glycine into serine via the reversible SHMT yielding in a depletion of the one-carbon pool[74].

Accordingly, the production of glycine was observed over the course of the process, which potentially is a result of the regulation of the serine to glycine ratio. The production of glycine from serine again confirms that serine is predominantly fed into the one-carbon metabolism in the NK-92 culture.

Methionine plays an important role in methylation pathways, including DNA- and RNA-methylation as well as the methylation of proteins as posttranslational modification[74]. S-adenosylmethionine, which derives from ATP and methionine, serves as methyl donor in these reactions[74]. After the methyl group transfer, the resulting homocysteine can be recycled back to methionine via the donation of a methyl group from methyl-THF[74]. This links the methionine recycling pathway to one-carbon metabolism and explains the observation that methionine was not constantly consumed over the process[74].

Besides its role as precursor for nucleotide synthesis aspartate is also used for the production of NADPH, via conversion into oxalacetate, followed by the conversion into malate which is oxidised into pyruvate while also producing NADPH[78]. The export of aspartate out of the mitochondrial matrix via the malate-aspartate shuttle is also necessary for the transport of NADH from the cytosol into the mitochondria[78, 79]. Aspartate cannot be derived from asparagine in mammalian cells, but from the transamination of oxalacetate and glutamate via aspartate aminotransferase, which is a part of the malate-aspartate shuttle[78, 80]

Thus, considering that aspartate is necessary for nucleotide synthesis and the lack of its synthesis from asparagine, it seems contradictory that aspartate is rather produced than taken up over the process. However, the production of aspartate can be explained by the high consumption of glutamine, which besides its contribution to the Warburg effect also has an anaplerotic function, due to its conversion to α-ketoglutarate. Therefore, glutamine can function as source to produce oxalacetate, which can be converted into aspartate. This indicates that the lack of aspartate uptake is a result of the high consumption of glutamine.

3.2.3 Essential amino acids

Here, the metabolic pathways of the group of essential amino acids will be summarised and the correlations of their concentrations with those of the other metabolites will be discussed. The group of essential amino acids involves histidine, isoleucine, leucine, lysine, methionine, phenylalanine, threonine tryptophane, and valine[81]. Moreover, arginine is considered as semi-essential amino acid, as it is synthesised in insufficient amounts[81]. Most of the strong correlations were found between the specific production rates of amino acids of this group,

which indicates that their uptake primarily serves protein biosynthesis, as this is their common function.

Over the whole process duration, a strong correlation was observed between the specific rates of the three aromatic amino acids tryptophane, phenylalanine, and tyrosine as well as the rate of leucine. Besides its role in protein synthesis, tryptophane is primarily degraded via the kynurenine pathway[82]. In this pathway tryptophane can be converted into different metabolites with distinct biological activities, including quinolinic acid, which can further be used for *de novo* NAD^+ synthesis[82]. The only metabolic pathway of phenylalanine is the conversion into tyrosine[83]. Tyrosine can be catabolised to fumarate and acetoacetate in five consecutive enzymatic reactions[83]. Thus, these two amino acids are both ketogenic and glucogenic[83].

Strong correlations were also observed between the specific rates of leucine, isoleucine, and arginine. While the prior two are essential amino acids, arginine is considered as semi-essential, which explains its correlations with the essential amino acids, as well as its strong correlation with the VCC over the whole process duration (R^2=0.78). The role of arginine as semi-essential amino acid is further corroborated by previous studies showing that low arginine concentrations lead to a decrease in NK-92 cell line proliferation, viability, and cytotoxic activity[84]. However the lowest concentrations reached 0.25 mM, which is higher than the reported threshold of 0,029 mM where negative effects on cell proliferation could be observed[84]. Besides the role as semi-essential amino acid, arginine also takes part in the cytotoxic activity of NK cells. NK cells are capable of NO production via the citrulline-NO cycle, where arginine is converted into NO via inducible nitric oxygen synthase (NOS) and endothelial NOS[85]. NO not only serves as an important key signalling molecule, but also takes part in NK cell mediated target cell lysis[85, 86]. Argininosuccinate synthase and argininosuccinate lyase convert the resulting citrulline into arginine, which ensures a continuous supply with NO for host defence[86]. Therefore, NK cell cytotoxic activity is suppressed under arginine deprivation[87]. This is for example observed in tumour microenvironments, where elevated arginase levels lead to decreased arginine availability[87]. On the other hand arginine can also be converted into ornithine via arginase, which can further be used by ornithine decarboxylase to form polyamines, required for cell proliferation[88]. In addition, arginine is also metabolically interconvertible into glutamate and proline[89].

The specific production rates of threonine and asparagine also show a strong correlation. While asparagine is a non-essential amino acid, it is the only amino acid that requires glutamine for its de novo synthesis[80]. Its synthesis involves the conversion of glutamine to asparagine via asparagine synthetase[80]. This implies that asparagine synthesis happens at the expense of anabolic pathways[80]. Thus, the predominant use of glutamine for energy production, nucleotide synthesis, and other anabolic pathways could explain the correlation of the specific rates of asparagine and the essential amino acid threonine. Moreover, asparagine cannot be converted into aspartate in mammalian cells[90]. Thus, asparagine does not have an anaplerotic function, and is predominantly taken up for proteins synthesis.

3.2.4 mTORC1 activation and upregulation of cMyc expression

To keep up the high glycolytic activity for the Warburg effect and high cell proliferation, activation of the mammalian target of rapamycin complex 1 (mTORC1) as well as the expression of cMyc are necessary[91, 92]. mTORC1 is a serine/threonine kinase that regulates aerobic glycolysis and cell growth and promotes lipid synthesis as well as protein synthesis via regulation of mRNA translation and ribosomal protein levels[91, 93]. mTORC1 is also necessary

for the initial activation of cMYC production[92]. Moreover, mTORC1-dependent elevated glycolytic activity is essential for NK cell effector function[94]. mTORC1 is activated by the presence of glucose and certain amino acids, such as serine, arginine, and the group of branched chain amino acids (BCAA)[91]. cMyc is a transcription factor, that also regulates the glycolytic activity of activated NK cells.[92]. In NK cells, the expression of cMyc is dependent on the availability of glutamine[92]. The role of each amino acid involved in mTORC1 activation and promotion of cMyc expression is summarised below and schematically depicted in Figure 22.

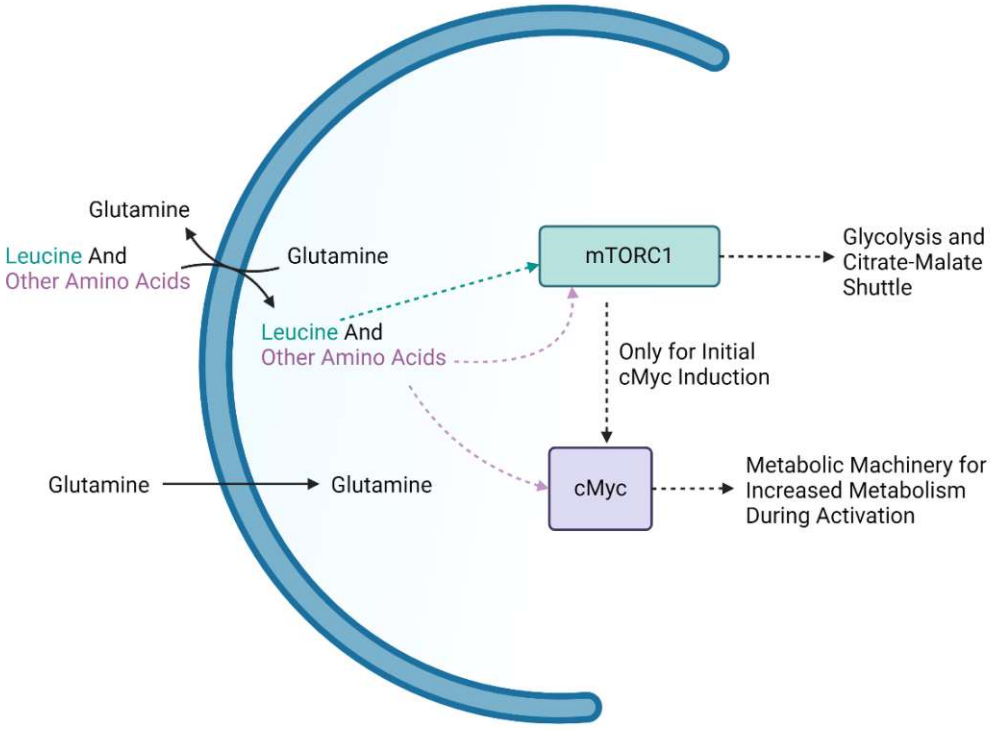

Figure 22: Summary of mTORC1 activation and cMyc induction in NK cells. Depicted is the amino acid dependent activation of mTORC1 and the induction of cMyc. mTORC1 is a protein complex, which is required for the induction of elevated glycolysis upon cytokine stimulation. cMyc is a transcription factor, that controls the metabolic machinery for increased metabolic function during NK cell activation. Apart from its' catabolic functions, glutamine can be transported out of the cell in exchange for other amino acids via the SLC7A5 amino acid transporter, which is an obligate antiporter. Some amino acids, such as leucine, arginine, tryptophane and phenylalanine were shown to be mTORC1 activators. Amino acid transport through SLC7A5 is also essential for the induction of cMyc protein expression. Dashed arrows indicate activation or induction, and continuous arrows indicate transport. The image was created with BioRender.com and references[68, 92, 95].

Serine, arginine and the group of BCAA, involving leucine, isoleucine, and valine directly contribute to the activation of mTORC1. For the import of leucine, which is the strongest mTORC1 activator, glutamine is used as an amino acid exchange factor[95]. First glutamine is taken up via the glutamine transporter SLC1A5[95]. In the next step a complex of SLC7A5 and SLC3A2, exchanges intracellular glutamine with extracellular leucine[95]. The group of branched chain amino acids share a common degradation step via cytosolic branched chain aminotransferase (BCATc)[96]. BCATc activity therefore serves as a regulator of intracellular BCAA concentrations thus controlling the availability of BCAA for mTORC1 signalling[97].

Also asparagine plays an important role as amino acid exchange factor, similar to the role of glutamine[80]. Asparagine is taken up for the exchange with other amino acids, including serine and arginine, which are necessary for mTORC1 activation[80]. Thus, the strong correlation between the VCC and the concentration of asparagine over the whole process duration (R^2=0.84) can be a result of its uptake for protein synthesis or for maintenance of intracellular asparagine concentrations for amino acid exchange.

The transport of amino acids via the L-amino acid transporter SLC7A5 is necessary for the expression of cMYC[68]. SLC7A5 is an obligatory antiporter which mainly exports glutamine and imports other amino acids into the cell[92]. Therefore, the availability of glutamine is necessary for the upregulation of glycolysis in NK cells[92].

3.2.5 NK-92 metabolism over the first process phase

The first process phase is characterized by a higher cell proliferation, compared to the second phase. Accordingly, the specific rates of the essential amino acids show a higher uptake during the first process phase. Also, the consumption of glutamine and glucose, as well as the production of lactate was higher in the first process phase than in the second phase. Over the first process phase, the concentrations of glycine and pyruvate exhibit a strong correlation with the VCC, while this was not observed for the whole process duration. The strong correlation of the concentration of glycine with the VCC (R^2=0.82) seems to be a consequence of the elevated cell proliferation. Highly proliferating cells exhibit a higher demand for intermediates of nucleotide synthesis. Serine meets this need by contribution of one-carbon units for nucleotide synthesis. This results in the production of glycine, which is exported out of the cell to maintain favourable serine to glycine ratios for serine conversion via SHMT. The correlation of the VCC with the pyruvate concentration (R^2=0.82), can be explained by the Warburg effect. The elevated demand of highly proliferating cells for glycolytic intermediates and NADPH, deriving from glutamine conversion into pyruvate, leads to excess intracellular pyruvate. The export of pyruvate is in part achieved by inhibition of pyruvate dehydrogenase function via pyruvate dehydrogenase kinase (PDK), limiting the entrance of pyruvate into the TCA cycle. The expression of PDK is elevated in cells exhibiting the Warburg effect[98]. It can be concluded that the higher proliferation in the first process phase is predominantly fuelled by the Warburg effect.

3.2.6 NK-92 metabolism over the second process phase and causes of the change in growth

The second process phase is characterized by a slower cell proliferation. This explains the lack of correlations between the VCC and the metabolite concentrations in the second process phase, as this seems to be a result of a lack in variability of those PPs. Also, in the second process phase most of the strong correlations can be observed among the group of essential amino acids. However, in contrast to the first process phase, no strong correlations were found for the specific rates of arginine and threonine with those of other amino acids. The loss of the strong correlation the rate of arginine with other amino acids could be a result of the continuous uptake of arginine for NO production.

The specific production rates of lactate and glutamine show a strong correlation over the second process phase. This correlation was not observed over the first process phase, indicating that the lactate production from glutamine was overshadowed by glucose-derived lactate in the first process phase. Thus, it can be derived that the Warburg effect was more pronounced during the first process phase.

Also, a strong correlation of the specific production rate of serine with glutamine and ammonia was, observed over the second process phase. As serine plays an important role in one-carbon metabolism, this correlation could be an indication that energy production via glutamine uptake is largely related to the production of one-carbon metabolism dependent products, such as purines, pyrimidines, and S-adenosylmethionine during the second process phase. The absence of this correlation in the first process phase indicates that the higher uptake of glutamine in the first process phase suffices to also fuel other anabolic pathways than the one-carbon metabolism. Another potential explanation is a more pronounced use of glutamine as to provide anabolic precursors via the TCA cycle.

Possible causes for the change in the growth behaviour are the accumulation of ammonia and lactate in the culture medium. An ammonia concentration of 2-3 mM has been reported to lead to lower cell growth and lower final cell concentrations, as well as to changes in metabolic rates in mammalian cell line cultures[99]. The cytotoxic activity of NK cells is also suppressed at ammonia concentrations of 2 to 3 mM[100]. Furthermore, it was shown that elevated concentrations of lactate (>12 mM) lead to an amplification of the growth inhibiting effect of ammonia[101]. One source of ammonia in the culture medium is the spontaneous decomposition of glutamine into pyrrolidonecarboxylic acid and ammonia, which was also observed in the stability flasks[102]. The other major source of ammonia is the conversion of glutamine to glutamate and ammonia by the cells[101]. The glutamine concentration showed an increase in the first process phase, reaching a local maximum at 4 mM on process day 4, followed by a decline to 3 mM. The peak in glutamine concentration is caused by the release of peptidase into the culture medium, leading to the hydrolysis of the alanine-glutamine dipeptide GlutaMAX, which also resulted in a peak in the alanine concentration[103]. The strong correlation between the VCC and the concentration of glutamine+GlutaMAX over the whole process duration (R^2=0.87) indicates that an increase in cell numbers also leads to an increase in peptidase release, resulting in increased GlutaMAX hydrolysation. The increase in GlutaMAX hydrolysation with increasing cell numbers also explains the correlation between the VCC and the concentration of ammonia over the whole process (R^2=0.89), as elevated glutamine concentrations lead to higher ammonia production. In the process, the critical ammonia concentration of 2 to 3 mM was already reached between process days 2 and 4. A high lactate concentration (15 mM), which was already reached between process days 6 and 8, results in impaired cytotoxicity of NK cells and in decreased expression of perforin and granzyme[104]. It also leads to the accumulation of reactive oxygen species in the mitochondria due to intracellular acidification, resulting in mitochondrial dysfunction and apoptosis[68, 105].

Since the specific rates of glucose, glutamine and most of the essential amino acids, show decrease in their uptake between process days 4 to 8, the decrease in metabolic activity could be a result of the inhibitory effects of ammonia and lactate. Furthermore, it was reported that already small decreases in the pH value (7.2 to 7.0) of the culture medium lead to a decline in mitochondrial activity.[106] However, the pH of the culture medium did not drop below a value of 7.3.

Another possible reason for the decrease in growth, could be the seeding cell density.[107] As the preculture was kept at cell densities between $0.7x10^6$ and $1x10^6$ viable cells/ml, which is significantly higher than the initial cell density of $1x10^5$ viable cells/ml for the process, it is possible that the decrease in growth was a consequence of an adaptation of the culture to this change of conditions. The delay of the response can be explained by the average doubling time of 67 h during the process. It is claimed that NK cells are capable of activating each other via

trans presentation of IL2[108]. Therefore, a potential reason for a deficient growth at lower cell densities could be that less cell to cell contact leads to a decrease of trans-activation. However, no recovery of the cell growth was observed at higher cell densities in the second process phase. A reason for this finding could be that beneficial effects of higher cell densities were masked by the inhibitory effects of elevated ammonia and lactate concentrations.

To sum up, an important role of serine in sustaining elevated cell proliferation was observed. This is primarily due to its contribution to one-carbon metabolism, which was corroborated by the production of glycine. Also, glutamine was identified as an important source to fuel OXPHOS and NADPH production for anabolic pathways. However, the high glutamine concentrations were simultaneously shown to be the main source of ammonia, which reached inhibiting concentrations during the process. Thus, the data presented in this thesis hint at future strategies for improvement of NK-92 expansion processes. An adaptation of the concentration of serine and glutamine in the cell culture medium could lead to more stable growth rates. However, it should be considered that reduced glutamine concentrations could make a supplementation with asparagine necessary, as asparagine is exclusively synthesised from glutamine. This was also observed in the second process phase, as the production rates of serine and asparagine showed a strong correlation (R^2=0.78) at lower glutamine levels. Moreover, the inhibiting effects of ammonia and lactate on NK-92 proliferation reveal the importance of monitoring of their concentrations during expansion processes. The continuous production of lactate and ammonia, additionally indicate the necessity of constant media renewal for sustained high proliferation.

3.3 Comparison of cytotoxicity measurement methods

For an accurate interpretation of the cytotoxicity measurement results it needs to be considered that K-562 cells do not express the Fas receptor[13]. Thus K-562 cells are not killed via the FasL-dependent pathway in these assays, which allows an easier interpretation of cytotoxicity results due to a reduction of available killing pathways[13].

In this section the three cytotoxicity assays performed in this thesis will be analysed and disadvantages and prerequisites of each method will be discussed in detail. Additionally, the results of the assays will be compared via t-tests and by testing for correlations and reasons for the differences will be investigated, as this could provide an objective basis for cytotoxicity measurement method decisions in future experiments[31, 109]. Previous studies have already shown discrepancies between the results of different cytotoxicity assays. An example is the comparison of the LDH- and the calcein assay using KHYG-1 cells as effector cells and Raji cells as target cells, resulting in a 20% higher cytotoxicity for the calcein release assay[110]. Another example is a study by Wong et al. comparing a FCM and the chromium release assay, showing an E:T ratio-dependent difference between the assays[111]. However, the three assays performed in this thesis have not been compared directly let alone in a time resolved set up.

Time-course plots of the results of each cytotoxicity measurement method are depicted in Figure 23. The cytotoxicity showed a variation over time for all three methods. Previous studies have already shown that NK cell function is dependent on the cell metabolism[92]. However, also other factors than changes in the metabolism of the effector cells could have had an additional influence on the variations in the cytotoxicity. For instance the cell density of the target cell culture, which is used for the co-culture has a severe influence on the cytotoxicity[112]. Therefore, it was tried to maintain the K-562 cultures at consistent cell densities throughout the whole

experiment duration. However, the viable cell concentration of the K-562 cultures still showed slight variations over the process, which could have contributed to the variations.

For the LDH release method the cytotoxicity values representing an effector to target ratio of 1:1 only show small variations over time, with an average value of 7.8%. The highest cytotoxicity values for the 1:1 E:T ratio are reached on process days 14-16. The cytotoxicity values representing an E:T ratio of 5:1 range from 12 to 35% and show a similar pattern to those of the 1:1 ratio, except for the value at process day 8.

For the calcein release method the cytotoxicity values of the 1:1 E:T ratio exhibit an average value of 14,38% with the highest values at the beginning of the process and levelling off after process day 4 slightly below 10% until an increase to over 20% can be observed on process day 14, followed by another decrease until process day 18 and an upward trend from process day 18-20. The cytotoxicity values of the 5:1 ratio show the same pattern as those of the 1:1 ratio, with an average of 5% higher values than the 1:1 ratio. The calcein release method exhibits the lowest difference between the cytotoxicity of the two E:T ratios of the three methods.

For the 1:1 E:T ratio the cytotoxicity determined via FCM exhibits a drop from 23% on process day 0 to 0% on process day 6 and stays between 0 and 10% until the end of the process. For the 5:1 E:T ratio the cytotoxicity exhibits an increase from 13 to 31% from process day 10 to 12 and stays between 27 and 41% until the end of the process.

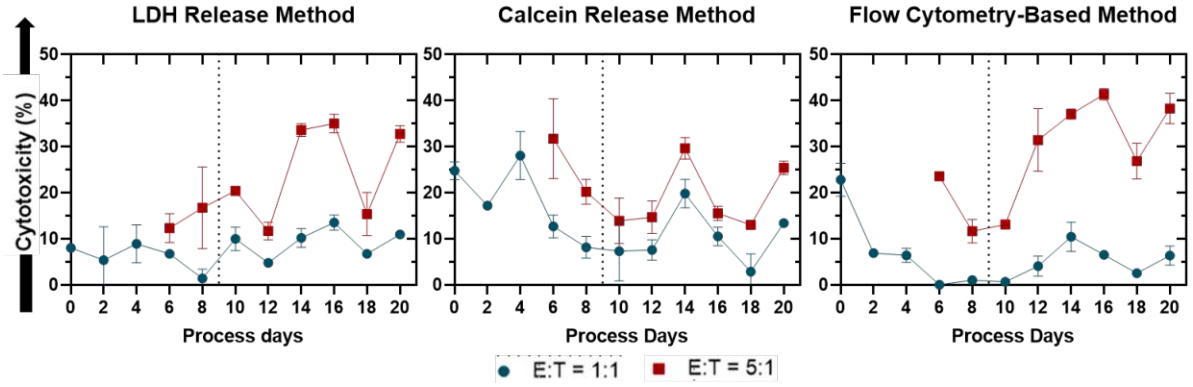

Figure 23: Time-course graphs of cytotoxicity results of each method NK-92 cells deriving from the NK-92 culture samples and K-562 cells from the K-562 culture samples were used for seeding of co-cultures and controls in 96 well conical (V) bottom plates. The co-cultures were performed under serum free conditions at E:T ratios of 1:1 and 5:1 at 37 °C for4 h in a humidified incubator. After the incubation time was finished, the plates were centrifuged (300 g, 5 min) and the supernatants were used for fluorescence measurement for the calcein assay and subsequent determination of the volumetric LDH activity. The cells were stained with fluorescent labelled antibodies and analysed via flow cytometry. Error bars indicate the standard deviation between the biological triplicates of NK-92 cultures. Vertical dotted lines indicate the separation between the two process phases.

While the LDH- and calcein release methods are based on the release of molecules from lysed cells, the FCM relies on the staining of lysed cells with an amine reactive dye. Accordingly, in the FCM dead cells can directly be identified, while in the release assays the proportion of dead target cells is represented by the fraction of released signal molecules to the maximum release.

The two release assays exhibit the problem that the spontaneous release of substances is cell density dependent, resulting in a higher spontaneous release in the co-culture wells than in the controls[110]. This error potentially occurs for the spontaneous release of LDH from the effector,

as well as the target cells. In contrast, the calcein release assay cannot be influenced by the spontaneous release from effector cells, as only target cells are labelled. Another difference between the LDH and calcein release method is that the LDH release assay can be influenced by variabilities in LDH expression of both the effector and target cells, which could influence the spontaneous release of LDH. However, the manual labelling step is a possible source of inconsistency in the calcein release assay.

A disadvantage of the LDH release assay is that the volumetric LDH activity in the K-562 control wells was below the detection limit of the used enzymatic assay at the applied cell numbers of $6.6x10^4$ target cells per well. To circumvent this issue, a well containing $6.6x10^5$ K-562 cells was seeded. The relative fluorescence of the K-562 control was assumed to be a tenth of the 10x K-562 well. However, this introduces an error in the cytotoxicity value since the LDH release is cell density dependent, leading to an overestimation of the cytotoxicity.

The correlations between the results of the cytotoxicity measurements are summarised in form of R^2-values in Figure 24. It can be observed that, at the 1:1 E:T ratio, the calcein- and LDH release methods show a strong correlation (R^2=0.77) during the first phase of the process, whereas the calcein release method and FCM exhibit a strong correlation in the second process phase (R^2=0.80).

A paired t-test was carried out for each combination of the methods with the null hypothesis that there is no significant difference between the means of the two methods at a level of significance of α=0.05. As a normal distribution of the difference of the cytotoxicity values of the two compared groups is a prerequisite to carry out a paired t-test, the normal distribution of the differences was tested with the Shapiro-Wilk test at a level of significance of α=0.05.

The results of the paired t-tests are summarised in Figure 25. It can be observed that the difference between the means of the cytotoxicity values of the LDH and calcein release assay as well as that of the calcein release assay and the FCM is significant at a 1:1 E:T ratio, while there is no significant difference between the means of the LDH and FACS method for the 1:1 ratio. For the 5:1 E:T ratio there is no significant difference of the means of the cytotoxicity values between any of the three methods.

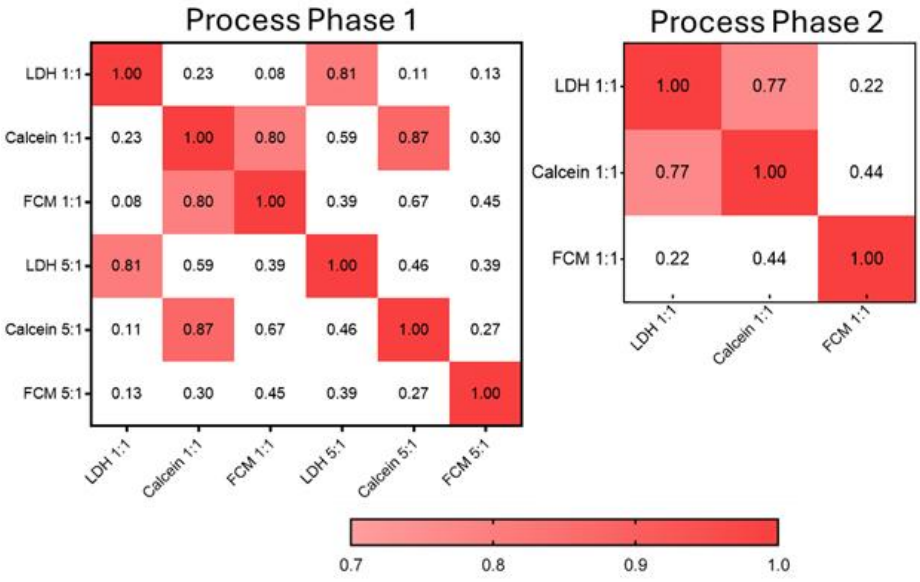

Figure 24: Matrix of R^2 values of the correlations between the cytotoxicity results Correlations over the whole process phase are not depicted as no strong correlations ($R^2 \geq 0.7$) were found.

The comparison via paired t-tests showed that the results of the calcein release assay are significantly higher than for the other two methods at an E:T ratio of 1:1. A possible reason for the overestimation of the cytotoxicity via calcein release compared to the other two methods could be the dependency of the spontaneous calcein release on the cell density. Another possible reason for the higher values of the calcein release method could be the automated gain setting of the fluorescence intensity measurement. When automated gain setting is applied, the plate reader performs a pre-scan of the wells involved in the measurement and identifies the well with the highest fluorescence intensity. The gain is then adjusted so that this well is at the upper limit of the dynamic range. As the 10x K-562 well was included into the fluorescence measurement, the automated gain was set assuming the 10x K-562 well to be at 100% of the target value. However, the relative fluorescence of the 10x K-562 well was always higher than that of the Triton lysed well (positive control). Thus, it is possible that the detector sensitivity was lower for the wells of interest due to the lower gain. This would also explain the small difference between the two E:T ratios for the calcein release assay. To determine if this was the case it would have been necessary to repeat the fluorescence measurement at different gain settings followed by evaluation of the influence of the gain setting on the cytotoxicity values.

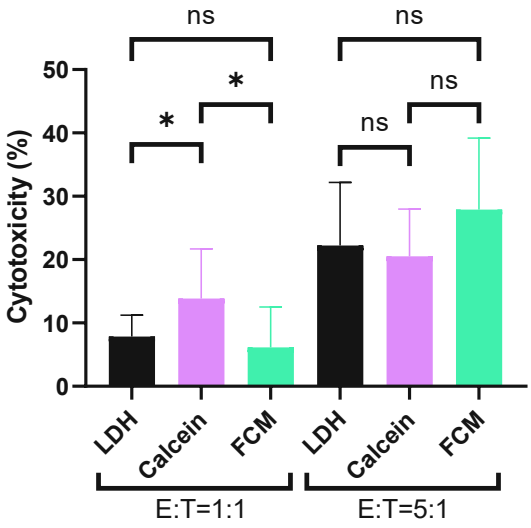

Figure 25: Graphic summary of results of paired t-tests comparing the mean of the results of the methods at a level of significance of α=0.05 To compare the results of cytotoxicity measurement of the three methods, paired t-tests at a level of significance of α=0.05 were performed. ns indicates that no significant difference was identified between the results of the methods and asterisk indicates that a significant difference was identified (P<0.05). Columns indicate the mean cytotoxicity of a method over all process days and error bars indicate the according standard deviation.

To sum up, even if the cytotoxicity values derived from different measurement methods seem to match at a certain measurement time point, a time-resolved consideration reveals that the above-described inherent differences between the three methods still lead to differences in the cytotoxicity profile over time. Thus, the results of cytotoxicity measurements derived from different methods cannot be compared to each other. Additionally, even if the same cytotoxicity determination method was used in the compared experiments, variations in parameters such as the incubation time of the co-culture, the E:T ratio, cell concentrations and the presence/absence of serum and interleukins need fall into consideration. This emphasizes the need for a standard cytotoxicity determination method.

3.4 Analysis of dead target cells via FCM

The applied gating strategy for the cytotoxicity determination via FCM, allows to simultaneously track the proportion of events in each category of cell death, which are necrotic, late apoptotic, and early apoptotic. Thus, the proportion of each cell death category within in the dead target cells in the co-culture was analysed, to monitor changes over time.

In Figure 26 the proportion of necrotic, late apoptotic, and early apoptotic cells within the population of dead target cells is depicted over the process time. For the 1:1 ratio, it can be observed that throughout the whole process duration, with exceptions on process days 0 and 10, necrotic cells (23-72%) represent the largest of the three categories, followed by late apoptotic (24-66%) and early apoptotic cells (3-28%). Over the first process phase the three populations show only small variations. In the second process phase a continuous increase of the proportion of necrotic cells and a decrease in the proportion of late and early apoptotic cells can be observed. The 5:1 ratio shows the same order and profile over time, with a higher difference of the proportion of necrotic (40-90%) to both late apoptotic (10-36%) and early apoptotic (1-23%) events.

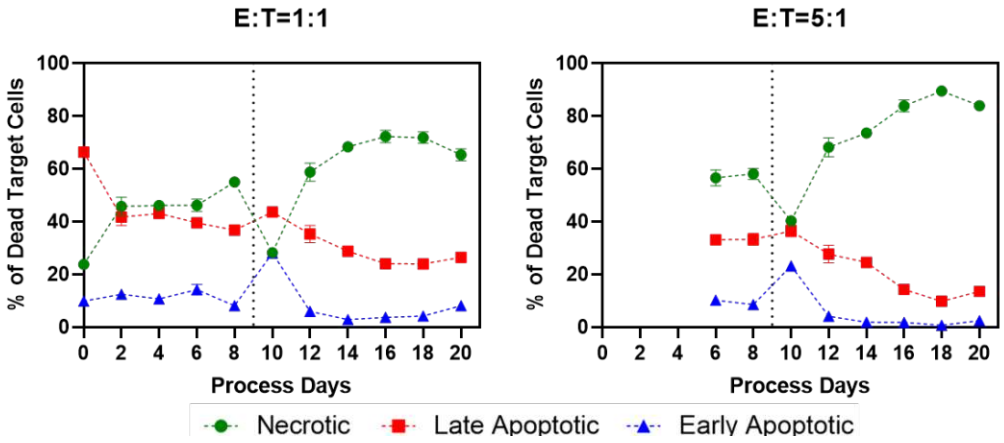

Figure 26: Time-course graphs of the proportions of necrotic-, early apoptotic- and late apoptotic cells in the population of dead target cells determined via FCM. To determine the proportion of necrotic-, late apoptotic- and early apoptotic events in the dead cell population of K-562 cells, the gating strategy described in section 2.9 was used. Depicted are the results of the FCM measurement of the co-culture wells. Error bars indicate the standard deviation of biological triplicates, and a dotted vertical line indicates the separation between the two process phases.

Multiple paired t-tests were conducted, comparing the mean proportion of each dead target cell category between the co-cultures and the K-562 control. The paired t-tests were performed at a level of significance of α=0.05. The results of the t-tests are summarised in Figure 27. No significant difference can be observed between the co-cultures of the 1:1 E:T ratio and the K-562 controls for all dead cell categories. However, the differences are significant for the 5:1 E:T ratio. This shows that the composition of the dead cells, only becomes significantly different from that of spontaneous cell death at elevated E:T ratios. This might be explained by the higher cytotoxicity which is concomitant with higher E:T ratios, leading to an increased signal to-noise ratio.

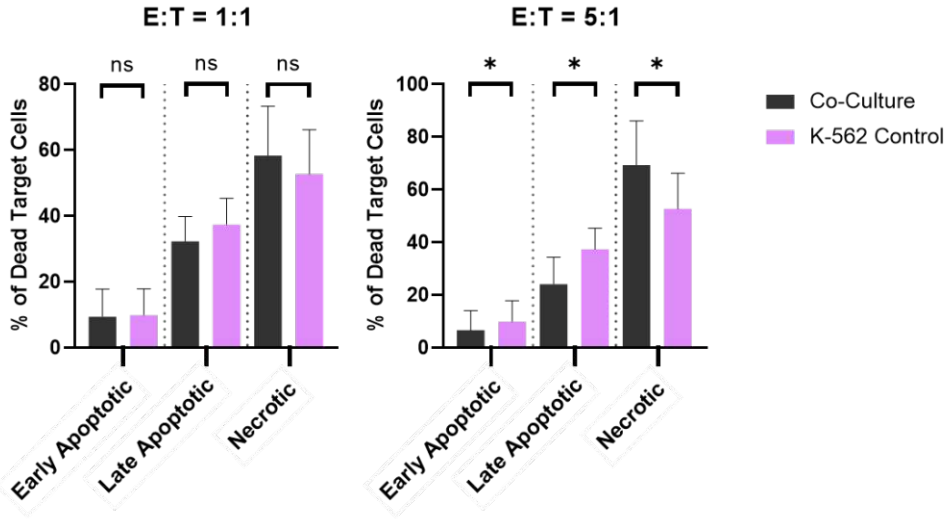

Figure 27: Graphic summary of paired t-tests comparing the means of the proportion of each dead cell category in the population of dead target cells between the co-culture and K-562 control wells. Columns indicate the proportion of dead target cells in the according category to the whole dead cell population, in form of mean values over all process days and error bars indicate the standard deviation. Asterisk indicates that a significant difference was found (P<0.05) between the mean values and ns indicates that no significant difference was found.

3.4.1 *Discussion of reasons for the change in mode of killing*

From the increasing difference between the proportion of necrotic cells to late apoptotic cells during the second process phase, it can be concluded that either apoptosis-inducing pathways were downregulated, or necrosis-inducing pathways were upregulated in the second process phase. A possible reason for the increase of necrotic events can be a change of the perforin to granzyme B ratio in the secretory granules of NK-92 cells[13]. Another possible reason for the increase of the proportion of necrotic cells over time could be the leakage of perforin and granzymes out of effector cells. It was stated that spontaneous LDH release from NK cells is concomitant with NK cell function deficiency, which was presumed of being linked to the co-release of perforin and granzyme B[113].

To investigate whether the variation of the ratio of necrotic to late- and early apoptotic cells is linked to spontaneous LDH leakage, the measured LDH activity of the NK-92-only well supernatant was plotted over the process time (Figure 28). Since the LDH activity of the NK-92 only wells was under the detection limit for the 1:1 E:T ratio, only those of the 5:1 ratio were considered. After an increase from process day 6 to 10, a decrease in the spontaneous LDH release can be observed in the second process phase after process day 10.

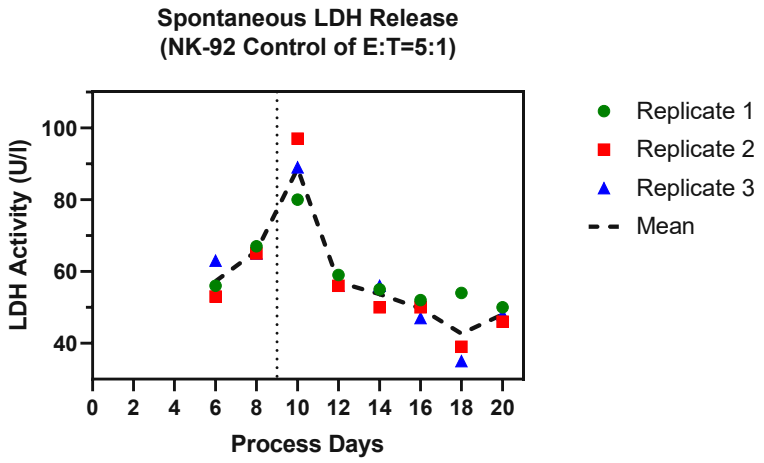

Figure 28: Time-course graph of the volumetric LDH activity measured in the supernatant of NK-92 control wells after an incubation time of 4 h The LDH activity values are derived from the LDH activity determination for the LDH release method. Error bars indicate the standard deviation between biological replicates and a vertical dotted line indicates the separation between the two process phases.

A potential relation between the spontaneous LDH release in the NK-92 controls and the death of NK-92 cells was investigated by calculation of the R^2 value of the correlation between the spontaneous LDH release and the viability of the NK-92 culture. A low correlation (R^2=0.14) was observed indicating that spontaneous LDH release is rather related to stressed cells than to already dead cells[114].

The correlation between the proportion of necrotic-, late apoptotic-, early apoptotic cells, spontaneous LDH release, and the cytotoxicity over the second process phase is summarised in form of R^2 values in Figure 29. For the 1:1 E:T ratio a moderate positive correlation can be observed between the spontaneous LDH release in the NK-92 controls and the proportion of both early apoptotic events (R^2=0.69) and late apoptotic events (R^2=0.64). The proportion of necrotic events shows a strong negative correlation with the spontaneous LDH release of the

NK-92 controls (R^2=0.75) For the 5:1 E:T ratio slightly stronger correlations between the spontaneous LDH release and the proportion of early apoptotic (R^2=0.81) and necrotic events (R^2=76) and a weaker correlation with the proportion of late apoptotic events (R^2=0.57) was observed, compared to the 1:1 E:T ratio.

Interestingly no strong correlation was found between the spontaneous LDH release from NK-92 controls and the cytotoxicity, determined with any of the three methods. This means that despite the mode of killing is correlated with the spontaneous LDH release, the total killing was not influenced by LDH leakage. This is consistent with the finding that the proportion of necrotic events is strong, inversely correlated with those of late- and early apoptotic events at the 1:1 E:T ratio and the 5:1 E:T ratio.

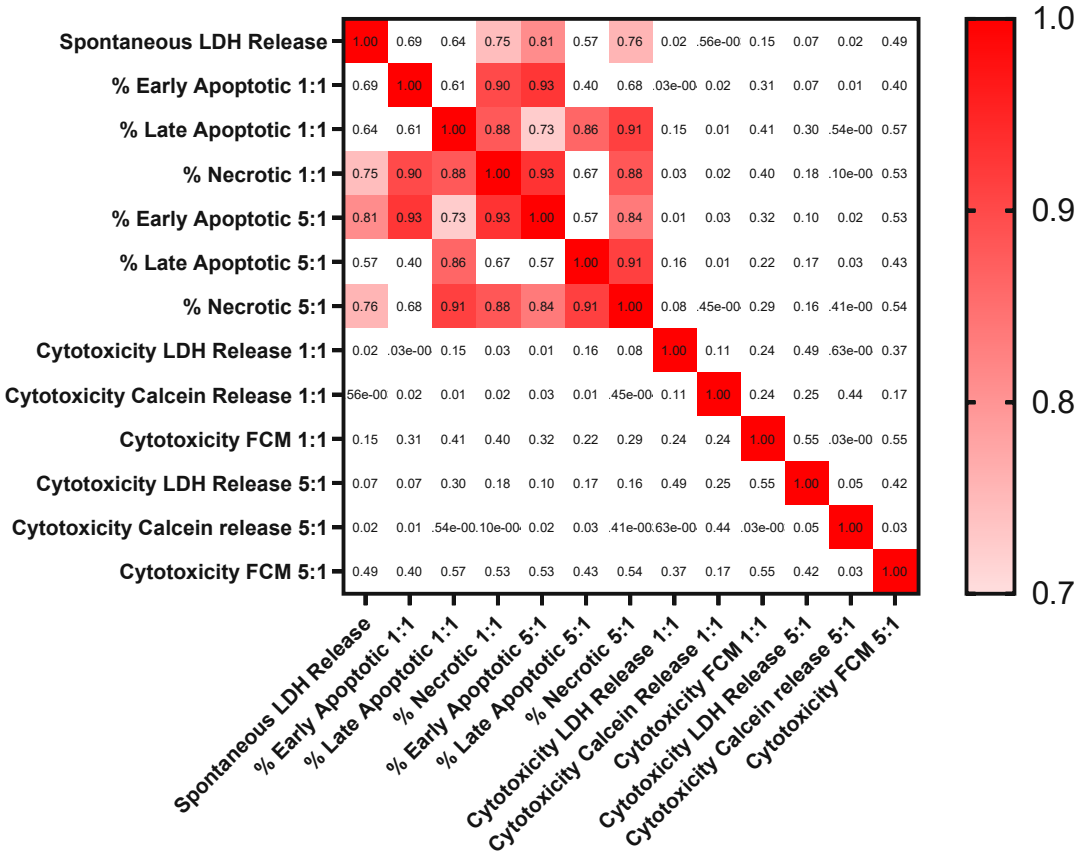

Figure 29: Matrix of R^2-values of the correlation between spontaneous LDH release, proportion of dead cell categories in the dead target cell population and cytotoxicity measurement results over the second process phase Coloured fields indicate a R^2-value ≥ 0.7 while the colouring gets more intensive for higher R^2-values.

As already mentioned, a possible explanation for the correlation between the mode of killing and the spontaneous LDH release could be the co-release of perforin and granzyme with LDH from NK-92 cells. As described in section 2, target cells die via necrosis if the plasma membrane damage cannot be restored after perforation via perforin release. If, however, the plasma membrane can be repaired, the target cell dies via apoptosis.

Thus, a possible explanation for the increase of necrosis while spontaneous LDH release is decreasing is that lower concentrations of perforin in the synaptic cleft are not sufficient to cause enough pore formation for necrosis, while the low concentrations of perforin and granzymes still enable apoptosis. Nevertheless, it was not yet shown that lytic molecules are

indeed co-released upon spontaneous LDH release from NK-92 cells. Hence it is also possible that spontaneous LDH release from NK-92 cells is linked to the mode of killing in other ways than the co-release of lytic molecules. For instance, as LDH leakage is linked to the plasma membrane integrity, it could be possible that Ca^{2+} influx control is disturbed, which also affects the killing behaviour of NK cells, as Ca^{2+} is necessary for lytic granule fusion as well as perforin functioning[115].

3.5 Cell aggregate analysis

Time course plots of the average aggregate size and the average aggregate count are depicted in Figure 30. It can be observed that the average aggregate size increases with the process time. The increase in aggregate size is higher in the first phase of the process, than in the second process phase. The aggregate count shows a drop from process days 2 to 4, followed by an increase until process day 12. After process day 12 the aggregate count exhibits a slight decrease until the end of the process. To determine the average number of cells contained in each aggregate, the aggregate areas were divided by the mean cell area of the corresponding process day. All aggregates were classified into four size categories, based on the calculated number of contained cells per aggregate. The definitions of the chosen size categories are listed in table 6. The size categories at the outer range were kept smaller as the most significant changes over time were expected in these categories.

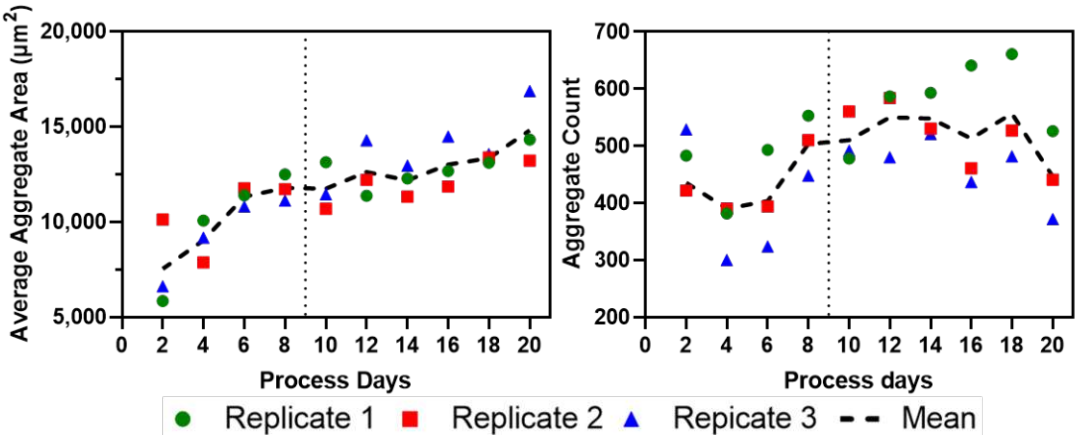

Figure 30: Time-course graphs of the average aggregate area and the aggregate count of the NK-92 cultures Depicted are the results derived from the bright field image analysis of the NK-92 cultures via image analysis software. A vertical dotted line indicates the separation between the two process phases.

Table 6: Overview of chosen aggregate size categories

Category designation	Cells per aggregate
Smallest aggregates	0-10.9
Small aggregates	11-50.9
Large aggregates	51-99.9
Largest aggregates	≥100

The proportions of aggregate counts in each size category to the total aggregate count are summarised in Figure 31. It can be observed that the proportion of the largest aggregates

increases from the beginning of the process until process day 12. From process day 12-16 the increase is interrupted by a slight decline. It can be deduced that the proportion of largest aggregates is linked to the viable cell concentration in the culture. Higher cell concentrations seem to facilitate the formation of larger aggregates, while the formation of small aggregates already takes place at lower cell concentrations. The proportion of large aggregates increases from 5% at the beginning of the process to close to 20% on process day 12 and exhibits a plateau at the end of the process. The proportion of small aggregates shows a decrease over time, while staying between 40 and 60%. The proportion of smallest aggregates exhibits the opposite course of curve than the aggregates containing more than 100 cells, but at higher values ranging between 40 and 10%. In general, it is noticeable that initially 10% of the aggregates contain more than 50 cells at the beginning of the process. However, this proportion reaches over 30% by process day 12.

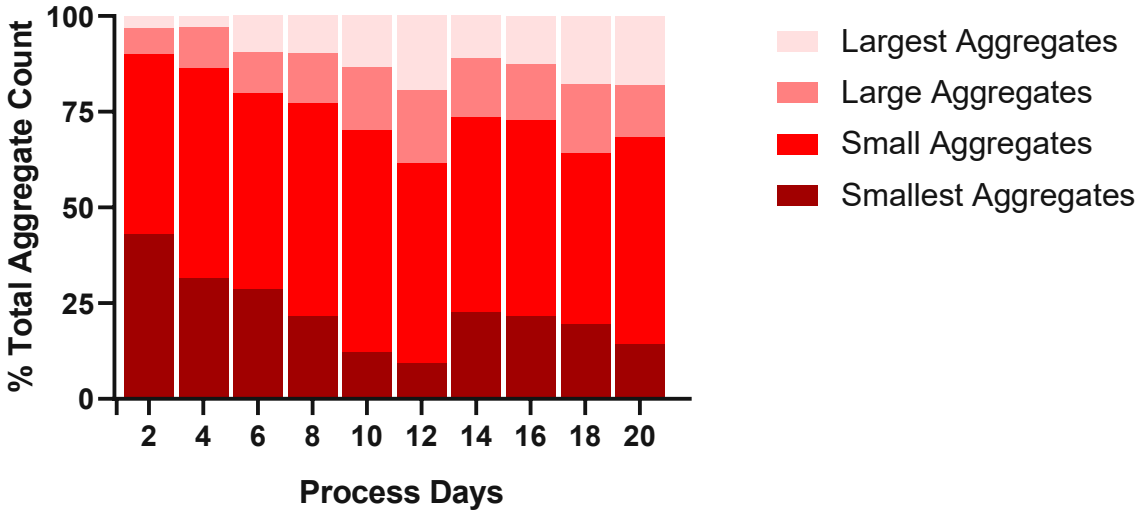

Figure 31: Time-course graph of the proportion of each aggregate category to the total aggregate count

The correlations between aggregate analysis derived data and the other PPs are summarised in form of R^2 values in Figure 32 to Figure 34. Correlations are considered as strong when R^2 is equal or higher than 0.7. The average aggregate area is strongly correlated with the proportion of the largest aggregates over the whole process duration (R^2=0.78). This was expected as the category of the largest aggregates delivers the biggest contribution to the average aggregate area.

Beneficial, as well as unfavourable effects of aggregate formation on the cell growth have been reported. On the one hand is claimed that the formation of cell aggregates enhances the activation of NK cells via the trans-presentation of IL-2 between NK cells and that contact between NK cells is beneficial for NK cell effector functioning[108, 116]. On the other hand, it was already shown that cell clustering also leads to a gradient of stimulant concentration, leading to a lower stimulant availability for cells inside of aggregates for B cells[60].

A strong correlation with the VCC can be observed for the average aggregate area (R^2=0,68) as well as for the proportion of the largest aggregates (R^2=0,72) over the whole process duration. This indicates that while higher cell densities do not lead to a variation in the number of aggregates, the formation of aggregates belonging to the category of largest aggregates is favoured when the cell concentration increases. The average cell size exhibits a strong negative

correlation with the proportion of largest aggregates (R^2=0,70) and a strong positive correlation with the proportion of smallest aggregates(R^2=0,76) over the whole process duration. A possible explanation for the inverse correlation between the proportion of largest aggregates and the average cell size could be that cells incorporated in larger aggregates encounter a different osmotic pressure than cells that participate in smaller aggregates, due to concentration gradients in cell aggregates. This could lead to a shrinkage of cells participating in larger cell aggregates. However, this theory is weakened by the fact that the average cell size is positively correlated with the viability over the whole process duration (R^2=0.73). Thus, it is possible that the cell shrinkage is derived from apoptotic volume decrease. Hence, smaller cells would be part of a less viable cell fraction, which could be linked to their ability of cell aggregate formation. A higher proportion of larger cells with a better capability of aggregate formation would lead to faster formation of smaller aggregates, leaving less cells available to join already larger aggregates, which would explain the negative correlation of the average cell size with the proportion of largest aggregates and the positive correlation with the proportion of smallest aggregates.

Moreover, the question appears why only the proportion of smallest aggregates (R^2=0.79) and not the proportion of largest aggregates (R^2=0.21) is strongly correlated with the average cell size over the second process phase. A reason for this finding could be that the formation of larger aggregates is only influenced by the faster formation of smaller aggregates at lower cell densities in the culture. This theory is corroborated by the fact that the proportion of smallest aggregates shows a moderate correlation with the proportion of largest aggregates in the first process phase (R^2= 0.61) while no correlation is observed over the second process phase (R^2=0.19)

A strong correlation can be observed between the proportion of the largest aggregates and the concentrations of multiple metabolites such as ammonia (R^2=0.77), glutamine+GlutaMAX (R^2=0.74), pyruvate (R^2=0.80), asparagine (R^2=0.80) and serine (R^2=0.81) over the whole process duration. These correlations can be explained by the dependence of those metabolite concentrations on the VCC. Thus, the proportion of largest aggregates, which also correlates with the VCC, is correlated with the cell concentration dependent metabolites. This assumption is corroborated by the fact that no correlations between any of the metabolites and the proportion of largest aggregates can be observed for the second process phase, where the cell growth was lower, and the concentrations of most metabolites showed a plateau.

The specific ammonia production rate is inversely correlated with the proportion of largest aggregates over the whole process duration (R^2=0.72). A possible explanation for this correlation could be that the availability of glutamine is lower inside of large aggregates, which would lead to a lower production of ammonia, which is corroborated by the moderate positive correlation between the glutamine production rate and the proportion of largest aggregates over the whole process duration (R^2=0.60). Thus, a consideration of potential effects of aggregate formation on the growth behaviour is necessary in NK-92 expansion processes.

The analysis of the aggregate formation revealed limitations of the representativeness of the acquired data. With an image size of 7 mm^2 and a sample size of 16 images, only 0,6% of the culture flask area are covered by the microscopy image data. This indicates that for a deeper understanding of the mechanism of cluster formation and the relationships between cluster formation, cell growth and metabolism it would be necessary to conduct experiments in smaller scales (i.e. in well plates) to achieve a higher representativeness of the collected data.

Furthermore, in the setup, which was chosen for this experiment, the formed aggregates were disrupted every 24 h. Accordingly, it is possible that potential effects of aggregate formation on cell growth and- metabolism, would only be recognizable with cultivation setups which allow cell aggregates to stay intact over longer time periods.

Figure 32: Matrix of R^2 values of correlations of aggregate data with other PPs over the whole process duration
Depicted are exclusively PPs which showed a strong correlation with the aggregate analysis-derived data.

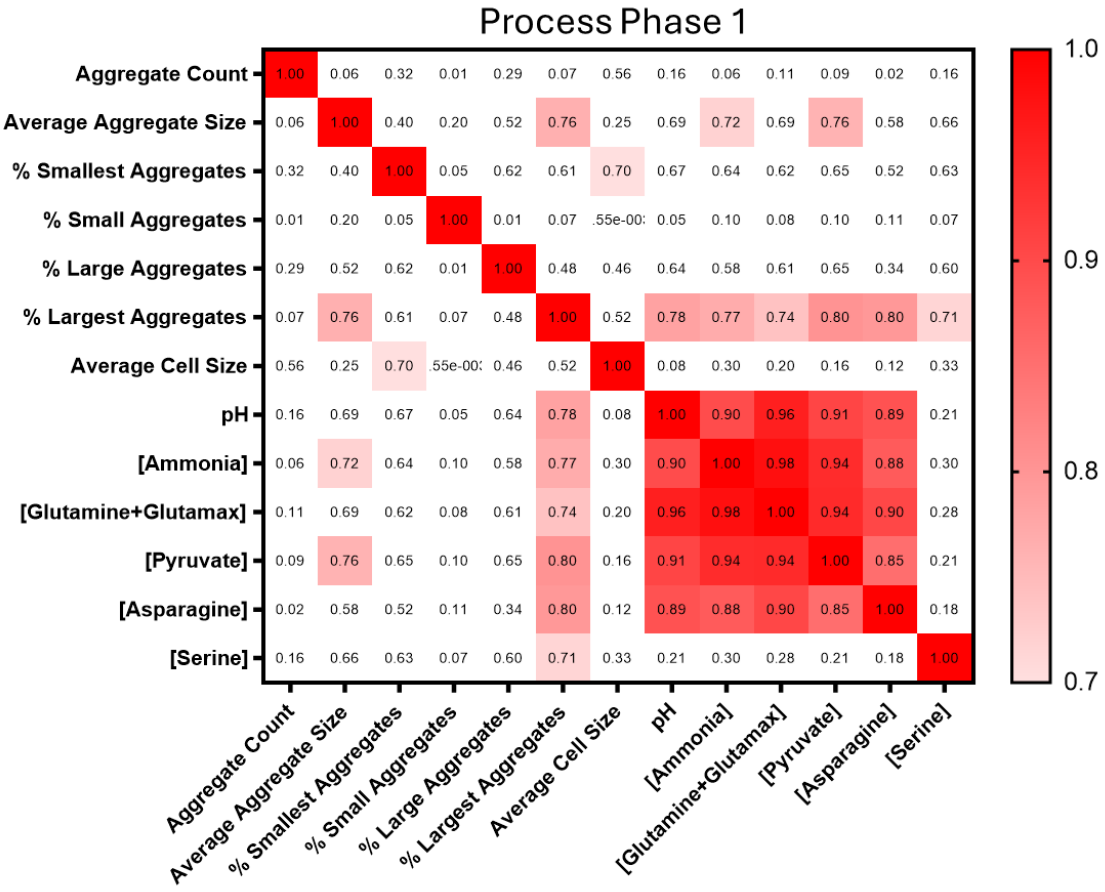

Figure 33: Matrix of R^2 values of correlations of aggregate data with other PPs over process phase 1 Depicted are exclusively PPs which showed a strong correlation with the aggregate analysis-derived data.

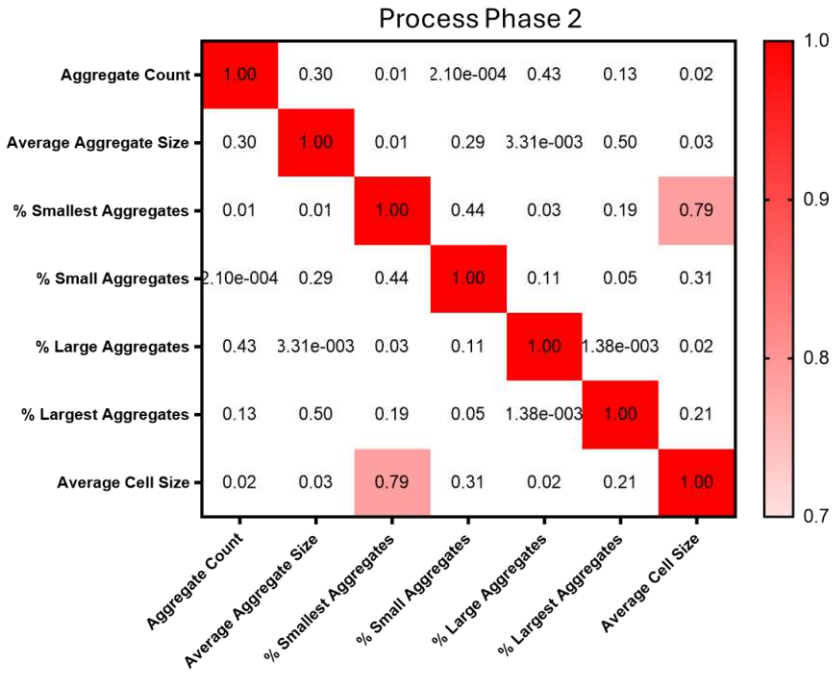

Figure 34: Matrix of R^2 values of correlations of aggregate data with other PPs over process phase 2 Depicted are exclusively PPs which showed a strong correlation with the aggregate analysis-derived data.

4 Conclusion

This thesis followed two major goals. One was to investigate the relationships among several cell culture process related parameters and quality attributes of NK-92 cultures. The other goal was to compare three different cytotoxicity assays to each other.

A static, pseudo-static NK-92 culture in biological triplicates was performed over a total duration of 21 process days. Samples of the culture were taken daily to monitor process parameters and quality attributes. The sampling process included the acquisition of cell aggregate morphology data via brightfield microscopy, measurement of pH and metabolite concentrations in the culture, measurement of VCC and viability of the culture, as well as the determination of the time resolved cytotoxicity against K-562 via a LDH release assay, a calcein release assay and a FCM.

A decline in the growth rate of the NK-92 culture was observed, which was the basis for the division of the process into two process phases. The change in growth behaviour was concomitant with changes in the production rates of several metabolites. As potential cause for the decline in growth, elevated levels of ammonia and lactate could be identified, indicating a sensitivity of NK-92 to elevated ammonia and lactate levels. As lactate and ammonia are continuously produced, monitoring of lactate and ammonia levels and constant media exchange are necessary for optimised expansion processes.

The evaluation of the specific metabolite production rates of the culture revealed that the specific consumption rates of most of the essential amino acids are strongly correlated. A production of aspartate, glutamate and glycine was observed, which could be explained in accordance with reports on NK cell and mammalian cell metabolism. High consumption of serine and glutamine during the process, revealed potential optimisation of NK-92 growth by adaptation of their concentrations in cell culture media. Increasing importance of asparagine for NK-92 growth was observed when glutamine levels were decreased, which should be considered for adaptation of the glutamine concentration.

The analysis of the cell aggregate formation revealed an inverse correlation between the formation of aggregates belonging to the largest of four size categories and the production of ammonia in the NK-92 cultures. Thus, it needs to be considered that aggregate formation potentially influences the growth behaviour in NK-92 expansion processes. A potential beneficial influence of aggregate formation on the growth behaviour could not be observed, which could be due to the inhibiting effects of ammonia and lactate on cell proliferation. No strong correlations were observed between the formation of aggregates and the cytotoxicity of the NK-92 cultures.

The three cytotoxicity determination methods exhibited different, not correlating profiles of cytotoxicity time courses. However, there was no significant difference between the means of the results of the methods at a 5:1 E:T ratio. At a 1:1 E:T ratio the results of the calcein release assay were significantly higher than those of the other two assays. It was shown that not only the choice of the method, but also the metabolic state of the effector and target cells could have an influence on the results of the cytotoxicity assay, as the cytotoxicity exhibited variations over the process time. This reveals a lack of comparability of results from different cytotoxicity assays.

An unexpected strong correlation between the spontaneous release of LDH from NK-92 cells and the ratio of necrotic and apoptotic target cells in the dead target cell population was observed. This shows that the amount of cell stress, which is linked to the membrane integrity, has an influence on the killing behaviour of NK-92 cells. Thus, LDH release in NK-92 culture supernatants could emerge as an easily accessible soft sensor for the killing behaviour of NK-92 cells.

5 Appendix

5.1 Reagents and consumables

Table 7: List of reagents and consumables used for the experiments

Name	Source	Identifier
3-Mercaptopropionic acid (MPA)	Sigma-Aldrich (St. Louis, MO, USA)	63768-25ML
Acetic acid, 100%	Carl Roth (Karlsruhe, Germany)	6755.3
Acetonitrile, HPLC grade	AppliChem (Darmstadt, Germany)	221881
AdvancedBio AAA UHPLC Guard 3PK	Agilent (Santa Clara, CA, USA)	823750-946
Agilent AdvanceBio AAA LC column	Agilent (Santa Clara, CA, USA)	695975-322
Ala-Gln Bio HT	Roche Diagnostics (Basel, Switzerland)	8056943001
Amino Acid Standard 18AAS	Sigma-Aldrich (St. Louis, MO, USA)	AAS18-5ML
BD Cytofix/Cytoperm	BD Biosciences (Franklin Lakes, NJ, USA)	554714
BD GolgiPlug	BD Biosciences (Franklin Lakes, NJ, USA)	51-2301KZ
BD GolgiStop	BD Biosciences (Franklin Lakes, NJ, USA)	51-2092KZ
Brilliant Stain Buffer	BD Biosciences (Franklin Lakes, NJ, USA)	563794
Calcein AM - Green	Invitrogen (Waltham, MA, USA)	C3100MP
Chromafil RC-20/15 MS	Macherey-Nagel (Düren, Germany)	729036
Dimethyl sulphoxide (DMSO)	Carl Roth (Karlsruhe, Germany)	A994.2
Disodium tetraborate decahydrate	Carl Roth (Karlsruhe, Germany)	T880.1
Fetal bovine serum (FBS)	ATCC (Manassas, VA, USA)	30-2025
Glucose Cedex Bio HT	Roche Diagnostics (Basel, Switzerland)	6608418001
Glutamate V2 Bio HT	Roche Diagnostics (Basel, Switzerland)	7395566001
GlutaMAX™ Supplement	Thermo Fisher Scientific (Waltham, MA, USA)	35050061
Glutamine V2 Bio HT	Roche Diagnostics (Basel, Switzerland)	7395612001
GolgiPlug - Protein Transport Inhibitor	BD Biosciences (Franklin Lakes, NJ, USA)	555029
GolgiStop - Protein Transport Inhibitor	BD Biosciences (Franklin Lakes, NJ, USA)	554724
Human interleukin-2 (IL-2) IS Premium grade	Milteny Biotec (Bergisch Gladbach, Germany)	130-097-749
Hydrochloric acid (HCl), 37%	Carl Roth (Karlsruhe, Germany)	9277.3
Iscove's Modified Dulbecco's Medium (IMDM)	Carl Roth (Karlsruhe, Germany)	12440046
Ionomycin	Cayman Chemical (Ann Arbor, MI, USA)	10004974
K-562 Cells	ATCC (Manassas, VA, USA)	CCL-243
L-Asparagine monohydrate	Carl Roth (Karlsruhe, Germany)	HN23.1
L-Glutamine	Carl Roth (Karlsruhe, Germany)	HN08.3
L-Tryptophane	TCI chemicals (Tokyo, Japan)	T0541
Lactate Bio HT	Roche Diagnostics (Basel, Switzerland)	6608485001
LDH Cedex Bio HT	Roche Diagnostics (Basel, Switzerland)	6608493001
Live or Dead Fixable Dead Cell Staining Kit	AAT Bioquest (Sunnyvale, USA)	22600
Methanol, HPLC grade	AppliChem (Darmstadt, Germany)	221091
NH3 Bio HT	Roche Diagnostics (Basel, Switzerland)	6608515001

Name	Source	Identifier
NK-92 Cells	ATCC (Manassas, VA, USA)	CRL-2407
Ortho-phthalaldehyde (OPA)	Sigma-Aldrich (St. Louis, MO, USA)	P0657-1G
Perchloric acid ($HClO_4$), 70%	Carl Roth (Karlsruhe, Germany)	HN51.1
Phorbol-12-myristate-13-acetate (PMA)	Cayman Chemical (Ann Arbor, MI, USA)	10008014
Pyruvate Bio HT	Roche Diagnostics (Basel, Switzerland)	7299818001
Stem Cell Growth Medium (SCGM)	CellGenix (Freiburg, Germany)	20802-0500
Sodium dihydrogen phosphate monohydrate	Carl Roth (Karlsruhe, Germany)	T878.1
Sodium hydroxide (NaOH)	Sigma-Aldrich (St. Louis, MO, USA)	1064691000
UltraComp eBeads™ Plus Compensation Beads	Thermo Fisher Scientific (Waltham, MA, USA)	01-3333-41

Table 8: List of antibodies used for flow cytometry-based analysis

Reactivity/Fluorophore	Clone	Source	Identifier	Lot
CD11a - PerCP/Cyanine 5.5	TS2/4	BioLegend (San Diego, CA, USA)	350614	B325240
CD25 - APC/Fire 750	M-A251	BioLegend (San Diego, CA, USA)	356136	B330219
CD49d - Super Bright 600	9F10	Thermo Fisher Scientific (Waltham, MA, USA)	63-0499-42	2308019
CD56 - PE-cF594	NCAM16.2	BD Biosciences (Franklin Lakes, NJ, USA)	564849	2192145
CD69 - BUV737	FN50	Thermo Fisher Scientific (Waltham, MA, USA)	367-0699-42	2560256
CD107a - PE-Cyanine5	eBioH4A3	Thermo Fisher Scientific (Waltham, MA, USA)	15-1079-42	2380466
CD244 - PE	C1.7	BioLegend (San Diego, CA, USA)	329508	B377962
CD314 - BV785	1D11	BioLegend (San Diego, CA, USA)	320830	B367221
CD335 - BV711	9E2	BioLegend (San Diego, CA, USA)	331936	B378731
CD337 - BUV395	p30-15	BD Biosciences (Franklin Lakes, NJ, USA)	743173	3027814
IFN-γ– - BV510	B27	BioLegend (San Diego, CA, USA)	506540	B357871
TNF-α– - PE-Vio 770	cA2	Miltenyi Biotec (Bergisch Gladbach, Germany)	130-120-492	5221103017
Phosphatidylserine - AF-488	1H6	Merck Millipore (Burlington, VT, USA)	16-256	3849118

5.2 List of abbreviations

acetoxymethyl (**AM**)
adenosyl triphosphate (**ATP**)
adoptive cell therapy (**ACT**)
american type culture collection (**ATCC**)
antibody dependent cellular cytotoxicity (**ADCC**)
chimeric antigen receptors (**CAR**)
common lymphoid progenitors (**CLPs**)
cytokine release syndrome (**CRS**)
branched-chain amino acids (**BCAA**)
cytosolic branched-chain aminotransferase (**BCATc**)
Fas ligand (**FasL**)
fetal bovine serum (**FBS**)
flow cytometry-based method (**FCM**)
high performance liquid chromatography (**HPLC**)
host versus graft rejection (**HvGR**)
immunoreceptor tyrosine-based activation motifs (**ITAMs**)
immunoreceptor tyrosine-based inhibitory motifs (**ITIMs**)
interleukin-2 (**IL-2**)
major histocompatibility complex class I(**MHC I**)
mammalian target of rapamycin complex 1 (**mTORC1**)
mature natural killer cells (**mNKs**)
3-mercaptopropionic acid (**3-MPA**)
natural killer cell activating receptors (**NKRs**)
nitric oxygen synthase (**NOS**)
oxidised nicotinamide adenine dinucleotide (**NAD^+**)
oxidised nicotinamide adenine dinucleotide phosphate (**$NADP^+$**)
ortho-phthaldialdehyde (**OPA**)
peripheral blood mononuclear cells (**PBMCs**)
phosphatidylserine (**PS**)
3-phosphoglycerate (**3-PG**)
phosphoglycerate dehydrogenase (**PHGDH**)
pyruvate dehydrogenase kinase (**PDK**)
pyruvate kinase M2 (**PKM2**)
reduced nicotinamide adenine dinucleotide (**NADH**)
reduced nicotinamide adenine dinucleotide phosphate (**NADPH**)
secondary lymphoid tissues (**SLTs**)
serine hydroxymethyltransferase (**SHMT**)
specific growth rate (**μ**)
Stem Cell Growth Medium (**SCGM**)
tetrahydrofolate (**THF**)
TNF-related apoptosis-inducing ligand (**TRAIL**)
tumour necrose factor (**TNF**)
umbilical cord blood (**UCB**)

5.3 List of figures

5.4 List of tables

5.5 Bibliography

(1) Lodoen, M. B.; Lanier, L. L. Natural killer cells as an initial defense against pathogens. *Curr Opin Immmunol* **2006**, *18* (4), 391-398. DOI: 10.1016/j.coi.2006.05.002.
(2) Xie, G.; Dong, H.; Liang, Y. CAR-NK cells: A promising cellular immunotherapy for cancer. *EBioMedinice* **2020**, *59*. DOI: 10.1016/j.ebiom.2020.102975.
(3) Abel, A. M.; Yang, C.; Thakar, M. S. Natural Killer Cells: Development, Maturation, and Clinical Utilization. *Frontiers in Immunology* **2018**, *9*. DOI: 10.3389/fimmu.2018.01869.
(4) Campbell, K. S.; Hasegawa, J. Natural killer cell biology: An update and future directions. *The Journal of allergy and clinical immunology* **2013**, *132* (3), 536-544. DOI: 10.1016/j.jaci.2013.07.006.
(5) Paul, S.; Lal, G. The Molecular Mechanism of Natural Killer Cells Function and Its Importance in Cancer Immunotherapy. *Frontiers in Immunology* **2017**, *8*. DOI: 10.3389/fimmu.2017.01124.
(6) Wang, W.; Erbe, A. K.; Hank, J. A.; Morris, Z. S. NK Cell-Mediated Antibody-Dependent Cellular Cytotoxicity in Cancer Immunotherapy. *Frontiers in Immunology* **2015**, *6*. DOI: 10.3389/fimmu.2015.00368.
(7) Lanier, L. L. Up on the tightrope: natural killer cell activation and inhibition. *Nature Immunology* **2008**, *9*, 495-502. DOI: 10.1038/ni1581.
(8) Prager, I.; Watzl, C. Mechanisms of natural killer cell-mediated cellular cytotoxicity. *Journal of leukocyte biology* **2019**, *105* (6), 1319-1329. DOI: 10.1002/JLB.MR0718-269R.
(9) Hoves, S.; Trapani, J. A.; Voskoboinik, I. The battlefield of perforin/granzyme cell death pathways. *Journal of leukocyte biology* **2010**, *87* (2), 237-243. DOI: 10.1189/jlb.0909608.
(10) Chowdhury, D.; Lieberman, J. Death by a Thousand Cuts: Granzyme Pathways of Programmed Cell Death. *Annu Rev Immunol.* **2008**, *26*, 389-420. DOI: 10.1146/annurev.immunol.26.021607.090404.
(11) Griffiths, G. M.; Argon, Y. Structure and biogenesis of lytic granules. *Current topics in Microbiology and Immunology* **1995**, *189*, 39-58. DOI: 10.1007/978-3-642-79414-8_3.
(12) Topham, N. J.; Hewitt, E. W. Natural killer cell cytotoxicity: how do they pull the trigger? *Immunology* **2009**, *128* (1), 7-15. DOI: 10.1111/j.1365-2567.2009.03123.x.
(13) Backes, C. S.; Friedmann, K. S.; Mang, S. Natural killer cells induce distinct modes of cancer cell death: Discrimination, quantification, and modulation of apoptosis, necrosis, and mixed forms. *Journal of Biological Chemistry* **2018**, *293* (42), 16348-16363. DOI: 10.1074/jbc.RA118.004549.
(14) Elmore, S. Apoptosis: A Review of Programmed Cell Death. *Toxicol Pathol* **2007**, *35* (4), 495-516. DOI: 10.1080/01926230701320337.
(15) Page, A.; Chuvin, N.; Valladeau-Guilemond, J. Development of NK cell-based cancer immunotherapies through receptor engineering. *Cellular & Molecular Immunology* **2024**, *21*, 315-331. DOI: 10.1038/s41423-024-01145-x.
(16) Zhang, P.; Zhang, G.; Wan, X. Challenges and new technologies in adoptive cell therapy. *Journal of Hematology & Oncology* **2023**, *16* (97). DOI: 10.1007/s00428-018-2484-0.
(17) Rohaan, M. W.; Wilgenhof, S.; Haanen, J. B. A. G. Adoptive cellular therapies: the current landscape. *Virchows Archiv* **2019**, *474* (4), 449-461. DOI: 10.1186/s13045-023-01492-8.
(18) Damodharan, S. N.; Walker, K. L.; Forsberg, M. H. Analysis of ex vivo expanded and activated clinical grade human NK cells after cryopreservation. *Cytotherapy* **2020**, *22* (8), 450-457. DOI: 10.1016/j.jcyt.2020.05.001.
(19) Klingemann, H. The NK-92 cell line—30 years later: its impact on natural killer cell research and treatment of cancer. *Cytotherapy* **2023**, *25* (5), 451-457. DOI: 10.1016/j.jcyt.2022.12.003.
(20) Liu, S.; Galat, V.; Galat, Y. NK cell-based cancer immunotherapy: from basic biology to clinical development. *Journal of Hematology & Oncology* **2021**, *14*. DOI: 10.1186/s13045-020-01014-w.
(21) Chu, J.; Gao, F.; Yan, M. Natural killer cells: a promising immunotherapy for cancer. *Journal of Translational Medicine* **2022**, *20*.
(22) Handgretinger, R.; Lang, P.; André, M. C. Exploitation of natural killer cells for the treatment of acute leukemia. *blood* **2016**, *127* (26), 3341-3349. DOI: 10.1182/blood-2015-12-629055.
(23) Klingemann, H. Chapter Twelve - Development and testing of NK cell lines. In *Natural Killer Cells Basic Science and Clinical Application*, Lotze, M. T., Thomson, A. W. Eds.; 2010; pp 196-175.

(24) Du, S.; Yan, J.; Xue, Y. Adoptive cell therapy for cancer treatment. *Exploration (Beijing)* **2023**, *3* (4). DOI: 10.1002/EXP.20210058.
(25) Chu, J.; Gao, F.; Yan, M. Natural killer cells: a promising immunotherapy for cancer. *Journal of Translational Medicine* **2022**, *20* (240). DOI: 10.1186/s12967-022-03437-0.
(26) Li, H.; Song, W.; Li, Z.; Zhang, M. Preclinical and clinical studies of CAR-NK-cell therapies for malignancies. *Frontiers in Immunology* **2022**, *13*. DOI: 10.3389/fimmu.2022.992232.
(27) Lapteva, N.; Szmania, S. M.; Rhee, F. v. Clinical Grade Purification and Expansion of Natural Killer Cells. *Critical Reviews in Oncogenesis* **2014**, *19* (0), 121-132. DOI: 10.1615/critrevoncog.2014010931.
(28) Li, Q. Natural Killer (NK) Cell Assays in Immunotoxicity Testing. In *Immunotoxicity Testing. Methods in Molecular Biology*, DeWitt, J. C., Rockwell, C. E., Bowman, C. C. Eds.; Vol. 1803; Humana Press, 2018; pp 231-241.
(29) Kim, J.; Phan, M.-T. T.; Kweon, S. A Flow Cytometry-Based Whole Blood Natural Killer Cell Cytotoxicity Assay Using Overnight Cytokine Activation. *Frontiers in Immunology* **2020**, *11*. DOI: 10.3389/fimmu.2020.01851.
(30) Lee, S.-b.; Cha, J.; Kim, I.-k. A high-throughput assay of NK cell activity in whole blood and its clinical application. *Biochemichal and Biophysical Research Communications* **2014**, *445* (3), 584-590. DOI: 10.1016/j.bbrc.2014.02.040.
(31) Kim, G.; Donnenberg, V.; Donnenberg, A. A novel multiparametric flow cytometry-based cytotoxicity assay simultaneously immunophenotypes effector cells: Comparisons to a 4 h 51Cr-release assay. *Journal of Immunological methods* **2007**, *325* (1-2), 51-66. DOI: 10.1016/j.jim.2007.05.013.
(32) Chava, S.; Bugide, S.; Gupta, R. Measurement of Natural Killer Cell-Mediated Cytotoxicity and Migration in the Context of Hepatic Tumor Cells. *Journal of Visualized Experiments* **2020**, (156). DOI: 10.3791/60714.
(33) Neri, S.; Mariani, E.; Meneghetti, A. Calcein-acetyoxymethyl cytotoxicity assay: standardization of a method allowing additional analyses on recovered effector cells and supernatants. *Clinical and diagnostic laboratory immunology* **2001**, *8* (6), 1131-1135. DOI: 10.1128/CDLI.8.6.1131-1135.2001.
(34) Lichtenfels, R.; Biddison, W. E.; Schulz, H. CARE-LASS (calcein-release-assay), an improved fluorescence-based test system to measure cytotoxic T lymphocyte activity. *Journal of Immunological methods* **1994**, *172* (2), 227-239. DOI: 10.1016/0022-1759(94)90110-4.
(35) Korzeniewski, C.; Callewaert, D. M. An enzyme-release assay for natural cytotoxicity. *Journal of Immunological methods* **1983**, *64* (3), 313-320. DOI: 10.1016/0022-1759(83)90438-6.
(36) Papadopoulos, N. G.; Dedoussis, G. V. Z.; Spanakos, G. An improved fluorescence assay for the determination of lymphocyte-mediated cytotoxicity using flow cytometry. *Journal of Immunological methods* **1994**, *177* (1-2), 101-111. DOI: 10.1016/0022-1759(94)90147-3.
(37) Vermes, I.; Haanen, C.; Reutelingsperger, C. Flow cytometry of apoptotic cell death. *Journal of Immunological methods* **2000**, *243* (1-2), 167-190. DOI: 10.1016/S0022-1759(00)00233-7.
(38) Kandarian, F.; Sunga, G. M.; Arango-Saenz, D. A Flow Cytometry-Based Cytotoxicity Assay for the Assessment of Human NK Cell Activity. *Journal of Visualized Experiments* **2017**, (126). DOI: 10.3791/56191.
(39) Heipertz, E. L.; Zynda, E. R.; Stav-Noraas, T. E. Current Perspectives on “Off-The-Shelf” Allogeneic NK and CAR-NK Cell Therapies. *Frontiers in Immunology* **2021**, *12*. DOI: 10.3389/fimmu.2021.732135.
(40) Lapteva, N.; Durett, A. G.; Sun, J.; Rollins, L. A. Large-scale ex vivo expansion and characterization of natural killer cells for clinical applications. *Cytotherapy* **2012**, *14* (9), 1131-1143. DOI: 10.3109/14653249.2012.700767.
(41) Garcia-Aponte, O. F.; Herwig, C.; Kozma, B. Lymphocyte expansion in bioreactors: upgrading adoptive cell therapy. *Journal of Biological Engineering* **2021**, *15*. DOI: 10.1186/s13036-021-00264-7.
(42) Curcio, E.; Piscioneri, A.; Salerno, S. Human lymphocytes cultured in 3-D bioreactors: Influence of configuration on metabolite transport and reactions. *Biomaterials* **2012**, *33* (33), 8296-8303. DOI: doi.org/10.1016/j.biomaterials.2012.07.065.

(43) Bröker, K.; Sinelnikov, E.; Gustavus, D. Mass Production of Highly Active NK Cells for Cancer Immunotherapy in a GMP Conform Perfusion Bioreactor. *Frontiers in Bioengineering and Biotechnology* **2019**, *7*, 194. DOI: 10.3389/fbioe.2019.00194.
(44) Shah, N.; Martin-Antonio, B.; Yang, H. Antigen Presenting Cell-Mediated Expansion of Human Umbilical Cord Blood Yields Log-Scale Expansion of Natural Killer Cells with Anti-Myeloma Activity. *PLoS ONE* **2013**, *8* (10). DOI: 10.1371/journal.pone.0076781.
(45) Zhao, X.; Cai, L.; Hu, Y. Cord-Blood Natural Killer Cell-Based Immunotherapy for Cancer. *Frontiers in Immunology* **2020**, *11*. DOI: 10.3389/fimmu.2020.584099.
(46) Tam, Y. K.; Martinson, J. A.; Doligosa, K.; Klingemann, H. Ex vivo expansion of the highly cytotoxic human natural killer-92 cell-line under current good manufacturing practice conditions for clinical adoptive cellular immunotherapy. *Cytotherapy* **2003**, *5* (3), 259-272. DOI: 10.1080/14653240310001523.
(47) Arai, S.; Meagher, R.; Swearingen, M. Infusion of the allogeneic cell line NK-92 in patients with advanced renal cell cancer or melanoma: a phase I trial. *Cytotherapy* **2008**, *10* (6), 625-632. DOI: 10.1080/14653240802301872.
(48) Tonn, T.; Schwabe, D.; Klingemann, H. G. Treatment of patients with advanced cancer with the natural killer cell line NK-92. *Cytotherapy* **2013**, *15* (12), 1563-1570. DOI: 10.1016/j.jcyt.2013.06.017.
(49) Piscopo, N. J.; Mueller, K. P.; Das, A. Bioengineering solutions for manufacturing challenges in CAR T cells. *Biotechnology Journal* **2018**, *13* (2). DOI: 10.1002/biot.201700095.
(50) Xie, Z.; Fu, Y.; Tan, W.-s. Fatty acids promote the expansion of NK-92 cells in vitro by improving energy metabolism. *Applied Microbial and Cell Physiology* **2021**, *105*, 4285-4295. DOI: 10.1007/s00253-021-11313-y.
(51) Klingemann, H.; Boissel, L.; Toneguzzo, F. Natural Killer Cells for Immunotherapy – Advantages of the NK-92 Cell Line over Blood NK Cells. *Frontiers in Immunology* **2016**, *7*. DOI: 10.3389/fimmu.2016.00091.
(52) Maki, G.; Klingemann, H.; Martinson, J. A.; Tam, Y. K. Factors Regulating the Cytotoxic Activity of the Human Natural Killer Cell Line, NK-92. *Journal of Hematotherapy & Stem Cell Research* **2001**, *10* (3), 369-383. DOI: 10.1089/152581601750288975.
(53) Aponte, O. F. G.; Kozma, B.; Egger, D. Kinetics of NK-92 growth and functionality in pseudo-static cultures. *Biochemical Engineering Journal* **2023**, *196*. DOI: 10.1016/j.bej.2023.108929.
(54) Palaniswamy, M. S. *Determination of Amino Acid Composition of Cell Culture Media and Protein Hydrosylate Standard*. Agilent Technologies, Ltd, 2021. (accessed 2024 30.05.2024).
(55) Frank, M. P.; Powers, R. W. Simple and rapid quantitative high-performance liquid chromatographic analysis of plasma amino acids. *Journal of Chromatography B.* **2007**, *852* (1-2), 646-649. DOI: 10.1016/j.jchromb.2007.01.002.
(56) *Bioprozesstechnik*; 2011. DOI: 10.1007/978-3-8274-2477-8.
(57) Perfetto, S. P.; Chattopadhyay, P. K.; Lamoreaux, L. Amine-Reactive Dyes for Dead Cell Discrimination in Fixed Samples. *Current Protocols in Cytometry* **2010**, *Chapter: Unit-9.34*. DOI: 10.1002/0471142956.cy0934s53.
(58) Fadok, V. A.; Bratton, D. L.; Frasch, S. C. The role of phosphatidylserine in recognition of apoptotic cells by phagocytes. *Cell Death & Differentiation* **1998**, *5*, 551-562. DOI: 10.1038/sj.cdd.4400404.
(59) Bortner, C. D.; Cidlowski, J. A. Ions, the Movement of Water and the Apoptotic Volume Decrease. *Frontiers in cell and developmental biology* **2020**, *8*. DOI: 10.3389/fcell.2020.611211.
(60) Vijayashankar, D. P.; Vaidya, T. Homotypic aggregates contribute to heterogeneity in B cell fates due to an intrinsic gradient of stimulant exposure. **2021**, *405* (1). DOI: 10.1016/j.yexcr.2021.112650.
(61) Mackenzie, C. G.; Mackenzie, J. B.; Beck, P. THE EFFECT OF pH ON GROWTH, PROTEIN SYNTHESIS, AND LIPID-RICH PARTICLES OF CULTURED MAMMALIAN CELLS. **1961**, *9* (1), 141-156. DOI: 10.1083/jcb.9.1.141.
(62) Dong, L.; Krewson, E. A.; Yang, L. V. Acidosis Activates Endoplasmic Reticulum Stress Pathways through GPR4 in Human Vascular Endothelial Cells. *International Journal of Molecular Science* **2017**, *18* (2), 278. DOI: 10.3390/ijms18020278.

(63) Carswell, K. S.; Papoutsakis, E. T. Extracellular pH affects the proliferation of cultured human T cells and their expression of the interleukin-2 receptor. *Journal of Immunotherapy* **2000**, *23* (6), 669-674. DOI: 10.1097/00002371-200011000-00008.
(64) Mazzio, E. A.; Smith, B.; Soliman, K. F. A. Evaluation of endogenous acidic metabolic products associated with carbohydrate metabolism in tumor cells. *Cell Biology Toxicology* **2010**, *26* (3), 177-188. DOI: 10.1007/s10565-009-9138-6.
(65) Bose, S.; Zhang, C.; Le, A. Glucose Metabolism in Cancer: The Warburg Effect and Beyond. In *The Heterogeneity of Cancer Metabolism [Internet]. 2nd edition*, Le, A. Ed.; Springer, 2021.
(66) Bouillaud, F.; Hammad, N.; Schwartz, L. Warburg Effect, Glutamine, Succinate, Alanine, When Oxygen Matters. *Biology (Basel)* **2021**, *10* (10). DOI: 10.3390/biology10101000.
(67) Assmann, N.; O'Brien, K. L.; Donnelly, R. P. Srebp-controlled glucose metabolism is essential for NK cell functional responses. *Nature Immunology* **2017**, *18* (11), 1197-1206. DOI: 10.1038/ni.3838.
(68) Cong, J. Metabolism of Natural Killer Cells and Other Innate Lymphoid Cells. *Frontiers in Immunology* **2020**, *11*, 1989. DOI: 10.3389/fimmu.2020.01989.
(69) Yoo, H. C.; Yu, Y. C.; Sung, Y. Glutamine reliance in cell metabolism. *Experimental & Molecular Medicine* **2020**, *52* (9), 1496-1516. DOI: 10.1038/s12276-020-00504-8.
(70) Li, X.; Yang, Y.; Zhang, B.; Lin, X. Lactate metabolism in human health and disease. *Signal Transduction and Targeted Therapy* **2022**, *7*. DOI: 10.1038/s41392-022-01151-3.
(71) Yi, H.; Talmon, G.; Wang, J. Glutamate in cancers: from metabolism to signaling. *Journal of Biomedical Research* **2020**, *34* (4), 260-270. DOI: 10.7555/JBR.34.20190037.
(72) Denker, N.; Dringen, R. Modulation of Pyruvate Export and Extracellular Pyruvate Concentration in Primary Astrocyte Cultures. *Neurochemical Research* **2024**, *49* (5), 1331-1346. DOI: 10.1007/s11064-024-04120-0.
(73) Kotzur, R.; Duev-Cohen, A.; Kol, I. NK-92 cells retain vitality and functionality when grown in standard cell culture conditions. *PLoS ONE* **2022**, *17* (3). DOI: 10.1371/journal.pone.0264897.
(74) Newman, A. C.; Maddocks, O. D. K. One-carbon metabolism in cancer. *British Journal of Cancer* **2017**, *116*, 1499-1504. DOI: 10.1038/bjc.2017.118.
(75) Alberghina, L. The Warburg Effect Explained: Integration of Enhanced Glycolysis with Heterogeneous Mitochondria to Promote Cancer Cell Proliferation. *International Journal of Molecular Science* **2023**, *24* (21). DOI: 10.3390/ijms242115787.
(76) Wu, Q.; Chen, X.; Li, J. Serine and Metabolism Regulation: A Novel Mechanism in Antitumor Immunity and Senescence. *Aging and Disease* **2020**, *11* (6), 1640-1653. DOI: 10.14336/AD.2020.0314.
(77) Kikuchi, G.; Motokawa, Y.; Yoshida, T. Glycine cleavage system: reaction mechanism, physiological significance, and hyperglycinemia. *Proc Jpn Acad Ser B Phys Biol Sci* **2008**, *84* (7), 246-263. DOI: 10.2183/pjab/84.246.
(78) Gorgoglione, R.; Impedovo, V.; Riley, C. L. Glutamine-Derived Aspartate Biosynthesis in Cancer Cells: Role of Mitochondrial Transporters and New Therapeutic Perspectives. *Cancers (Basel)* **2022**, *14* (1), 245. DOI: 10.3390/cancers14010245.
(79) Birsoy, K.; Wang, T.; Chen, W. An essential role of the mitochondrial electron transport chain in cell proliferation is to enable aspartate synthesis. *Cell* **2015**, *162* (3), 540-551. DOI: 10.1016/j.cell.2015.07.016.
(80) Krall, A. S.; Xu, S.; Graebner, T. G. Asparagine promotes cancer cell proliferation through use as an amino acid exchange factor. *Nature Communications* **2016**, *7*. DOI: doi.org/10.1038/ncomms11457.
(81) Lopez, M. J.; Mohiuddin, S. S. *Biochemistry, Essential Amino Acids*; StatPearls Publishing, 2024.
(82) Platten, M.; Nollen, E. A. A.; Röhrig, U. D. Tryptophan metabolism as a common therapeutic target in cancer, neurodegeneration and beyond. *Nature Reviews Drug Discovery* **2019**, *18*, 379-401. DOI: 10.1038/s41573-019-0016-5.
(83) Parthasarathy, A.; Cross, P. J.; Dobson, R. C. J. A Three-Ring Circus: Metabolism of the Three Proteogenic Aromatic Amino Acids and Their Role in the Health of Plants and Animals. *Frontiers in Molecular Biosciences* **2018**, *5*. DOI: 10.3389/fmolb.2018.00029.

(84) Lamas, B.; Vergnaud-Gauduchon, J.; Goncalves-Mendes, N. Altered functions of natural killer cells in response to L-Arginine availability. *Cellular Immunology* **2012**, *280* (2), 182-190. DOI: 10.1016/j.cellimm.2012.11.018.
(85) Cifone, M. G.; Ulisse, S.; Santoni, A. Natural killer cells and nitric oxide. *International Immunopharmacology* **2001**, *1* (8), 1513-1524. DOI: 10.1016/S1567-5769(01)00095-9.
(86) Xiao, L.; Eneroth, P. H.; Qureshi, G. A. Nitric oxide synthase pathway may mediate human natural killer cell cytotoxicity. *Scandinavian Jounal of Immunology* **1995**, *42* (5). DOI: 10.1111/j.1365-3083.1995.tb03687.x.
(87) Domagala, J.; Lachota, M.; Klopotowska, M. The Tumor Microenvironment—A Metabolic Obstacle to NK Cells' Activity. *Cancers (Basel)* **2020**, *12* (12). DOI: 10.3390/cancers12123542.
(88) Albaugh, V. L.; Pinzon-Guzman, C.; Barbul, A. Arginine Metabolism and Cancer. *Journal of Surgical Oncology* **2017**, *115* (3), 273-280. DOI: 10.1002/jso.24490.
(89) Morris, S. M. J. Arginine Metabolism: Boundaries of Our Knowledge. *Journal of Nutrition* **2007**, *137* (6), 1602-1609. DOI: 10.1093/jn/137.6.1602S.
(90) Pavlova, N. N.; Hui, S.; Ghergurovich, J. M. As Extracellular Glutamine Levels Decline, Asparagine Becomes an Essential Amino Acid. *Cell Metabolism* **2018**, *27* (2), 428-438. DOI: 10.1016/j.cmet.2017.12.006.
(91) Kim, L. C.; Cook, R. S.; Chen, J. mTORC1 and mTORC2 in cancer and the tumor microenvironment. *Oncogene* **2017**, *36* (16), 2191-2201. DOI: 10.1038/onc.2016.363.
(92) Loftus, R. M.; Assmann, N.; Kedia-Mehta, N. Amino acid-dependent cMyc expression is essential for NK cell metabolic and functional responses in mice. *Nature Communications* **2018**, *9*, 2341. DOI: 10.1038/s41467-018-04719-2.
(93) Takahara, T.; Amemiya, Y.; Sugiyama, R. Amino acid-dependent control of mTORC1 signaling: a variety of regulatory modes. *Journal of Biomedical Science* **2020**, *27*. DOI: 10.1186/s12929-020-00679-2.
(94) Donnelly, R. P.; Loftus, R. M.; Keating, S. E. mTORC1-dependent metabolic reprogramming is a prerequisite for Natural Killer cell effector function. *Journal of Immunology* **2014**, *193* (9), 4477-4484. DOI: 10.4049/jimmunol.1401558.
(95) Nicklih, P.; Bergam, P.; Zhang, B. Bidirectional Transport of Amino Acids Regulates mTOR and Autophagy. *Cell* **2009**, *136* (3), 521-534. DOI: 10.1016/j.cell.2008.11.044.
(96) Holeček, M. Branched-chain amino acids in health and disease: metabolism, alterations in blood plasma, and as supplements. *Nutrition & Metabolism* **2018**, *15*. DOI: 10.1186/s12986-018-0271-1.
(97) Ananieva, E. A.; Powell, J. D.; Hutson, S. M. Leucine Metabolism in T Cell Activation: mTOR Signaling and Beyond. *Advances in Nutrition* **2016**, *7* (4). DOI: 10.3945/an.115.011221.
(98) Jaworska, M.; Szczudło, J.; Pietrzyk, A. The Warburg effect: a score for many instruments in the concert of cancer and cancer niche cells. *Pharmacol Rep.* **2023**, *75* (4), 876-890. DOI: 10.1007/s43440-023-00504-1.
(99) Schneider, M.; Marison, I. W.; Stockar, U. v. The importance of ammonia in mammalian cell culture. *Journal of Biotechnology* **1995**, *46* (3), 161-185. DOI: 10.1016/0168-1656(95)00196-4.
(100) Domagala, J.; Grzywa, T. M.; Baranowska, I. Ammonia inhibits antitumor activity of NK cells by decreasing mature perforin. **2023**. DOI: 10.1101/2023.11.20.567708.
(101) Hassel, T.; Gleave, S.; Butler, M. Growth inhibition in animal cell culture. The effect of lactate and ammonia. *Applied Biochemistry and Biotechnology* **1991**, *30* (1), 29-41. DOI: 10.1007/BF02922022.
(102) Tritsch, G. L.; Moore, G. E. Spontaneous decomposition of glutamine in cell culture media. *Experimental Cell Research* **1962**, *28* (2), 360-364. DOI: 10.1016/0014-4827(62)90290-2.
(103) Zhao, M.-H.; Kim, N.-H.; Cui, X.-S. GlutaMAX prolongs the shelf life of the culture medium for porcine parthenotes. *Theriogenology* **2016**, *85* (3), 368-375. DOI: 10.1016/j.theriogenology.2015.08.014.
(104) Husain, Z.; Huang, Y.; Seth, P. Tumor-Derived Lactate Modifies Antitumor Immune Response: Effect on Myeloid-Derived Suppressor Cells and NK Cells. *Journal of Immunology* **2013**, *191* (3), 1486-1495. DOI: 10.4049/jimmunol.1202702.

(105) Harmon, C.; Robinson, M. W.; Hand, F. Lactate-Mediated Acidification of Tumor Microenvironment Induces Apoptosis of Liver-Resident NK Cells in Colorectal Liver Metastasis. *Cancer Immunology Research* **2019**, *7* (2), 335-346. DOI: 10.1158/2326-6066.CIR-18-0481.
(106) Müller, B.; Fischer, B.; Kreutz, W. An acidic microenvironment impairs the generation of non-major histocompatibility complex-restricted killer cells. *Immunology* **2000**, *99* (3). DOI: 10.1046/j.1365-2567.2000.00975.x.
(107) Johnson, C.; Jesuraj, N. J. Seeding density is critical for optimizing scalable feeder-free natural killer cell expansion. *Cytotherapy* **2020**, *22* (5), 126. DOI: 10.1016/j.jcyt.2020.03.240.
(108) Kim, M.; Kim, T.-J.; Kim, H. M. Multi-cellular natural killer (NK) cell clusters enhance NK cell activation through localizing IL-2 within the cluster. *Scientific Reports* **2017**, *7*. DOI: 10.1038/srep40623.
(109) Somanchi, S. S.; McCulley, K. J.; Somanchi, A. A Novel Method for Assessment of Natural Killer Cell Cytotoxicity Using Image Cytometry. *PLoS ONE* **2015**, *10* (10). DOI: 10.1371/journal.pone.0141074.
(110) Tanito, K.; Oshiro, Y.; Tagawa, H. Comparative Evaluation of Natural Killer Cell-mediated Cell Killing Assay Based on the Leakage of an Endogenous Enzyme or a Pre-loaded Fluorophore. *Analytical Sciences* **2021**, *37* (11), 1571-1575. DOI: 10.2116/analsci.21P117.
(111) Wong, W.-Y.; Wong, H.; Cheung, S. P. Measuring natural killer cell cytotoxicity by flow cytometry. *Pathology* **2019**, *51* (3), 286-291. DOI: 10.1016/j.pathol.2018.12.417.
(112) Nishimura, Y.; Kumagai-Takei, N.; Lee, S. A New Method to Determine Natural Killer Cell Activity Without Target Cells. In *Natural Killer Cells*, Aribi, M. Ed.; 2017.
(113) Konjevic, G.; Jurisic, V.; Jovic, V. Investigation of NK cell function and their modulation in different malignancies. *Immunologic Research* **2012**, *52*, 139-156. DOI: 10.1007/s12026-012-8285-7.
(114) Keilhoff, G.; Wolf, G. Comparison of double fluorescence staining and LDH-test for monitoring cell viability in vitro. *Neuroreport* **1993**, *5* (2), 129-132.
(115) Schwarz, E. C.; Qu, B.; Hoth, M. Calcium, cancer and killing: The role of calcium in killing cancer cells by cytotoxic T lymphocytes and natural killer cells. *BBA-Molecular Cell Research* **2013**, *1833* (7), 1603-1611. DOI: 10.1016/j.bbamcr.2012.11.016.
(116) Lee, K.-M.; Forman, J. P.; McNerney, M. E. Requirement of homotypic NK-cell interactions through 2B4(CD244)/CD48 in the generation of NK effector functions. *blood* **2006**, *107* (8), 3181-3188. DOI: 10.1182/blood-2005-01-0185.